KINETIC STUDIES FOR THE PRODUCTION OF TERTIARY ETHERS USED
AS GASOLINE ADDITIVES

A THESIS SUBMITTED TO
THE GRADUATE SCHOOL OF NATURAL AND APPLIED SCIENCES
OF
THE MIDDLE EAST TECHNICAL UNIVERSITY

BY

NEZAHAT BOZ

IN PARTIAL FULFILLMENT OF THE REQUIREMENTS FOR THE DEGREE OF
DOCTOR OF PHILOSOPHY
IN
THE DEPARTMENT OF CHEMICAL ENGINEERING

JUNE 2004

Approval of the Graduate School of Natural and Applied Sciences

                                                    _____
                                                    Prof. Dr. Canan Özgen
                                                           Director

I certify that this thesis satisfies all the requirements as a thesis for the degree of Doctor of Philosophy.

                                                    _____
                                                    Prof. Dr. Timur Doğu
                                                     Head of Department

This is to certify that we have read this thesis and that in our opinion it is fully adequate, in scope and quality, as a thesis and for the degree of Doctor of Philosophy.

_____   _____
Prof. Dr. Gülşen Doğu   Prof. Dr. Timur Doğu
   Co-Supervisor   Supervisor

Examining Committee Members

Prof. Dr. Hayrettin Yücel   (METU, CHE) _____

Prof. Dr. Gülşen Doğu   (GU, CHE) _____

Prof. Dr. Timur Doğu   (METU, CHE) _____

Prof. Dr. Suna Balcı   (GU, CHE) _____

Assoc. Prof. Dr. Kırali Mürtezaoğlu (GU, CHE) _____

I hereby declare that all information in this document has been obtained and presented in accordance with academic rules and ethical conduct. I also declare that, as required by these rules and conduct, I have fully cited and referenced all material and results that are not original to this work.

Name, Last name : Nezahat Boz

Signature   :

ABSTRACT

KINETIC STUDIES FOR THE PRODUCTION OF TERTIARY ETHERS USED AS GASOLINE ADDITIVES

Boz, Nezahat

Ph. D., Department of Chemical Engineering

Supervisor: Prof. Dr. Timur Doğu

Co-supervisor: Prof. Dr. Gülşen Doğu

June 2004, 174 pages

In the present study, the kinetics studies for etherification reactions were investigated in detail.

In the first phase of present study, different acidic resin catalysts were prepared by the heat treatment of Amberlyst-15 catalysts at 220°C at different durations of time and also by the synthesis of sulfonated styrene divinylbenzene cross-linked resins at different conditions. A linear dependence of reaction rate on hydrogen ion-exchange capacity was in 2M2B+ethanol reaction. However, in the case of 2M1B+ethanol reaction hydrogen ion-exchange capacities over 2.8 meq.H^+/g did not cause further increase in reaction rate, which was concluded to be majorly due to significance of diffusional resistances.

DRIFTS experiments carried out with alcohols, isobutylene, isoamylenes and TAME (tert-amyl-methyl-ether) in a temperature range of 333-353 K supported a Langmuir-Hinshelwood type reaction mechanism involving adsorbed isoolefins molecules forming a bridged structure between $-SO_3H$ sites of the catalyst and adsorbed alcohol molecules. A rate expression derived basing on the mechanism proposed from the DRIFTS results gave good agreement with the published data. Reaction rate was found to give a sharp maximum at ethanol activity of around 0.1.

The third phase of this work included evaluation of effective diffusivities and adsorption equilibrium constants of methanol, ethanol and 2M2B, in Amberlyst-15 from moment analysis of batch adsorber dynamic results. Models proposed for monodisperse and bidisperse pore structures were used for the evaluation of effective diffusivities. It was shown that surface diffusion contribution was quite significant.

In the last phase of the work, a batch Reflux-Recycle-Reactor (RRR) was proposed, modeled and constructed to achieve high yields and selectivities in equilibrium limited reactions. The batch reflux recycle reactor was modeled by assuming plug flow in the reactor section, perfect mixing in the reboiler and vapor-liquid equilibria between the liquid in the reboiler and reactor inlet stream. In this system conversion values of isoamylenes reaching to 0.91 were achieved at 82°C with almost 100% selectivity. Such conversion values were shown to be much higher than the corresponding equilibrium values that could be obtained in vapor phase fixed bed reactors. The activation energies evaluated in this system were found to be much less than the activation energies evaluated in the fixed bed reactor studies. This was concluded to be majorly due to the significance of transport resistant in the batch Reflux-Recycle-Reactor in which catalyst particles are partially wet.

As a result of catalyst development, characterization, kinetic and reactor development studies carried out in this study, it was concluded that tert-amyl-ethyl-ether (TAEE) could be effectively produced and used as a gasoline blending oxygenate.

Keywords: MTBE, ETBE, TAME, TAEE, DRIFTS, reaction mechanism, batch Reflux-Recycle-Reactor, Amberlyst-15, diffusion resistance.

ÖZ

BENZİN KATKI MADDESİ OLARAK KULLANILAN TERSİYER ETERLERİN ÜRETİMİ ÜZERİNE KİNETİK ÇALIŞMALAR

Boz, Nezahat

Doktora, Kimya Mühendisliği Bölümü

Tez Yöneticisi: Prof. Dr. Timur DOĞU

Ortak Tez Yöneticisi: Prof. Dr. Gülşen DOĞU

Haziran 2004, 174 sayfa

Bu çalışmamızda, eterleşme reaksiyonlarının kinetiği ve reaksiyon mekanizması detaylı bir şekilde araştırılmıştır.

Çalışmamızın ilk kısmında, eterifikasyon reaksiyonları için hem Amberlit-15'in ısı ile muamelesi sonucunda hem de stiren divinilbenzen polimerik katalizörün sentezlenmesi ve asitlendirilmesi sonucunda alternatif katalizörler sentezlenmiştir. Reaksiyon hızının hidrojen iyon değişim kapasitesine bağlılığı, 2M2B+etanol sisteminde lineer olarak değişmektedir. Fakat, 2M1B+etanol sisteminde, hidrojen iyon değişim kapasitesinin 2.8 meq.H^+/g üzerinde reaksiyon hızına etkisi olmadığı bulunmuştur.

Çalışmamızın ikinci bölümünde; alkoller, izobüten, isoamilenler ve tert-amyl-ethyl-ether (TAME) ile 333-353 K sıcaklık aralığında, DRIFT deneyleri yapılmıştır. Elde edilen sonuçlar izoolefinlerin katalizör yüzeyinde tutunduğunu, katalizörün $-SO_3H$ aktif siteleri ile adsorplanan alkollere tutunarak köprülü bir yapı oluşturduğunu, böylece eterleşme reaksiyonunun Langmuir-Hinshelwood mekanizmasına uyduğunu desteklemiştir. DRIFT sonuçlarına dayanarak önerilen mekanizmaya uygun olarak elde edilen hız ifadesi literatür dataları ile uyum göstermiştir. Reaksiyon hızının, etanol aktivitesinin 0.1 olduğu yerde keskin bir maksimumdan geçtiği bulunmuştur.

Çalışmamızın üçüncü bölümünde, methanol, etanol, ve 2M2B'in Amberlit 15 üzerinde etkin difuzyon katsayıları ve adsorpsiyon denge sabitleri, literatürden alınan kesikli adsorpsiyon sistemi deney verilerinden hesaplanmıştır. Etkin difüzyon katsayılarının hesaplanmasında moment ifadelerinden elde edilen difuzyon direncinin makro gözeneklerde ve jel-tipi mikro tanecikler de olduğunu içeren; farklı modeller kullanılarak bulunmuştur. Yüzey difuzyon katsayısının katkısının makro gözeneklerde oldukça önemli olduğu bulunmuştur

Çalışmamızın son bölümünde, kesikli geri döngü reaktörü önerilerek, modelleme çalışmaları yapılmış ve reaksiyon denge limitasyonlarının olduğu reaksiyonlarda, yüksek ürün seçiciliği elde edilmiştir. Bu reaktörün modellenmesinde; reaktör bölümünde tapa akışı, kazan bölümünde ise mükemmel bir karışım olduğu ve kazanın içerisindeki sıvı ile reaktör girişinde gaz-sıvı dengesinin olduğu varsayımı yapılmıştır. Bu sistemde, 82°C'de dönüşüm değerleri 0.91'e kadar ulaşmıştır. Bu dönüşüm değerleri, gaz fazı dolgulu reaktörlerde elde edilen denge dönüşümlerinden çok yüksektir. Bu sistemde elde edilen aktivasyon enerjileri, dolgulu reaktörde elde edilen aktivasyon enerji değerlerinden düşük bulunmuştur. Bu sonuç daha çok kesikli geri döngü

reaktöründeki kısmen ıslanmış olan katalizör partiküllerindeki taşınım dirençleri ile açıklanabilir.

Bu çalışmada gerçekleştirilen; katalizör geliştirme ve karakterizasyonu, kinetik ve reaktor geliştirme sonuçlarına dayanarak, tert-amyl-ethyl-ether (TAEE)'in verimli bir şekilde üretilebileceği ve benzin katkı maddesi olarak kullanılabileceği sonucuna varılmıştır.

Anahtar kelimeler: MTBE, ETBE, TAME, TAEE, İzoamilen, DRIFTS, reaksiyon mekanizması, Kesikli Geri Döngü Reaktörü, Amberlit-15, Difüzyon limitasyonları.

x

To My Family,

x

ACKNOWLEDGEMENTS

My deepest and sincerest thanks go to my advisors Prof. Dr. Timur Doğu and Prof. Dr. Gülşen Doğu. This work would not have been possible without their constant support, encouragement and patience that helped me get past all those frustrating times when research would end up in a blind alley. I am also grateful to them for all the great ideas and insights, and for steering this dissertation in the right direction. Through their character, leadership, and scientific spirit, they were great role models to me for which I will be ever thankful. I also would like to send my sincere thanks to Assoc. Prof. Dr. Kırali Mürtezaoğlu for his endless support and helpful way every stage of my PhD studies.

I would like to thank Prof. Dr. Hayrettin Yücel for serving on my thesis progressive committee and for giving his valuable advise and comment throughout this work. I also would like to thank Prof. Dr. Suna Balcı for serving on my thesis examining committee and for sharing her own experience.

My sincere thanks go to Dr. Nuray Oktar for sharing her scientific ideas with me and always being a good friend in lab and outside whenever I needed. I would also like to thank to Gazi University Research Group, especially, Dr. Meltem Doğan and Dr. Sena Yaşyerli, they are always there whenever I needed.

In some parts of this work I studied with Dr. Nuray Oktar and Ms. Ebru Aydın. As a result of this collaboration some joint papers are prepared. I would like to express my sincere thanks both of them for their contributions and help.

My special thanks go to our METU Kinetic Research Group Members; Yeşim Güçbilmez, Gülsün Karamullaoğlu, Dilek Varışlı, Zeynep Obalı and Berker Fıçıcılar for their constant support and friendship during my PhD studies.

Thanks are also due to all the staff and technicians of the Chemical Engineering Department.

Above all, words cannot describe my gratitude to my parents, sisters, brother, and my husband and lovely son for their love, support, encouragement, and the innumerable sacrifices they have made to help me achieve my goals. I dedicate this dissertation to them.

TABLE OF CONTENTS

LIST OF TABLES

LIST OF FIGURES

NOMENCLATURE

C_M^V	concentration of alcohol in vapor phase, mol/cm^3
C_{IA}^L	concentration of IA in liquid phase in reboiler, mol/cm^3
$C_{IA,o}^V$	initial concentration of IA in vapor phase, mol/cm^3
a_i	Activity of species i
X_{TAA}	Conversion of olefin to TAA
X_{TAEE}	Conversion of olefin to TAEE
K_j	Equilibrium Constant for reaction j
x_i	Mole fraction of species i in the mixture
A_{ij}	The NRTL model energy parameter for ij binary pair
k_{ij}	The Wong Sandler Model binary interaction parameter
Bi_m	Biot number, $Bi_m = \dfrac{k_m R_o}{D_a}$
C_{Ao}	initial bulk concentration of olefins, mol/lt
D_a	macropore effective diffusivity, cm^2/s
D_i	effective diffusivity within gel-like micrograins, cm^2/s
D_M	molecular diffusion coefficient, cm^2/s
D_s	surface diffusion coefficient, cm^2/s
G	the ratio of diffusion times in the micrograins and macropores
K	apparent adsorption equilibrium constant, ml/g
$K^{(V)}$	vapor phase chemical equilibrium constant
k_1	apparent rate constant, cm^3/g.s
$K1^{(L)}$	liquid phase chemical equilibrium constant for TAME synthesis
$K2^{(L)}$	liquid phase chemical equilibrium constant for TAEE synthesis
K_{IA}	vapor liquid equilibrium constant of IA evaluated at the reboiler composition
M	ratio of initial concentration of ether to isoamylene; $C_{E,o}^V / C_{IA,o}^V$

Q	vapor stream flow rate, cm^3/s
R_A	observed reaction rate, moles/g.s
R_{IA}	observed reaction rate, moles/g.s
R_o	catalyst particle radius, cm
r_o	gel-like micrograin radius, cm
V	reactor volume, cm^3
W	catalyst weight, g
X_E, X_{IA}	mole fractions of ether (TAME or TAEE) and isoamylene in the reboiler, respectively.
$y_{IA,o}$	inlet mole fraction of IA in vapor phase.
y_M,o	inlet mole fraction of alcohol in vapor phase.

Greek Letters

ε_a	macroporosity
ρ_p	apparent density of catalyst, g/ml
ξ_{IA}^V	conversion of IA in vapor phase
$\xi_{IA,e}^V$	vapor phase equilibrium conversion
$\xi_{IA,f}^V$	conversion of IA in vapor phase at the reactor outlet
γ_i	Activity coefficients of species i
τ	tortuosity factor

Abbreviations:

2M2B	2 methyl 2 butene
2M1B	2 methyl 1 butene
MTBE	Methyl tert butyl ether
ETBE	Ethyl tert butyl ether
TAME	Tert amyl methyl ether
TAEE	Tert amyl ethyl ether
MeOH	Methanol
EtOH	Ethanol
TAA	Tert amyl alcohol
TBA	Tert butyl alcohol
RVP	Reid vapor Pressure
FCC	Fluid Catalytic Cracking

CHAPTER 1

INTRODUCTION

Due to high octane numbers and also due to CO and unburned hydrocarbon exhaust emission lowering properties of oxygenates, wide attention was focused on the kinetic studies for synthesis of t-ethers, such as methyl tert-butyl ether (MTBE), ethyl tert-butyl ether (ETBE), tert-amyl methyl ether (TAME) and tert-amyl ethyl ether (TAEE) (Ancillotti and Fattore, 1998; Tejero et al., 1996; Linnekoski et al., 1997). Following the Clean Air Act Amendments of 1990, oxygen content of the reformulated gasoline was increased up to 2.7 wt %. To achieve this, fuels containing about 15% MTBE have been produced during the last decade. However, the bad smell and taste of MTBE, even at very low concentration levels in the drinking water created a problem in extensive use of MTBE as a gasoline additive. This problem of MTBE diverted the attention of researchers to other alternative oxygenates as gasoline additives. Higher vapor pressure and phase separation problems of ethanol make it an unattractive fuel additive. However, ETBE, TAME and TAEE are considered as possible alternates to MTBE.

TAME or TAEE may be produced by the etherification of isoamylenes (2-methyl-1-butene (2M1B) and 2-methyl-2-butene (2M2B)) on acidic catalysts. Considering that about 20 % of FCC gasoline constituted C_5, C_6 and C_7 reactive olefins (Pescarolla et al., 1993), direct etherification of FCC gasoline with

methanol or ethanol attracted the attention of researchers (Rihko et al.,1996; Zhang and Datta, 1995) and the number of studies focusing on the kinetics of TAME and TAEE synthesis were significantly increased in recent years (Rihko et al., 1995; Oost and Hoffmann, 1996; Oktar et al., 1999a,b; Dogu et al., 2001; Dogu et al., 2003).

Acidic macroreticular resins, zeolites and more recently heteropolyacids were used as catalysts in the kinetic studies carried out for the etherification of tert i-olefins. In number of studies, Langmuir-Hinsherwood (LH) type rate models involving adsorption of alcohols (methanol or ethanol) and i-olefins on the $-SO_3H$ acid sites of acidic resin catalysts were proposed (Subramaniam and Bhatia, 1987; Ali and Bhatia, 1990; Zhang and Datta, 1995; Linnekoski et al., 1997). However, in some other studies, Rideal-Eley (RE) type mechanisms involving adsorbed alcohol molecules and fluid phase i-olefins were considered (Al-Jarallah et al.,1988; Parra et al., 1994; Rihko et al., 1995; De lasa et al., 1999). In the review of Tejero et al. (1996) it was shown that, a transition between the Rideal-Eley and Langmuir-Hinshelwood mechanisms might be assumed depending upon the alcohol concentration.

In the first phase of present study, different acidic resin catalysts were prepared by the heat treatment of Amberlyst 15 catalysts at 220°C at different durations of time and also by the synthesis of sulfonated styrene divinylbenzene cross-linked resins at different conditions. Activities and characterization of these catalysts were performed.

In the second phase of this study, diffuse reflectance FT-IR spectra (DRIFTS) obtained with alcohols (methanol and ethanol), *i*-amylenes and TAME in adsorption and reaction experiments were used to obtain detailed information

about the reaction mechanism. A rate expression derived basing on the mechanism proposed from the DRIFTS results gave good agreement with the published data on the rate of production of TAME and TAEE by using independent adsorption equilibrium constants of reagents and related ethers.

The third phase of this work included evaluation of effective diffusivities and adsorption equilibrium constants of methanol, ethanol and 2M2B, in Amberlyst 15. For this purpose, moment expressions were derived for a batch adsorber using different models involving diffusion resistances in the macropores and within the gel-like micrograins. Experimental data reported in an earlier work (Aydın, 1999) were used to evaluate the effective diffusivities using the moment expressions derived here. Contribution of surface diffusion to the diffusion flux within the macropores was found to be quite significant. Also, it was found that diffusion resistance in liquid filled macropores was much more significant than diffusion resistance within the gel-like micrograins of Amberlyst 15, for methanol, ethanol and 2M2B.

In the last phase of the work, a batch reflux recycle reactor was proposed, modeled and constructed to achieve high yields in equilibrium limited reactions. Production of both TAME and TAEE were investigated in this reactor at different temperatures.

CHAPTER 2

OXYGENATES FOR REFORMULATED GASOLINE

Increasing environmental pollution problems and the subsequent emergence of more strict regulations on fuel exhaust gases led to progressive changes in gasoline compositions. Impact of gasoline chemical and physical properties on human health, air quality and the environment, is the issue of greatest relevance for the definition of proper quality standards, which could really affect the end result of environmental legislations. Among the other issues concerned, the levels set for Reid Vapor Pressure (RVP), light olefins and oxygenates will be of the greatest interest for the refineries.

Although the final recipes for motor gasoline after the year 2000 have not been fixed, much speculation on the subject has been published. Future legislation concerning motor gasoline made by the European Union will have a major influence on the time schedule and extend of reformulated gasoline use in other parts of Europe.

Reformulated gasoline is regular gasoline that is blended to reduce volatile organic compounds and toxic emissions relative to conventional gasoline. The gasoline is blended with additives that contain oxygen. Oxygenates help fuels burn cleaner and more completely, thereby reducing levels of carbon monoxide

and ozone-forming compounds emitted via the tailpipe. Reformulated gasoline also reduces the rate at which pollutants evaporate into the air.

2.1 Specifications for Reformulated Gasoline

To produce reformulated gasoline refiners reformulated gasoline by blending fuels with oxygenates and by reducing gasoline components that contribute to air toxics and to ozone formation. In the United States, the Clean Air Act Amendments (CAAA) of 1990 parameters for reformulated gasoline was (Schipper et al., 1990):

- ✓ at least 2% oxygen by weight;
- ✓ a maximum benzene content of 1% by volume;
- ✓ a maximum of 25% by volume of aromatic hydrocarbons.
- ✓ No heavy metals, specifically lead and manganese
- ✓ Detergent additives for deposit prevention

Specifications for gasoline and diesel fuel were enforced by Amendments of the Clean Air Act and two new fuels were mandated:

I. Oxygenated gasoline during the winter months in areas that do not comply with CO emission standard and reformulated gasoline all year round in areas that do not comply with ozone emission standard.

II. Reformulated gasoline differs from conventional fuels at least three features: lower volatility, presence of oxygenate and lower aromatics.

Other quality considerations, such as toxic or air toxic content (eg. Lead, benzene, etc) also come into play for a variety of other effects. Reformulated gasoline produces 15-17% less pollution than conventional gasoline. Benzene is

reduced up to 24%, carbon monoxide (CO) is decreased by as much as 13%, nitrogen oxide (NOx) drops 3%, hydrocarbons (HC) drop 15%, and particulates are reduced up to 9% compared to conventional gasoline.

Oxygenates in reformulated gasoline are not new, but have been used as gasoline additives around the world since the late 1970s. Their most widespread use has been in premium gasoline to improve the octane ratings. Producing oxygenates from all potential Fludized Catalytic Cracking (FCC) tertiary olefins is one of the most economic methods for reducing olefins and RVP in motor gasoline. This route allows higher levels of oxygenate production, thereby lowering Reid Vapor Pressure and the proportion of olefins in the gasoline pool and maximizing the use of FCC olefins. Higher ethers (TAME and TAEE) can be used to meet the amended blend Reid Vapor Pressure levels, and the limits on the olefin content of reformulated gasoline. TAME and TAEE have lower blend Reid Vapor Pressure values than the isoamylenes from which they are produced. Production of TAME and TAEE from isoamylenes thus reduces the olefin content of the light FCC gasoline.

2.2 Oxygenates

Oxygenates are compounds such as alcohols and ethers which contain oxygen in their molecular structure. Oxygenates improve combustion efficiency, thereby reducing polluting emissions. Many oxygenates also serve as excellent octane enhancers when blended with gasoline.

At the end of the 1950's, petroleum refinery seemed to have reached a satisfactory technological level representing a good energy/economy balance. However, great increase in energy consumption and deterioration of the environment led to the recognition during the 1960's that energy production and automotive transportation were major causes of air-quality deterioration. By the

1970's it became clear that petroleum refining had to meet a new goal: energy, economy, and environment together (Ancillotti and Fattore, 1998).

The most publicized environmental measure adopted in the 1970's was the progressive phasing-out of lead additives in motor fuels and the introduction of severe emissions limits for 1975 that could be met only by the application of catalytic converters for the oxidation of CO and HC in automobile exhaust.

By 1978, NO_x emissions had to be reduced drastically. This requirement brought about the development of the three-way catalytic converter, which allowed simultaneous reduction of CO, HC and NO_x.

The complete removal of lead additives from gasoline was necessary for the technical operability of catalytic converters, because the catalysts were intolerant to lead. An important technical consequence of the reduction of lead concentration in gasoline was a notable drop in gasoline octane number, which could not be tolerated by millions of automobiles designed for high-octane-number fuel. The immediate solution for the problem was to raise octane number with increasing concentration of butanes and aromatics in gasoline. However, aromatics and especially benzene were known as carsinogenic species. Recent environmental regulations require total aromatics and benzene to be less than 15% vol and 1% (vol), respectively (Schipper et al., 1990). A second and more innovative solution was the use of a new class of high-octane oxygenated components, called as oxygenates. According to the ASTM D 4814 'Standard Specification for Automotive Spark-Ignition Engine Fuel' an oxygenate is defined as an oxygen containing, ashless organic compound, such as an alcohol or ether, which can be used as a fuel supplement.

Knowledge of the good antiknock properties of some oxygenated compounds dates back to the 1930s, when improvements in aircraft performance resulted in demand for fuels of increasingly higher antiknock performance. It was proved that some branched methyl ethers, like MTBE, ETBE had very interesting octane behaviour.

Oxygenates began to be added to gasoline and to play an increasingly important role in gasoline formulation, as octane booster replacing alkyl lead, from 1973. In the last decade, the oxygenate market was dominated by MTBE, due to its octane blending value, relatively low volatility, complete miscibility with gasoline, low susceptibility to phase separation in the storage and relatively low cost of methanol as compared to ethanol.

Both 'oxygenated gasoline' and reformulated gasoline require certain oxygen content. The CAAA gave to oxygenate the new role of clean air additives, advancing that of octane supplier. Despite the controversial future of oxygenates as "clean air additive", they are expected to maintain and extend the role of "octane supplier" to replace butanes and aromatics.

2.3 Properties and Production of Oxygenates

Oxygenates improve hydrocarbon burning efficiency of gasoline and reduce carbon monoxide (CO) emissions. They also help reduce atmospheric ozone resulting from gasoline evaporative emissions due to their lower volatility and atmospherics characteristics in comparison with hydrocarbon constituents of the refinery gasoline they replace. Because oxygenates clean burning characteristics, they are expected to play a significant role in most of the countries in the world, where clean burning light octane fuels are needed.

Oxygenates which are commonly used in the blending of gasoline are alcohols, mainly methanol and ethanol, and tertiary ethers, such as MTBE, ETBE, TAME, and TAEE. Some properties of alcohols, isoolefins and corresponding ethers are presented in Table 2.1.

Table 2.1 Properties of some hydrocarbons and oxygenates (Ancillotti et al., 1998)

Compound	Octane Number (R+M)/2	Atmospheric reactivity*	Oxygen (wt%)	Boiling Point (°C)	Blending RVP (psi)
Isobutylene		55	-	-3	66
2M2B	91 pure 158 blend	85		38	15
2M1B	92 pure	70	-	31	19
Methanol	116 blend	1	49.9	65	60
Ethanol	113 blend	3.4	34.7	78	18
MTBE	109 blend	2.6	18.2	55	9
ETBE	110 blend	8.1	15.7	72	3-5
TAME	104 blend	7.9	15.7	86	1-2
TAEE	105 blend		13.8	101	0-2

*Gas phase reaction rate with the hydroxyl radical related to the methanol one.

Tertiary ethers are the preferred compounds to alcohols, among the oxygenates for reformulated gasoline, because of their lower Reid Vapor Pressure (RVP; vapor pressure of component at 37.7°C), lower vaporization latent heats, and also they avoid phase separation in the presence of water, which accounts for their full compatibility with the petroleum refining and distribution systems.

2.3.1 MTBE (Methyl Tert Butyl Ether)

MTBE is an oxygenates which has been used in recent years in the US and Canada as an octane-enhancer for gasoline. A significant step to improve the

gasoline quality is the removal of lead by adding an octane enhancer such as MTBE. Another advantage of using oxygenates as gasoline additives to reduce emissions of CO and unburned hydrocarbons from motor vehicles. Schipper et al. (1990) indicated that blending of 15-vol % MTBE in gasoline decreased exhaust hydrocarbons by 5-7% and the presence of MTBE in gasoline reduced CO emissions.

MTBE is produced by the reaction methanol with isobutene. This is a reversible exothermic reaction, which might take place in gas or liquid phase, depending on the system pressure. In liquid phase, the reaction proceeds selectively and with high conversion if the equilibrium is attained at conveniently low temperatures (40-60°C). The reaction is:

$$
CH_3OH \; + \; H_2C{=}\underset{\underset{CH_3}{|}}{C}{-}CH_3 \; \Longleftrightarrow \; CH_3{-}\underset{\underset{O{-}CH_3}{|}}{\overset{\overset{CH_3}{|}}{C}}{-}CH_3
$$
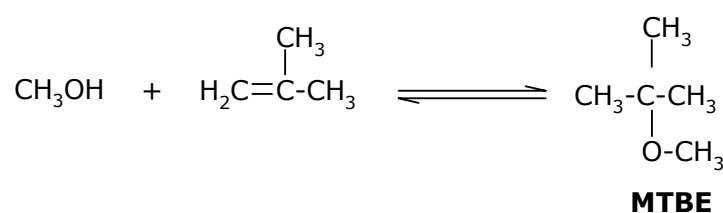
MTBE

Some side reactions can accompany the formation of MTBE, such as isobutene dimerization to 2,4,4-trimethyl-1-pentene and 2,4,4-trimethyl-2-pentene and methanol dehydration to dimethyl ether (DME). Traces of water in the reactants lead to formation of tert-butyl alcohol (TBA) due to the competitive addition of water to isobutene. This reaction proceeds to equilibrium conversion. However, because of the low amount of water in the reactants, TBA does not, generally, reach a concentration level above 0.5-1% in MTBE.

The thermodynamics of the reaction was first studied by Colombo et al. (1983). Also, Rehfinger and Hoffmann (1990), and Izquierdo et al. (1994) and Zhang and Datta (1995) proposed different correlations for the equilibrium constant vs. temperature for MTBE synthesis reaction in the liquid phase. A

substantial agreement between the Rehfinger and Hoffmann and Zhang and Datta data can be noted especially in the temperature range of 40°-90°C. Equilibrium constants calculated through the Colombo expression meet quite well those of Rehfinger and Hoffmann data at low temperatures.

Considering the nature of the reaction, the selection of catalyst for this synthesis was oriented to acid substrates. All the industrial plants built till today have adopted acidic cation exchange resins as catalysts. Less attention was given to inorganic acids that seem not offering, as a whole, convincing performances to substitute the resins in industrial applications. Related to ion exchange resin catalysts used for this reaction, a fundamental work was reported in the early work of Ancillotti et al. (1978).

The increasing demand of MTBE has for a long time been conditioned by the isobutene availability. Industrial quantities of isobutene were coming from C_4 streams of catalytic cracking processes for gasoline production and of ethylene manufacture. The availability of methanol is another key element in MTBE manufacture, but, unlike isobutene, methanol is extensively produced by number of firms from inexpensive natural gas and other carbon sources.

In 1998, MTBE's total worldwide production was 6.6 billion gallons (Ahmed, 2001), with the US consuming the most, about 4.3 billion gallons annually and is considered as one of the top 50 chemicals in production (WHO, 1998). MTBE can be found in the environment during all phases of the petroleum fuel cycle (e.g. auto emissions, evaporative losses from gasoline stations and vehicles, storage tank releases, pipeline leaks and accidental spills, and refinery stock releases). Ahmed (2001) reviewed that, when MTBE was released into air, the greater part will exist in the atmosphere, with small amounts entering soil and water, with chemical degradation being the major removal source from air. When released

into water, a significant amount of MTBE remains dissolved in surface water, with some partitioning into air and a much smaller amount into soil; the key removal process being volatilization (WHO, 1998). Because its high solubility, once released, it moves through the soil and into ground water more rapidly than other chemicals present in gasoline.

Once in ground water, it is slow to biodegrade and is more persistent than other gasoline-related compounds (EPA, 1999). Thus, the potential exposure for humans to MTBE is considerable. These exposures generally occur through inhalation. Inhalation from fumes while fueling automobiles was reported as the principal route for human exposure (Dourson and Felter, 1997).

MTBE is mainly used as an octane enhancer in high-octane gasoline and to achieve the specified oxygen content requirements, 5–15% MTBE in gasoline is required (Dekant et al., 2001) in Europe. Due to the high concentrations of these ethers in gasoline, human exposure to these compounds is likely during production, gasoline blending, and refueling and by evaporation (Stern et al., 1997 and Vainiotalo et al, 1999). MTBE has also been found to leak from storage tanks and is a widely found water contaminant (Brown, 1997). Thus, the potential exposure for humans to MTBE is considerable However, recent studies have indicated that MTBE is claimed to be carsinogenic. MTBE is an animal carcinogen, but its human carcinogenic potential remains unclear. EPA based on animal studies which looked primarily at inhalation effects, concluded that MTBE poses a potential for carcinogenicity to humans at high doses. Some studies suggested that carcinogenicity of MTBE might be due to its two main metabolites, formaldehyde or tributanol. Concern over ground and surface water contamination caused by persistent MTBE has lead the Environmental Protection Agency (EPA) to proposed reducing or eliminating its use as a gasoline additive.

2.3.2 ETBE (Ethyl Tert Butyl Ether)

The major potential alternatives to MTBE are other forms of ethers such as ETBE, TAME and TAEE.

ETBE has a slightly higher octane number and lower blending Reid vapour pressure. Also, it is produced from renewable ethanol. Moreover, there has been no evidence that ETBE is carsinogenic. In a computer-automated structure evaluation study, where ETBE structure was compared with the structure of known determinants of carcinogenicity in rodents, ETBE was predicted to be neither a genotoxicant nor a carcinogen (Rosenkranz and Klopman, 1991). Thus, ETBE is a potential alternative to MTBE in spite of its higher cost at present. Recent advances in ethanol production from biomass may decrease the price of ethanol and the cost of ethanol-based ethers may become comparable to the cost of MTBE in the near future.

The formation of ETBE from ethanol and isobutene is an acid catalyzed, reversible, moderately exothermic reaction. The reaction can be represented as:

$$H_2C{=}\overset{\overset{\displaystyle CH_3}{|}}{C}\text{-}CH_3 \quad + \quad C_2H_5OH \quad \rightleftharpoons \quad CH_3\text{-}\underset{\underset{\displaystyle O\text{-}C_2H_5}{|}}{\overset{\overset{\displaystyle CH_3}{|}}{C}}\text{-}CH_3$$

ETBE
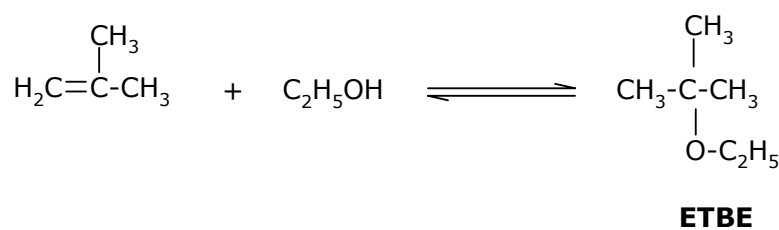
The reaction is equilibrium limited in the industrially significant ranges of temperatures so that the equilibrium conversion from a stoichiometric mixture of reactant at 70 °C is only 84.7% in liquid phase (Sneesby et al., 1997). At higher temperatures, which are needed to increase the reaction rate, even lower equilibrium conversions were expected.

The preferred catalysts appear to be the macroreticular ion exchange resins in the production of ETBE. Tau and Davis (1989) investigated the synthesis of ETBE in liquid and vapour phase on acid resins (Amberlyst-15, Amberlyst-35, fluorocarbonsulphuric acid polymer (FCSA), and phenylphosphoric acid (PPA) on active carbon) and on zeolites (ZSM-5 and S115 of Union Carbide). In the vapour phase Amberlyst-15 was found to be the most active catalyst. In the liquid phase, FCSA and ZSM-5 showed performances near to those of Amberlyst-15 but at much higher temperatures. This prevents to attain equilibrium conversion at the more favorable lower temperatures. The selectivity is very high, but some byproducts such as diisobutene and diethyl ether may appear if the temperature is high enough and ethanol/isobutene molar ratio is far from the stoichiometric ratio. Side products become more important at longer residence times of reactants in the reactor. It is worth noting that the water impurity accompanying ethanol can be higher than with methanol, therefore the competitive formation of TBA is a more important side reaction in ETBE synthesis.

Izquierdo et al. (1994) and Jensen and Datta (1995) have investigated thermodynamic equilibrium of the liquid phase ETBE synthesis.

Çersu et al. (1995) have investigated kinetics of vapor phase production of ETBE using Amberlyst-15 as a catalyst in a fixed bed reactor. In their detailed study, adsorption equilibrium constants of both reactants and ETBE were evaluated using the moment technique.

2.3.3 TAME (Tert Amyl Methyl Ether)

TAME received serious consideration as an oxygenate in the early 1990s, in spite of its slightly lower octane content than other ethers, as it compares

favorably for vapor pressure, boiling point, energy density and water mixability (Caprino, 1998).

The formation of TAME proceeds through the methanol addition on two reactive isoamylenes (2M1B and 2M2B). The third C_5 branched olefin, 3-methyl-1-butene, is completely inert toward the reaction with methanol. Like MTBE and ETBE, TAME synthesis is an acid catalyzed reversible reaction where equilibrium reactions proceed simultaneously. The reaction can be represented as:

2M1B

$$CH_3$$
$$|$$
$$H_2C{=}C{-}CH_2{-}CH_3$$

$$CH_3$$
$$|$$
$$CH_3{-}C{-}CH_2{-}CH_3$$
$$|$$
$$O{-}CH_3$$

$+$ CH_3OH ⇌

TAME

$$CH_3$$
$$|$$
$$H_3C{-}C{=}CH{-}CH_3$$

2M2B
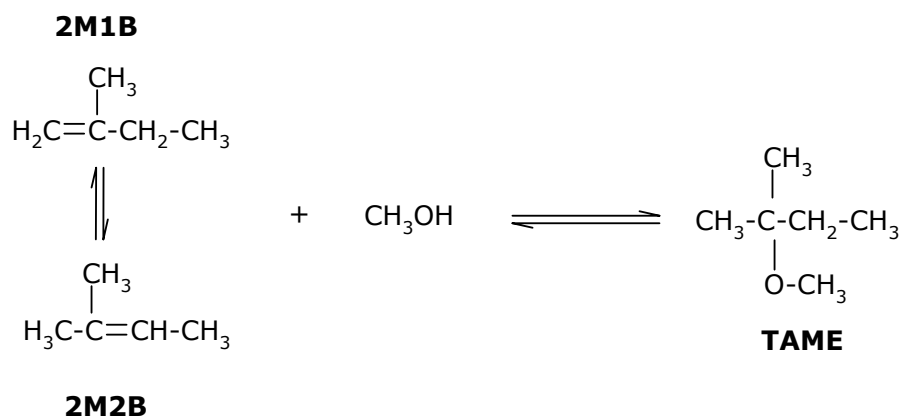
Krause and Hammarström (1987) investigated the reaction giving the limits of the thermodynamic equilibrium at various temperatures and pressures. Rihko et al. (1994) experimentally measured the reaction equilibrium in the liquid phase. In the study of Solà et al. (1997) it was given that under standard operation conditions, working pressure of 700-900 kPA, temperature range of 313-373 K, isoamylene equilibrium conversion was about 70%.

During TAME synthesis, isomerization reaction between 2M2B and 2M1B takes place in addition to reaction of olefins with methanol. The initial rate of double bond isomerization is faster than methanol addition, so two isoamylenes equilibrate before TAME equilibrium is achieved and the initial etherification rate

15

for the two isomers proved to be different, 2M1B being 10 times more reactive (Ancillotti et al., 1998 and Oktar et al., 1999a).

TAME contributes to meet three important requirements of reformulation: introduction of oxygen, reduction of volatility and removal of highly volatile and photochemically reactive olefins.

The TAME potential capacity is strictly related to the reactive isoamylene present in the light gasoline cracking plants. An additional minor contribution to TAME capacity can arise from C_5 coming from naphtha steam cracking for ethylene manufacture, after a selective hydrogenation to remove dienes.

In their detailed study, Oktar et al. (1999b) reported adsorption equilibrium constants and diffusivities of alcohols (methanol and ethanol), isobutylene and corresponding ethers (MTBE, ETBE and TAME) in Amberlyst-15, in gaseous phase in a packed bed flow system.

2.3.4 TAEE (Tert Amyl Ethyl Ether)

TAEE presently is not on the market but that could have some interest if ethanol would be available at a competitive price. In view of this possible alternative use of isoamylenes, some fundamental studies have been devoted to TAEE. TAEE has been identified as a suitable additive to gasoline in order to reduce pollution and to enhance octane ratings.

Kinetic studies on the production of TAEE are very few. Major kinetic studies on TAEE synthesis have been using isoamylene from fuel cracking streams, and ethanol as reactants were carried out by Rihko and Krause (1993), Linnekoski & Krause (1994), Kitchaiya & Datta (1995), Linnekoski et al., (1997), Linnekoski et al., (1998), Oktar et al. (1999a).

2M1B

$$
\begin{array}{c}
\text{CH}_3 \\
|\\
\text{H}_2\text{C}=\text{C-CH}_2\text{-CH}_3
\end{array}
\quad
\begin{array}{c}
\text{CH}_3 \\
|\\
\text{H}_3\text{C-C}=\text{CH-CH}_3
\end{array}
\quad + \quad \text{C}_2\text{H}_5\text{OH} \quad \rightleftharpoons \quad
\begin{array}{c}
\text{CH}_3 \\
|\\
\text{CH}_3\text{-C-CH}_2\text{-CH}_3 \\
|\\
\text{O-C}_2\text{H}_5
\end{array}
$$

TAEE

2M2B
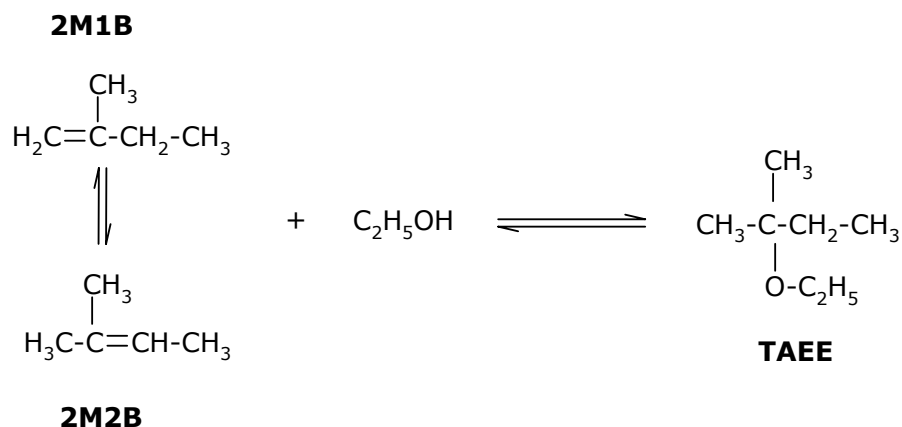
Rihko and Krause (1993) obtained conversion data for etherification and isomerization of isoamylenes using plug flow and batch reactors and showed that etherification conversions declined above 60°C due to the equilibrium limitations.

Kitchaiya and Datta (1995) have studied this reaction in a wide range of compositions and temperatures. They reported a thermodynamic analysis of the liquid phase synthesis of TAEE and of the accompanying mutual isomerisation of the two olefins. The etherification reactivity of isoamylenes with ethanol in liquid phase has been studied by Rihko and Krause (1993), the liquid phase equilibrium by Rihko et al. (1994) and Kitchaiya and Datta (1995) and the kinetics by Linnekoski et al. (1997).

Oktar et al. (1999a) investigated the reactivities of 2-methyl-1-butene (2M1B) and 2-methyl-2-butene (2M2B) in the etherification reaction with ethanol catalysed by a strongly acidic macroreticular resin catalyst in a temperature range of 333-360 K using liquid phase differential flow reactor. They showed that 2M1B was more reactive than 2M2B and its activation energy was also lower in the etherification reaction.

A particular advantage of TAEE is that ethanol, the other reagent, can be produced by fermentation from renewable resources, such as molasses,

sugarcane, sugar, corn and potatoes. Although ethanol is higher in price than methanol, using a less pure ethanol that is an azeotropic or sub-azeotropic mixture of ethanol and water could diminish the difference.

TAEE presents lower blending Reid vapor pressure (less than 5.3 kPa) and lower solubility in water than in other oxygenates. Despite the positive convenience for hot places and underground water contamination, TAEE is not yet on the market (Ancillotti & Fattore, 1998).

Ethyl ethers show slightly better blending octane properties than methyl ethers and lower blend Reid Vapor Pressure that favors the blending with more low cost butanes. The alternative use of methyl or ethyl ethers will mainly depend on availability and price of the two alcohols.

Producing oxygenates from all potential FCC tertiary olefins is one of the most economic methods for reducing olefins and Reid Vapor Pressure in motor gasoline. This route allows higher levels of oxygenate production, thereby lowering Reid Vapor Pressure and the proportion of olefins in the gasoline pool and maximizing the use of FCC olefins. Higher ethers (TAME and TAEE) can be used to meet the amended blend Reid Vapor Pressure levels, and the limits on the olefin content of reformulated gasoline.

TAME and TAEE have lower blend Reid Vapor Pressure values than the isoamylenes from which they are produced. Production of TAME and TAEE from isoamylenes thus reduces the olefin content of the light FCC (Fluid catalyst cracking) gasoline. The FCC unit can be identified as a major issue, because almost all light olefins and a large proportion of aromatics come from here. The typical composition of FCC light gasoline is given in Table 2.1.

Table 2.1 The typical composition of FCC light gasoline (Ignatus et al., 1995)

Component	Fraction, wt %
C4 or lighter	2.1
C5 reactive	13.0
C5 inerts	31.3
C6 reactive	11.7
C6 inerts	25.7
Dienes	1.0
Benzene	1.5
C7 reactives	3.0
C7 inerts + heavier	10.7

By using all the components, produced by an FCC efficiently, many gasoline problems can be solved. But, little attention has been given to the fact that FCC light gasoline contains much more reactive olefins that can be converted to ethers. This way, more octanes are produced and less octanes from reformate are required. Therefore, olefins and aromatics content of the gasoline pool can be reduced. The trend in FCC development allows much deeper conversion to light olefins and lower amounts of aromatics-rich FCC heavy gasoline. By producing more oxygenates like MTBE, TAME and heavier ethers, a refinery can be sufficient in blending reformulated gasoline and oxygenates need to be purchased. The olefin content in the FCC light gasoline stream represents roughly 90% of the gasoline pool olefins. By converting the reactive light olefins into ethers, the FCC gasoline RVP decreases by 0.9 psi (6 kPa). The olefin content is reduced by about 23% (Ignatius et al., 1995).

2.3.5 TAA (Tert-Amyl Alcohol)

Tert-amyl alcohol (TAA) is one of the major products of fusel oil, issued from biomass fermentation. It has been used as an alternative reactant to

isoamylenes so that the synthesized TAEE is completely obtained from renewable resources (Aiouache and Goto, 2003).

The hydration of 2M1B and 2M2B to produce tert-amyl alcohol can be represented as:

2M1B

$$CH_3$$
$$|$$
$$H_2C=C-CH_2-CH_3$$

$$CH_3$$
$$|$$
$$H_3C-C=CH-CH_3$$

$$+ \quad H_2O \quad \rightleftharpoons$$

$$CH_3$$
$$|$$
$$CH_3-C-CH_2-CH_3$$
$$|$$
$$OH$$

TAA

2M2B
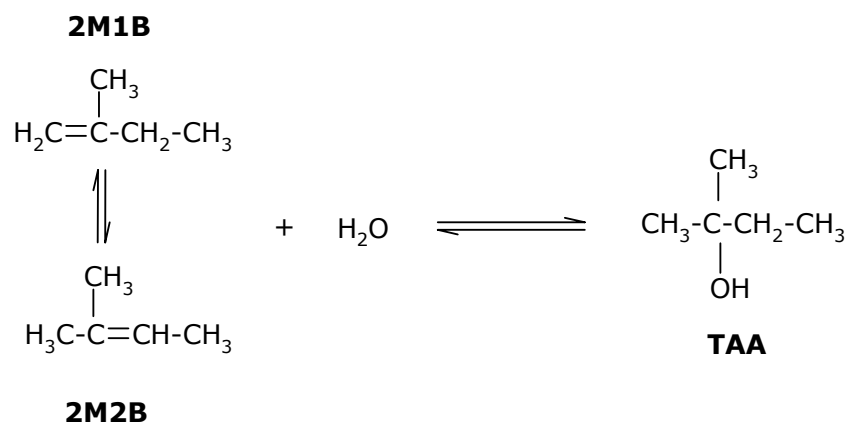
The reaction of isoamylene and water to produce TAA is very similar to the well-studied etherification reactions to produce MTBE, TAME, and ETBE. All of these reactions are carried out in the presence of strongly acidic macroporous resins, at a temperature range of 50-90°C and pressure range of 300-1500 kPa. The polar compound (water or alcohol) adsorbs preferentially in the resin, inhibiting favorable adsorption of the olefin. All reactions are proceeding by the formation of a stable tertiary carbenium ion and they are thermodynamically equilibrium limited, and are moderately exothermic (heats of reaction 25-40 kJ/mol) (González and Fair, 1997).

As indicated by Linnekoski et al. (1998) the hydration reactivity of isoamylenes was studied about this subject. The kinetics of simultaneous hydration and etherification of isoamylenes with sub-azeotropic mixture of ethanol and water and the equilibrium was studied by Jayadeokar and Sharma (1993) using a batch reactor.

20

Several kinetic and thermodynamic studies have been reported on the dehydration/hydration of TAA (Gonzalez & Fair, 1997). But, in our knowledge, there is not available data for the octane number of TAA in the literature.

Linnekoski et al. (1998) studied the simultaneous etherification and hydration of 2-methyl-2-butene and 2-methyl-1-butene in a continuous stirred tank reactor. They founded that addition of a small amount of water to the feed, caused a marked drop in the overall olefin conversion and in the etherification rate.

Varisli (2003) studied the simultaneous production of TAEE and TAA in a reactive distillation column. The elimination of equilibrium limitation was achieved by continuous removal of products from the reaction medium and high conversion values were obtained. Also, the effect of temperature, reactant composition, reactive plate location on the overall olefin conversion and selectivities of TAEE and TAA was investigated.

2.4 The Catalysts Used in Etherification Reactions

Acidic macroreticular ion-exchange resins are the mostly used catalysts for the etherification of reactive isoolefins, such as isobutylene, isoamylenes etc., with methanol and ethanol. Sulphonated polystyrene cross-linked with divinylbenzene is known to show high activity and selectivity in these etherification reactions. These macroreticular ion exchange resin catalysts are composed of gel-like microspheres bonded at the interfaces. The $-SO_3H$ groups attached to the polymer network are the active sites and 95% of these sites are reported to be present within the gel phase (Ancillotti and Fattore, 1998) forming a hydrogen bonded network. In the early work of Thornton and Gates (1974), interaction of alcohols with the matrix-bound sulphonic acid groups was illustrated in the dehydration of alcohols and it was shown that the proton donor-

acceptor tendencies of the network were significantly stronger than those of the solvated acid groups.

Ancillotti et al. (1978) did a fundamental study about ion exchange resins as catalyst for the production of MTBE, firstly. Amberlyst 15 is a macroreticular sulfonic resin manufactured by Rohm and Haas. It is a sulphonated copolymer of styrene and divinylbenzene. In the study of Oktar et al. (1999a) detail information about the pore size distribution, surface area (59.2 m^2/g), porosity (ε_a= 0.32), average macropore diameter (2.28×10^{-8}m) and apparent density (ρ_p =0.99 g/cm^3) were reported.

The morphology and the active sites were mentioned in the work of Ancillotti and Fattore (1998). Differently from gel type resins, where the polymeric gel phase occupies, as a continuum, the macroreticular porous resins are structurally composed of small microgel particles to form clusters bonded at the interfaces. The geometry of microgel tends towards spherical symmetry and the diameter of the individual microgel can range from 0.01 to 15 μm (Dooley et al., 1985). In our recent publication (Doğu et al., 2003), the average micrograin diameter of the catalyst was reported as 8.2×10^{-8}m from the SEM photographs. Also, in the same study, from the SEM photographs, the average micrograin diameter of $FeCl_3$ or NaCl treated catalyst particles was estimated as about 9.4×10^{-8} m, which corresponded to about 50% volume swelling of these microspheres.

The porosity arises from the void spaces between and within the clusters. The void region is a continuous system with essentially all the pores are interconnected. The gel phase is also a continuum, so that a macroreticular porous polymeric particle is constructed of two phases; a continuous pore phase

and a continuous gel phase. The surface area arises from the exposed surface of microgel glued together into clusters.

The pore system makes macroreticular resins suitable for anchoring catalytic sites, namely SO_3H groups, that can lie either on the surface of microspheres or inside the gel phase. Increasing the crosslinking density of the polymer, it is possible to raise the porosity and the surface area but at the same time a less penetrable and less effective gel phase is obtained. Porous macroreticular resins generally show an enhanced catalytic activity compared with nonporous gel polymers of the same level of crosslinking but an increase in porosity and in area surface of a functionalized macroreticular polymer does not univocally result in an increased catalytic activity. In fact, the most part of sulfonic groups in macroreticular resins are located inside the gel phase, more than 95% for Amberlyst-15, and such a situation remains also increasing the surface area unless very high surface areas are obtained.

It is clear that, when the most part of the catalytic sites are inside the microgel particles, the gel phase is the working one. So, till the working phase is the gel phase, an excessive surface area, obtained by increasing the crosslinking density, could reduce the catalytic effectiveness, due to a reduced penetrability of microgel particles.

It is worthy to note that macroreticular resins, when the gel phase is the working one, have advantage on gel type polymer due to the smaller dimensions and enhanced accessibility of the gel domine. If the gel phase has sufficient penetrability for the molecules involved in reaction, macroreticular resins with the gel phase working represent the best solution, since sulfonic groups in the gel portion are more active than those on the surface (Panneman et al., 1995).

Synthetic zeolites were demonstrated to be good catalyst in different reactions requiring acidic properties. Chu and Kuhl (1987) investigated zeolites for MTBE synthesis in vapour phase conditions. Their work considered large (Y, mordenite, etc), medium (ZSM5 and 11) and small (ferrierites) pore zeolites. All zeolites tested were shown to be less active than resins and the optimum performances were given at higher temperature (80°-110°C instead of 60°-90°C).

Chu and Kuhl (1987) utilized the most promising zeolites selected (namely ZSM5 and ZSM11) in liquid phase reaction conditions and made a comparison with Amberlyst 15. The results are quite near to those of A15 and the authors claim higher thermal stability, regenerability by calcination, low sensitivity to the methanol/isobutene ratio and higher productivity.

The heteropoly acid possesses strong acidity to be applicable to several acid-catalyzed reactions in the liquid phase at moderate temperatures. HPA catalyzes methanol addition to isobutene much more effectively than the ordinary protonic acids. It was proposed that high catalyst efficiency of HPA is essentially due to those specific properties of heteropoly anion that can be characterized by very weak basicity and great softness, in addition to a large molecular size of polyhedral heteropoly anion (Izumi et al., 1983).

Knifton and Edwards (1999) demonstrated 12-tungstophosphoric acid and 12-molybdophosphoric acid, on Group III and IV oxide supports, such as titania, HF-treated montmorillonite clays, as well as mineral acid-activated clays to be effective for MTBE syntheses from methanol/*tert*-butanol feed mixtures using a continuous, plug-flow, reactor system. Gas phase synthesis MTBE from methanol and isobutylene was studied with several heteropolyacids at different

temperature (Shikata et al. 1995). Major problem of using HPA's in such etherification reactions is their solubility in alcohols.

Obali (2003) investigated the applicability of bulk and supported heteropoly acid, to the etherification reaction of isoamylene (2M2B) with ethanol in a continuous differential flow reactor. The effect of temperature and the effect of loading amount of heteropoly acid on the conversion and reaction rate were studied.

2.5 Reactive Distillation Applications

Etherification reactions of isoamylenes are limited by chemical equilibrium. Reactive distillation processes are generally recommended to achieve high yields in such equilibrium limited reactions (Sundmacker and Hoffmann, 1995; Baur and Krihna, 2002, 2003; Noeres et al., 2003). Production of side products by the dimerisation and oligomerisation of isoamylenes or formation of dimethyl ether by methanol condensation may cause a decrease in the selectivities of TAME and TAEE production, especially at excessive contact times of reactants with the catalyst (Kitchaiya and Datta, 1995; Oost and Hoffmann, 1996). Another possible side reaction is the formation of tert-amyl alcohol by the reaction of isoamylene with water present as a feed impurity.

CHAPTER 3

LITERATURE SURVEY ON KINETIC STUDIES FOR PRODUCTION OF OXYGENATES

Reaction modeling is essential for interpretation of kinetic data in chemical kinetic studies. Depending on the reaction medium, the mechanism of strong acid ion exchange catalysis can be described in various ways ranging from homogeneous to heterogeneous catalysis.

According to the Helfferich approach (Ancilotti at al., 1977), catalysis performed in the liquid phase in the presence of a protophilic solvent such as water or alcohol that completely swells the resin can be conveniently interpreted as a homogeneous catalysis confined within the catalyst mass, wherein reactants, products and solvent are in equilibrium with the external solution. In this picture the same reaction mechanism is displayed by resins and the corresponding dissolved electrolytes; experimental differences in catalytic performances can be attributed to a selective adsorption and to a different local concentration of active sites. As previously reported, macroreticular resins have two continuous phases, the gel phase and the macropores, and if the gel phase of the microparticles could be assimilated to a homogeneous catalytic working phase, the diffusion through macropores introduces some difficulties in assuming a completely homogeneous picture.

In fact, heterogeneous kinetic models such as Langmuir–Hinselwood (LH) or Rideal-Eley (RE) fit the experimental data better than a homogeneous approach. It can be assumed that a specific competitive adsorption of one or more molecules of reactants or products causes local concentration to be different from their value in the pore liquid. This leads Panneman and Beenackers (1995) to conclude that reaction catalyzed by sulfonic ion exchange resins usually are best characterized as *quasi-homogeneous* and *quasi-heterogeneous*.

A number of kinetic investigations have been published along the years. In number of studies, Langmuir-Hinsherwood type rate models involving adsorption of alcohols (methanol or ethanol) and isoolefins on the $-SO_3H$ acid sites of acidic resin catalysts were proposed (Subramaniam and Bhatia, 1987; Ali and Bhatia, 1990; Zhang and Datta, 1995; Linnekoski et al., 1997). However, in some other studies, Rideal-Eley type mechanisms involving adsorbed alcohol molecules and fluid phase isoolefins were considered (Al-Jarallah et al.,1988; Parra et al., 1994; Rihko et al., 1995; De lasa et al., 1999). In the review of Tejero et al. (1996) it was shown that, a transition between the Rideal-Eley and Langmuir-Hinshelwood mechanisms might be assumed depending upon the alcohol concentration.

In some other studies (Tejero et al., 1987, 1988, 1989) and Piccoli and Lovisi (1995) proposed a simplified Langmuir-Hinshelwood-Hougen-Watson (LHHW) formalism for the TAME formation reaction. To develop the kinetic expression, a model is required to relate the rate and amount of adsorption to the concentration of the component of the fluid in contact with the surface (Froment and Bischoff, 1990). That is the basis of the Hougen-Watson methodology, widely employed to formulate rate equations. According to the

LHHW mechanism proposed in these studies, methanol completely covers the active sites solvating the sulfonic group and forming a methanol liquid layer around the active site. The isoolefins should migrate through that "methanol layer" to react on the same acidic site already occupied by methanol.

3.1 Kinetic Studies on MTBE synthesis

The first kinetic data for the MTBE synthesis available in literature are due to Ancillotti et al. (1977, 1978). The experiments were conducted assuming a homogeneous mechanism and limiting the investigation to the initial rates of the forward reaction with no attention to the effect of the reverse MTBE decomposition reaction. Evidence was given to the negligible influence of mass transfer resistance. These authors showed different mechanisms depending on the ratio of reactants. Reducing the initial methanol concentration and increasing the olefin / alcohol ratio, a negative order on the methanol appears and the rates increase till a maximum. Operating at the ratio isobutene/methanol a higher than 10, a zero order on olefin and a first order on methanol were observed.

A mechanism transition in reactions catalyzed by ion exchange resins was firstly observed by Gates and Rodrigues (1973). The negative effect of protic substances was shown by Thornton and Gates (1974). These authors supposed that at low protic concentration the more active undissociated sulfonic groups are operating. In the absence of protic substances, in fact, resins show a network of undissociated hydrogen bonded -SO_3H groups. The progressive addition of protic compounds destroys this array, firstly breaking the hydrogen bonds among –SO_3H and lastly dissociating and solvating the protons. According to Ancillotti et al. (1978) such a mechanism should be applicable also in the liquid phase MTBE synthesis.

Gicquel and Torck (1983) confirmed that the catalytic activity of resins is enhanced as the methanol concentration is lowered, attributing this trend to the alcohol effect on the proton activity of resin sulfonic group. The kinetics of MTBE synthesis on resins were also studied by Al Jarallah et al. (1988) that found a good fit of experimental data with a Rideal–Eley model, being the methanol the adsorbed reactant. Moreover, these authors confirmed that the catalyst is more active at low methanol / isobutene ratios. Subramaniam and Bhatia (1987) found that homogeneous and heterogeneous Langmuir–Hinshelwood models both correlated satisfactory their kinetic data. Several other studies on the kinetics of the reaction were conducted in the eighties; none arrived to propose a rate equation valid in the whole industrially interesting concentration and temperature range of application of the synthesis.

Amberlyst-15 was also studied by Tejero et al. (1987, 1988, 1989) for the reaction conducted at atmospheric pressure in vapour phase. A LHHW reaction mechanism was proposed and this was found consistent with the adsorption of methanol on one center and isobutene on two catalytic centers.

Rehfinger and Hoffmann (1990) determined the intrinsic rate of MTBE formation carrying out experiments in a CSTR reactor, operating at specific conditions high methanol concentration, small particle size of catalyst, high stirrer speed, where the influence of internal and external transport phenomena mass and heat transfer was eliminated. Amberlyst-15 and a specially prepared resin (CVT) were comparatively tested evidencing an undifferentiated behavior, so that the authors inferred that the reaction is neither influenced by microsphere diffusion nor the internal surface area and the whole microsphere contributes to the reaction with an effectiveness factor of 1. The microkinetic model was developed assuming that the reaction takes place within the gel

29

phase of macropores between molecules in the sorbed state, being the chemical reaction of sorbed molecules the rate-limiting kinetic step, described as a first-order reaction in the reacting species. With these assumptions, they described the experimental results adopting a three-parameter model based on a Langmuir–Hinshelwood rate expression in liquid phase activities from UNIQUAC method.

Ali and Bhatia (1990) studied on MTBE formation in a catalytic bed reactor. They found that the reaction rate data were interpreted using a heterogeneous model based on LH kinetics.

More recently other kinetic investigations on the liquid phase MTBE synthesis appeared. Sola et al. (1994) contributed with a study of the reaction in liquid phase in a calorimeter; the heat flow rate representing an indirect measure of the reaction rate. Among the literature proposed models, the Rehfinger model provided the best correlation with the experimental data of Sola. Zhang and Datta (1995) investigated the liquid phase MTBE reaction in an isothermal integral packed-bed reactor. The intrinsic kinetics were determined under conditions free of diffusional influence. Intraparticle diffusional limitations were however investigated, evidencing that with Amberlyst-15 catalyst of average diameter 0.74 mm, the reaction is substantially limited by interparticle diffusion resistance at temperatures above 60°C at isobutene conversion closer to the equilibrium.

Panneman and Beenackers (1995) have explored the influence of solvent, of the isobutene / methanol ratio and of MTBE product on the reaction rate. They found that the forward rate constant decreases continuously increasing the isobutene/methanol ratio, while an increase in the rate constant is observed with

an increased amount of MTBE in the reaction mixture. Applying a pseudo homogeneous model combined with the transition state theory, they explain their results on the basis of changes in activity of the reactants, of the catalyst and of the activated complex. The pseudo-homogenous model previously known from the literature considered the changes in reactant activities only. These authors found that, differently from Rehfinger and Hoffmann (1990), the differences in cross-linking and acid concentration greatly affect the values of the kinetic parameters. According to Panneman and Beenackers (1995), the differences found in the catalytic activity of some tested commercial resins should be attributed not only to the proton activity but also to the different positions of the sulfonic groups, leading to a different stabilization of the activated complex.

Fite et al. (1998) has studied the kinetics of MTBE synthesis. They compared the experimental results with calculated ones using the models from the literature. The experimental rate of reactions deviated from the calculated results, mainly in cases when the initial mol ratio of the reagents deviated from 1. With excess methanol the experimental reaction rates were lower than those calculated with the models. They concluded that the polarity of the whole reaction medium influences the activity of an ion-exchange resin. The kinetic model of the synthesis was improved by including a solubility parameter of the reaction medium in the model.

In the review article of Ancillotti and Fattore (1998), the main catalytic studies on MTBE synthesis were summarized in detailed. DRIFTS experiments (Section 5.2) showed that a LH type reaction mechanism involving adsorbed alcohols and tert-olefins gave good agreement with the kinetic data. It was concluded that the ether molecules (MTBE and ETBE) are formed on the

catalysts surface in the adsorbed state. In Table 3.1 gives a summary of the mechanisms proposed for MTBE synthesis, with different acidic ion exchange catalysts, in liquid and vapor phase.

Table 3.1 Mechanisms Proposed in Literature for MTBE Production on Acidic Ion Exchange Resins

source	Catalyst	Phase	Kinetic Model
Ancillotti et al. (1977, 1978)	Amberlyst-15	liquid	initial rate
Gicqual and Torck (1983)	Amberlyst-15	liquid	LH
Subramaniam and Bhatia (1987)	Amberlyst-15	liquid	homogeneous LH
Tejero et al. (1987, 1988,1989)	Amberlyst-15	gaseous	LHHW
Al-Jarallah et al. (1988)	Amberlyst-15	liquid	RE
Rehfinger and Hoffmann (1990)	Amberlyst-15 CVT (synthesized)	liquid	LH
Ali and Bhatia (1990)	Amberlyst-15	Liquid+ gaseous	LH
Sola et al. (1994)	Lewatit K2631	liquid	pseudo homogeneous
Parra et al. (1995)	Bayer K-2631	liquid	RE
Caetano et al. (1995)	Amberlyst 18	liquid	RE
Zhang and Datta, (1995)	Amberlyst-15	liquid	LH
Panneman and Beenackers (1995)	Amberlyst-15 and Several resins	liquid	pseudo homogeneous and transition state
Tejero et al. (1996)	Amberlyst-15	liquid	Transition between LH and RE
Fite et al. (1998)	Bayer K-2631	liquid	LHHW
Venimadhauan (1999)	Amberlyst-15	liquid	LHHW
de Lasa et al. (1999)	Amberlyst-15	liquid	-

Due to the different experimental procedures and also to discussed ambiguities in the resins mechanism, the reported kinetic approaches appear to be scarcely comparable and the different results difficult to be rationalized in a common reaction mechanism.

In their detailed study of Tejero et al. (1996), two reaction mechanism proposed for the reaction of MTBE synthesis in liquid phase. The first involves the reaction between isobutene in solution and methanol hydrogen bonded in the network of sulfonic groups (ER mechanism). The second involves the reaction between isobutene and methanol immobilized on $-SO_3H$ groups (LH mechanism). The ER mechanism is assumed to occur at large excess of methanol, whereas at very low contents of methanol the reaction would proceed according to the LH mechanism. They concluded that a transition between a RE and LH mechanism could be assumed depending on methanol concentration of the liquid phase.

In LH Mechanism, both the alcohol and the iso-olefin are adsorbed on the active sites of the catalsyst and the surface reaction takes place between adsorbed species to give the product, ether, which is then, desorbed. During the reaction step additional active sites may be involved. In chemical equations, the reaction of methanol (MeOH) with isobutylene (IB) to produce MTBE can be summarized with LH Mechanism as follows:

MeOH + S $\leftrightarrow$ MeOH.S

IB + S $\leftrightarrow$ IB.S

MeOH.S + IB.S + (n − 2)S $\leftrightarrow$ MeOH.S + (n - 1).S

MTBE.S $\leftrightarrow$ MTBE + .S
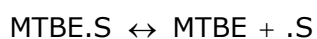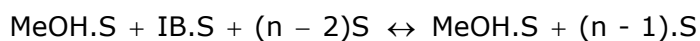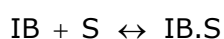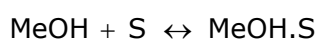
Here, S stands for an active site. In total, n active sites are used. From molecular point of view, it is assumed that a concerted proton transfer involving adsorbed isobutene begins to be operative. Adsorption of isobutylene leads to a t-butyl cation-like structure immolized on $-SO_3H$ groups, which reacts with the methanol hydrogen bonded to adjacent sulfonic groups. The cooperative action of three $-SO_3H$ groups is necessary to stabilize the t-butyl structure and the proton transfer can occur MTBE is also hydrogen bonded to $-SO_3H$ groups (Tejero, et al., 1996).

Taking the surface reaction as the rate limiting step, the resulting rate equation can be denoted as follows:

$$r = \frac{k_F K_{IB} K_{MeOH}(a_{IB} a_{MeOH} - a_{MTBE}/K)}{(1 + K_{IB} a_{IB} + K_{MeOH} a_{MeOH} + K_{MTBE} a_{MTBE})^n} \tag{3.1}$$

where, k_F denotes the forward reaction rate constant, K_i is the adsorption equilibrium constant of species i (dimensionless), a_i is the activity of the species in liquid phase at the specified temperature, and n is a constant. The non-ideality of the reaction medium, liquid phase activities calculated by the UNIFAC method was used in the kinetic expression (Eqn. 3.1).

On the other hand, in the Rideal-Eley type of reaction mechanism, the ether synthesis proceeds between iso-olefin from bulk solution and adsorbed alcohol, to give the product, ether, which is then desorbed, the surface reaction being the rate limiting step. The RE Mechanism for the reaction of methanol and isobutylene can be shown as follows:

MeOH + S ↔ MeOH.S

MeOH.S + IB + (n − 1).S ↔ MTBE.S + (n - 1).S

MTBE.S ↔ MTBE + .S
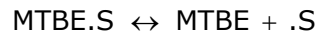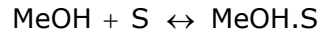
From a molecular standpoint, MTBE synthesis would occur by a concerted proton transfer in liquid phase. The methanol is hydrogen bonded in the three-dimensional network of $-SO_3H$ groups, and reacts with isobutene in solution within the pores and the gel phase. The cooperative action of three $-SO_3H$ is needed so that a t-butyl cation-like structure can be induced, and the concerted proton transfer takes place. The ether is hydrogen bonded to $-SO_3H$ groups inhibiting the reaction (Tejero et al., 1996).

The surface reaction being the rate-limiting step, the rate equation can be written as follows:

$$r = \frac{k_F K_{MeOH}(a_{IB}a_{MeOH} - a_{MTBE}/K)}{(1 + K_{MeOH}a_{MeOH} + K_{MTBE}a_{MTBE})^n}$$
(3.2)

For the verification of proposed reaction mechanisms, and for evaluation of adsorption parameters which appear in the rate expressions, a detailed investigation of iso-olefins, alcohols and corresponding ethers on acidic ion-exchange catalsyst is required.

3.2 Kinetic Studies on ETBE Synthesis

Tau and Davis (1989) investigated the synthesis of ETBE in liquid and vapor phase on acid resins. They discussed two different mechanisms for ETBE production. One of them is the RE mechanism whereby adsorbed t-butyl

carbenium ion would react with gas phase alcohol. They have mentioned about another mechanism where alcohol protonation was considered as the first step in the reaction mechanism.

Françoisse and Thyrion (1991) and Fite et al. (1994) studied the reaction assuming the Eley–Rideal kinetic mechanism. They have shown that ethanol is preferably adsorbed on the active sites and reacts with isobutene in solution. The surface reaction was the rate limiting step, and two additional centers take part in this step.

Sola et al. (1995) did a kinetic study of the liquid phase synthesis of this ether using a reactor calorimeter. The approach is the same followed for the MTBE reaction. An Eley–Rideal kinetic model, based on the involvement of two active sites in the rate determining step, is proposed.

Cunill et al. (1993) studied the influence of water in the liquid phase synthesis. Iborra et al. (1992) studied the influence of the resin structure on the reaction in vapour phase.

Cersu (1995) have investigated the kinetics of vapour phase production of ETBE using Amberlyst-15 as a catalyst in a fixed bed reactor. In their detailed study, adsorption equilibrium constants of both reactants and ETBE were evaluated using the moment tehnique. Their investigation showed that, a LH type of rate expression gave good aggreement with the kinetic data. Effects of pore diffusion and film mass transfer resistance on the observed rate were found to be negligible.

Schwarzer et al. (2000) have compared and tested microkinetics approaches from the literature against the available data and their own data in liquid phase ETBE synthesis. The adjustment of the parameter for n=2 to the

their own data and Fite et al. (1994) data, both models (LH or RE) seemed to describe the ETBE microkinetics well. They suggested the approach with n=2 that has been proven for MTBE synthesis and it was also prefered by Sola et al. (1995).

The main catalytic studies on ETBE synthesis quoted in the literature were summarized in Table 3.2, in liquid and vapor phase.

Table 3.2 Mechanisms Proposed in Literature for ETBE Production on Acidic Ion-Exchange Resins

source	Catalyst	Phase	Kinetic Model
Tau & Davis (1989)	Amberlyst-15 and other type of catalysts	Liquid and vapor	RE
Françoisse & Thyrion, 1991	Amberlyst-15	liquid	RE
Iborra et al., 1992	Amberlyst-15	vapor	LHHW
Jayadeokar and Sharma, 1992	Amberlyst-15	vapor	LH
Fite et al., 1994	Lewatit K-2631	liquid	RE
Sola et al., 1995	Lewatit K-2631	liquid	RE
Cersu, 1995	Amberlyst-15	vapor	LH
Schwarzer et al., 2000	Bayer K-2631	liquid	LH & ER for set to n=2

3.3 Kinetic Studies on TAME Synthesis

The isoamylene reactivity toward the methanol addition was first investigated by Ancillotti et al. (1977). These authors evidenced that 2M2B and 2M1B react giving both methanol addition and double bond isomerization. The initial rate of double bond isomerization is faster than methanol addition, so two isoamylenes equilibrate before TAME equilibrium is achieved. Moreover, the

initial etherification rate for the two isomers proved to be different, 2M1B being 10 times more reactive. Ancillotti et al. (1996) assumed an ionic mechanism in two steps: olefin protonation to a carbenium ion and addition of the nucleophile (methanol) on carbenium ion; since the two isoamylenes originate the same carbenium ion by protonation, it was inferred that the first step had to be the rate-determining step.

Since the etherification of isoamylenes to TAME production is a relatively new process, there are few published works concerning its kinetic. The liquid phase synthesis was studied by Pavlova et al. (1986). They proposed a kinetic model taking in consideration the activities of the chemical species involved in the reaction and following a Langmuir-Hinshelwood mechanism approach. Randriamahefa et al. (1988) proposed a quasi-homogeneous model for TAME synthesis, where the TAME splitting was described by a LH mechanism.

Piccoli and Lovisi (1995) proposed a simplified LHHW formalism for the TAME formation reaction. They pointed out that the presented model was only valid for reaction in the liquid phase with a molar ratio of MeOH/isoamylenes>1.

A kinetic investigation of TAME synthesis has been published by Rihko and Krause (1995). The effects of process variables pressure, temperature, reagent concentration on the forward and reverse reactions were measured. Three kinetic equations, one based on homogeneous mechanism and two based on heterogeneous mechanism (LH and RE), have been applied to the experimental results. The best fitting was obtained with an heterogeneous mechanism, where ether and alcohol adsorb on the catalyst active site and where the rate-determining step is the surface reaction (RE mechanism).

In other study of Rihko et al. (1997), the kinetics and equilibrium of the heterogeneously catalyzed liquid phase formation of TAME were investigated. The measured reaction rates were fitted to three kinetic models; homogeneous, RE type , and LH type. Of these, the LH type model described the experimental results best. This model was based on single-site adsorption of every component, with the surface reaction being the rate-limiting step.

In their detailed study, Kiviranta-Paakkonen et al. (1998) tested various kinetic models against batch reactor data for TAME sythesis. The temperature was varied between 333 and 353 K and the MeOH/isoamylene molar ratio between 0.2 and 2. They concluded that the activity-based models predicted the experimental results better within a wider range of conditions than the concentration-based models.

The main catalytic studies on ETBE synthesis quoted in the literature were summarized in Table 3.3, in liquid and vapor phase.

Table 3.3 Mechanisms Proposed in Literature for TAME Production on Acidic Ion Exchange Resins

Source	Catalyst	Phase	Kinetic Model
Pavlova (1986)	Amberlyst-15	liquid	LH
Randriamahefa and Gallo (1988)	Amberlyst-15	liquid	LH
Piccoli and Lovisi (1995)	Amberlyst-15	liquid	LHHW
Rihko and Krause (1995)	Amberlyst 16	Liquid	RE
Rihko et al. (1997)	Amberlyst 16	liquid	RE
Kiviranta-Paakkonen et al. (1998)	Amberlyst 16	liquid	RE
Rihko-Struckmann et al. (2001)	Amberlyst 16	liquid	RE

3.4 Kinetic Studies on TAEE Synthesis

Despite the growing interest in higher ethers and ethanol-based ethers, few studies have been published regarding the formation of TAEE. Rihko and Krause (1993) published a report of the reactivity of isoamylenes with ethanol. The reaction equilibrium in the synthesis of TAEE has been studied by Rihko et al. (1994) and Kitchaiya and Datta (1995).

In their detailed work of Linnekoski et al. (1997), the most common models proposed in the literature for the etherification reactions were summarized for the formation of TAEE: a pseudohomogeneous model, an RE type model, and a LH type model. Of these, they found that the LH type model described the experimental results best. The rate limiting step, in the model, is the surface reaction between adsorbed alcohol and isoamylene.

The simultaneous etherification and hydration of isoamylenes with an azeotropic mixture of ethanol and water have been studied by Jayadeokar and Sharma (1993). They proposed a concentration-based kinetic model of LH type for both etherification and alcohol formation of lumped isoamylenes and obtained reaction rate constants.

In recent study of Linnekoski et al. (1998), the simultaneous etherification and hydration of isoamylenes were investigated in a continuous stirred tank reactor. The measured reaction rates of the etherification and alcohol formation were fitted to kinetic models of LH type. These models are based on single site adsorption of every component and the surface reaction being the rate limiting step.The main catalytic studies on TAEE synthesis were summarized in Table 3.4.

Table 3.4 Mechanisms Proposed in Literature for TAEE Production on
Acidic Ion-Exchange Resins

source	Catalyst	Phase	Kinetic Model
Rihko and Krause (1993)	Amberlyst 16	liquid	LH
Jayadeokar and Sharma (1993)	Amberlyst-15	liquid	LH
Linnekoski et al. (1997)	Amberlyst 16	liquid	LH
Linnekoski et al. (1998)	Amberlyst 16	liquid	LH

For the verification of proposed reaction mechanisms, and for evaluation of adsorption parameters which appear in rate expressions, a detailed investigation of isoolefins, alcohols and corresponding ethers on acidic ion exchange catalyst is required. Related publications are summarized in the following section.

3.5. Adsorption Studies

No independent adsorption data were quoted in literature for isobutylene, isoamylenes, alcohols (methanol and ethanol), MTBE, ETBE, TAME, and TAEE on Amberlyst-15. For alcohols, Sola et al. (1997), and Fite et al. (1994) reported heat of adsorption values extracted from kinetic data. Zhang and Datta (1995) reported some information about adsorption of liquid ethanol in n-heptane as solvent, and C_6 olefins on Amberlyst-15.

In detailed study of Oktar et al. (1999b), the adsorption equilibrium constants of alcohols, isoamylenes and corresponding ethers on Amberlyst-15, in gaseous phase in a packed bed flow system between 323 and 373 K. The results of this study are tabulated in Table 3.5.

Table 3.5 Vapor Phase Adsorption Equilibrium Constants ($\rho_p K$) of Methanol, Ethanol, C_4 and C_5 i-olefins and the Corresponding Tertiary Ethers (Oktar et al., 1999b)

Tracer	323 K	340 K	358 K	373 K
Ethanol	1.44×10^4	1.14×10^4	1.06×10^4	1.87×10^4
Methanol	0.97×10^4	0.88×10^4	0.76×10^4	1.09×10^4
Isobutylene	635	260	113	38
2M1B	133	63	40	19
2M2B	94	68	42	24
MTBE	238	124	43	26
TAME	56	37	32	21

In our more recent study (Dogu et al., 2001), adsorption equilibrium constants of ethanol were calculated in liquid phase batch adsorption system on Amberlyst-15 at different temperature. Liquid phase adsorption isotherms corresponding to ethanol concentrations lower than 0.5 mole % were obtained of four different temperatures. The regression analysis of the adsorption data, by using a Langmuir type isotherm,

$$\frac{q}{q_m} = \frac{K_{AL} \, C_{AL}}{\left(1 + K_{AL} \, C_{AL}\right)} \tag{3.3}$$

yielded the liquid phase adsorption equilibrium constant K_{AL} and maximum adsorption capacity q_m. The linear adsorption equilibrium constant ($K_{AL} \, q_m$) values expected at very dilute concentrations were then estimated. The results were summarized in Table 3.6. As shown in this table, liquid phase adsorption equilibrium constant K_{AL} decreased with an increase of temperature up to 334 K. Further increase in temperature caused an increase in K_{AL}. The maximum adsorption capacity q_m also showed an increasing trend with an increase in temperature. Vapor phase adsorption equilibrium constants reported in our earlier publication (Oktar et al., 1999b) were also reported in the same table. A

similar trend was seen for vapor phase adsorption. The increasing trend of maximum adsorption capacity q_m with temperature indicated the increased availability of active sites for adsorption due to swelling of the catalyst and higher penetration of alcohol molecules into gel-like structure of the polymer at higher temperatures. This increasing trend of q_m with temperature also contributed to the increasing trend of linear adsorption equilibrium constant (q_m K_{AL}) with temperature. The maximum adsorption capacity values were found to be in the order of magnitude of 10 mmol/g, which is about twice the maximum hydrogen exchange capacity of Amberlyst-15. This is another indication of multilayer adsorption of alcohol molecules forming a network of hydrogen bridges over the first layer of adsorbed molecules.

The increasing trend of adsorption equilibrium constant K_{AL} over a certain temperature is a strong indication of chemisorption of ethanol molecules on the $-SO_3H$ sites of the catalyst. This result supported the DRIFT results which will be discussed in the coming sections.

As it was shown in Table 3.6, the vapor phase adsorption equilibrium constants are two orders of magnitude higher than the liquid phase adsorption equilibrium constants. Following analysis gave an approximate relationship between the vapor and the liquid phase adsorption equilibrium constants and explained this difference. In the liquid phase, some adsorption of the solvent (in our work, n-heptane) was also expected. Using the Langmuir model, the relation between the adsorbed concentration of alcohol (*q*) and vapor phase concentrations C_{AV} and C_{BV}, which are in equilibrium with the liquid phase solution concentrations C_{AL} and C_{BL} may be written as,

$$\frac{q}{q_m} = \frac{K_{AV}C_{AV}}{1 + K_{AV}C_{AV} + K_{BV}C_{BV}}$$

(3.4)

Table 3.6 Adsorption equilibrium parameters of ethanol on Amberlyst-15 (Doğu et al., 2001)

temperature (K)	Liquid phase[a]			Vapor phase[b]
	K_{AL} (mL/mmol)	q_m (mmol/g)	$q_m K_{AL}$ (mL/g)	$q_m K_{AV}$ (mL/g)
306	44.7	9.1	407	-
320	16.6	10.3	171	-
323	-	-	-	1.44×10^4
334	13.7	15.8	217	-
340	-	-	-	1.14×10^4
347	36.7	13.2	484	-
358	-	-	-	1.06×10^4
373	-	-	-	1.87×10^4

[a]Doğu et al. (2001)

[b]Oktar et al. (1999)

A similar approach was used by Boulicaut et al. (1998) to find the relation between liquid and vapor phase adsorption equilibrium constants for an ideal system. Ethanol n-heptane mixtures were known to be quite non-ideal. For this system, the relation between the vapor phase and the liquid phase concentrations can be approximately expressed as,

$$C_{AV}RT = P_A^o \gamma_A \left(C_{AL} / C_o \right) \quad (3.4)$$

where, C_o and γ_A are the total concentration of the liquid and the activity coefficient, of ethanol respectively. For low concentrations of alcohol, the liquid phase concentration of the solvent (n-heptane) can be approximated to be about the same as total concentration of liquid $C_{BL} \cong C_o$. For this case, Eqn. 3.4 reduces to Eqn. 3.3, where

$$K_{AL} = K_{AV}\left(\frac{P_A^o \gamma_A}{RT\,C_o}\right)\left(\frac{1}{1 + \left(\dfrac{K_{BV}}{RT}\right)P_B^o\,\gamma_B}\right) \qquad (3.6)$$

Eqn. 3.6 gives the relation between the vapor and liquid phase adsorption equilibrium constants. For a case with negligible sorption of solvent on the catalyst, this equation reduces to,

$$K_{AL} = K_{AV}\left(\frac{P_A^o \gamma_A}{RT\,C_o}\right) \qquad (3.7)$$

The vapor phase adsorption equilibrium constants of ethanol were estimated from the experimental liquid phase adsorption equilibrium data using Eqn. 3.7. In this calculation, activity coefficients were estimated from the UNIFAC method (Sandler, 1999) and vapor pressures $\left(P_A^o\right)$ were estimated from the Antoine relations. Results are shown in Figure 3.1, together with the experimental values of vapor and liquid phase adsorption equilibrium constants. Satisfactory agreement was obtained between the experimental and predicted values of equilibrium constants. The differences between the experimental and predicted values are, majorly due to the neglection of possible adsorption of solvent (n-heptane) in the calculation procedure and due to the possible differences in swelling of Amberlyst-15 in vapor and liquid phase adsorption of alcohols. The major conclusions reached from this analysis are that, the temperature dependences of vapor and liquid phase adsorption equilibrium constants are similar and the increased availability of the active sites due to swelling together with chemisorption of ethanol molecules contributed to the increase of the q_m K_{AL} values with temperature.
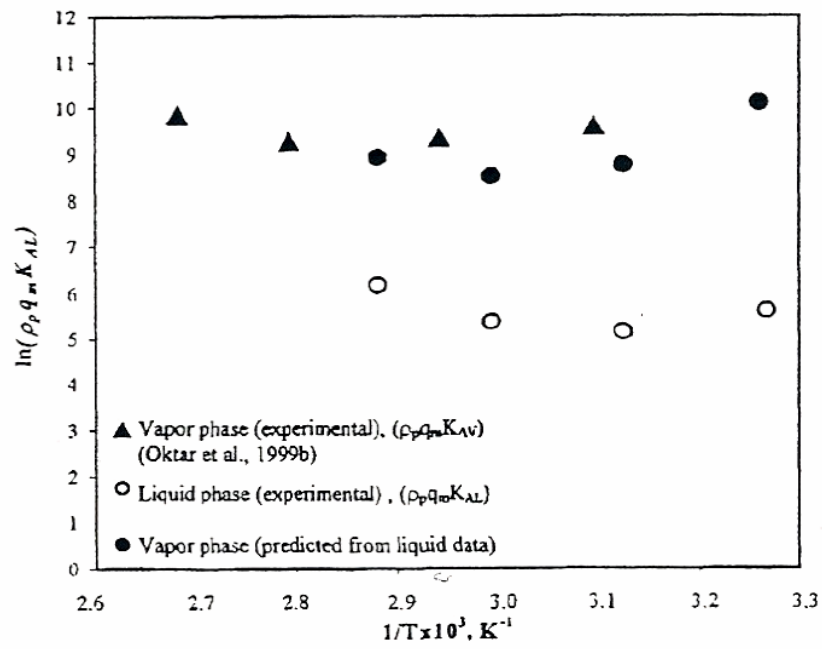
Figure 3.1 Liquid and vapor phase adsorption equilibrium constants of ethanol on Amberlyst-15 (Doğu et al., 2001).

CHAPTER 4

EXPERIMENTAL

The experimental work of this study consisted of three main parts. In the first part of the study, new acidic resin catalysts and heat treated Amberlyst-15 were prepared and characterized to find the effect of hydrogen ion-exchange capacity of resins on activity in the etherification reactions. Physical properties of the catalysts such as, surface area and pore size distribution and total ion-exchange capacity measurements were performed. In the second part, the surface of the catalyst during adsorption of the reactants and products was investigated with Diffuse Reflectance Infrared Fourier Transform (DRIFT) to obtain detailed information about the adsorbed species. Third part of study, a novel batch Reflux-Recycle-Reactor was proposed for TAME and TAEE production in order to get high conversion in the etherification reactions.

4.1 Chemicals Used in the Experiments

Methanol and ethanol of analytical grade (purity 99.8%) and 2M2B (purity>95%) from Merck was used as the reactants in the liquid phase etherification reactions. In DRIFT experiments, additionally, gaseous isobutylene from Uçar and TAME (>97%) from Aldrich were used. For the chromatographic analysis again TAME (>97%) from Aldrich and TAA from Merck were used

performing calibration experiments. The properties and other details of the chemicals are listed in Table 4.1.

Table 4.1 Properties of Chemicals Used in the Etherification and DRIFT Experiments

Chemical	Chemical Formula	Boiling Point (°C)	Purity	Density (g/ml)	Molecular Weight (g/mol)	Source
Methanol	CH_3OH	65	99.8%	0.790	32.04	Merck
Ethanol	C_2H_5OH	78-79	Min99.8 Vol%	0.790	32.04	Merck
Ethanol	C_2H_5OH	78	96 Vol%	0.800	32.04	Birpa
2M1B	C_5H_{10}	38	97%	0.660	70.14	Fluka
2M2B	C_5H_{10}	38	95%	0.660	70.14	Merck
TAME	$C_6H_{14}O$	85-86	97 %	0.770	102.18	Merck
Isobutene	C_4H_8	-7	-	-	56.11	Ucar
TAA	$C_5H_{12}O$	102	99.5%	0.81	88.15	Merck

In the preparation of alternative catalysts in the etherification reactions, styrene and divinylbenzene (DVB) were used as the monomers. Styrene was stored in the refrigerator until use. A divinlybenzene isomer mixture (65% divinylbenzene isomers and 33% ethylvinylbenzene isomers, Merck A.G.) was treated with aqueous NaOH solution (5% w/v) to remove the inhibitor. Benzoyl peroxide (BPO, including 98% of the active compound, Merck A.G.) was selected as an initiator. N-heptane (>99%) from Merck was used as the diluent during polymerization. In the preparation of another catalyst, ammonium bisulfate powder from Merck was used instead of n-heptane. During sulfonation of crushed resin particles, chlorosulfonic acid from Merck was used. The properties of chemicals used in the synthesizing alternative catalysts were summarized in Table 4.2.

Table 4.2 Properties of Chemicals Used in the Preparation of Alternative Catalysts

Chemical	Chemical Formula	Boiling/ Melting Point (°C)	Purity (vol %)	Density (g/cm^3)	Molecular Weight (g/mol)	Source
Styrene	C_8H_8	145	99%	0.906	104.15	Merck
Divinylbenzene	$C_{10}H_{10}$	200	65%	0.914	130.19	Merck
Benzoyl peroxide	$C_{14}H_{10}O_4$	225-228	98%	0.470	242.23	Merck
n-heptane	C_7H_{16}	98.4	99%	0.680	100.21	Merck
Chlorosulfonic acid	$HClO_3S$	152	97%	1.75	116.52	Merck

4.2 Acidic Ion-exchange Resin Catalyst Used in the Experiments

Acidic macroreticular resin catalysts are the mostly adopted catalysts for the etherification reactive isoolefins, such as isobutylene, isoamylenes, etc., with methanol and ethanol. Polystyrene sulfonic acid resins cross-linked by divinlybenzene are known to show high activity and selectivity in these etherification reactions. These macroreticular ion-exchange resin catalysts are composed of gel-like microspheres bonded at the interfaces. The –SO$_3$H groups with strong proton donor-acceptor properties acted as the active sites. The -SO$_3$H groups attached to the polymer network are the active sites and 95% of these sites are reported to be present within the gel phase (Ancillotti and Fattora, 1998) forming a hydrogen bonded network. As alcohol molecules enter into the network of the hydrogen-bonded –SO$_3$H groups of such catalysts, swelling of the catalyst particles was observed. In the early work of Thornton and Gates (1974), it was shown that proton donor-acceptor tendencies of the network of –SO$_3$H groups were significantly stronger than those of the solvated acid groups. A typical macroreticular resin catalyst used in such etherification reactions is Amberlyst-15, commercially available from Sigma. Mercury

porosimeter analysis of Amberlyst-15 indicated a very narrow pore size distribution (Oktar et al. 1999a) with an average macropore radius of 2.28×10^{-8} m. Average micrograin diameter of Amberlyst-15 was reported as 8.2×10^{-8} m (Dogu et al., 2003) from SEM photographs, while the average radius of the resin particles was around 0.037 cm. Its properties are given in Table 4.5 in Diffuse Reflectance Infrared Fourier Transform (DRIFT) section.

4.3 Acidic Ion-Exchange Catalyst Preparation and Characterization

Sulfonated styrene-divinylbenzene cross-linked resin catalysts having different porosities and different hydrogen ion-exchange capacities were prepared in our laboratory. Another set of catalysts having different hydrogen ion-exchange capacities were prepared by heat treatment of commercial Amberlyst-15 at 220°C at different durations. Activities of these catalysts were compared with the activities of Amberlyst-15 in the etherification of 2M1B and 2M2B with ethanol. Major objective of this part was to search for a relation between the hydrogen ion-exchange capacities of such catalysts and their activities in the etherification reactions.

4.3.1. Heat Treated Amberlyst-15 Catalysts

Commercial Amberlyst-15 (Sigma) catalyst particles were heat treated at 220°C at different durations in a constant temperature oven. With such a heat treatment procedure, some of the $-SO_3H$ groups were expected to be removed from the catalyst structure, causing a decrease in hydrogen exchange capacity. Pore size distributions and surface areas of these catalysts were determined using mercury intrusion porosimetry (Quantachrome 60) and BET sorptometer (Micrometrics ASAP 2000). Hydrogen ion-exchange capacities of these catalysts

were evaluated following a direct titration procedure as described by Fisher and Kunin (1955). Details of the direct titration method are given in Appendix 4.1. Physical properties of the catalysts prepared by heat treatment of Amberlyst-15 will be discussed in Results and Discussion part.

4.3.2 Synthesized Acidic Resin Catalysts

A group of catalysts were synthesized by copolymerisation of styrene with divinylbenzene (DVB) which was the cross-linking agent. About 0.1 wt % benzoyl peroxide was used as the initiator during polymerisation. These polymers were then sulfonated according to the procedure reported in the literature (Thornton and Gates, 1974; Zundel, 1969). Amount of divinylbenzene in the solution was varied between 8-16 wt %. A set of catalysts were prepared by adding n-heptane as a diluent into the reaction medium to create pores of various sizes by removal of diluent from the gel after synthesis. Amount of diluent was varied between 50-70 vol%. In the preparation of another catalyst, ammonium bisulfate powder was used instead of n-heptane for the same purpose.

Polymerisation reaction proceeded for 7 days at 70°C and then samples were kept at 70°C for 5 days under vacuum for complete removal of the diluent from the structure. Cross-linker (divinyl benzene) concentration was varied between 8-16 wt % while polymerisation temperature and time were kept constant. Crushed resin particle were sulfonated by using chlorosulfonic acid. Sulfonation was carried out at different durations of time ranging between 5 to 72 h. Most of the sulfonation was carried out at 45°C. In some experiments, sulfonation temperature was varied between 23 and 90°C. A summary of experimental conditions used in the synthesis of these resin catalysts is given in Table 4.3. In the preparation of Catalyst M used in Diffuse Reflectance Infrared Fourier Transform (DRIFTS) experiments, 8% cross-linker (divinylbenzene) was

51

used and polymerisation was completed in 5 days, at 70°C. Then, it was kept at 90°C for 2 days. The chemical composition of this catalyst was quite similar to that of Amberlyst-15.

Table 4.3 Experimental conditions used in synthesis of resin catalysts

Catalyst	DVB Wt %	Diluent Vol %	Sulfonation Temperature, °C	Sulfonation time, h
Cat M	8	No diluent	45	72
2A	16	n-heptane, 50 vol %	45	72
7A	16	n-heptane, 70 vol %	45	72
14A	13	n-heptane, 70 vol %	45	72
12A	10	n-heptane, 70 vol %	45	72
13A	8	n-heptane, 70 vol %	45	72
23A	16	NH_4HSO_4	45	72
2A1	16	n-heptane, 50 vol %	23	5
2A2	16	n-heptane, 50 vol %	45	5
2A3	16	n-heptane, 50 vol %	60	5
2A4	16	n-heptane, 50 vol %	90	5

4.4 Testing Activities of Acidic Resin Catalysts: Etherification Reactions

Activities of all the synthesized catalysts and heat treated Amberlyst-15 catalysts were tested in the etherification reactions of 2M2B and 2M1B with ethanol in a liquid phase differential flow reactor. Different temperatures at constant initial concentration were studied throughout the experiments while the pressure was always constant as 8×10^{-5} Pa, to make sure that reaction takes place in liquid phase. A Gas Chromatograph was used for the determination of fractional conversion and reaction rates. Sample calculation is given in Appendix D.1.

4.4.1 Experimental Set-up

Etherification reactions were carried out using 2M2B and 2M1B with ethanol in a liquid phase differential flow reactor system shown in Figure 4.1 schematically.
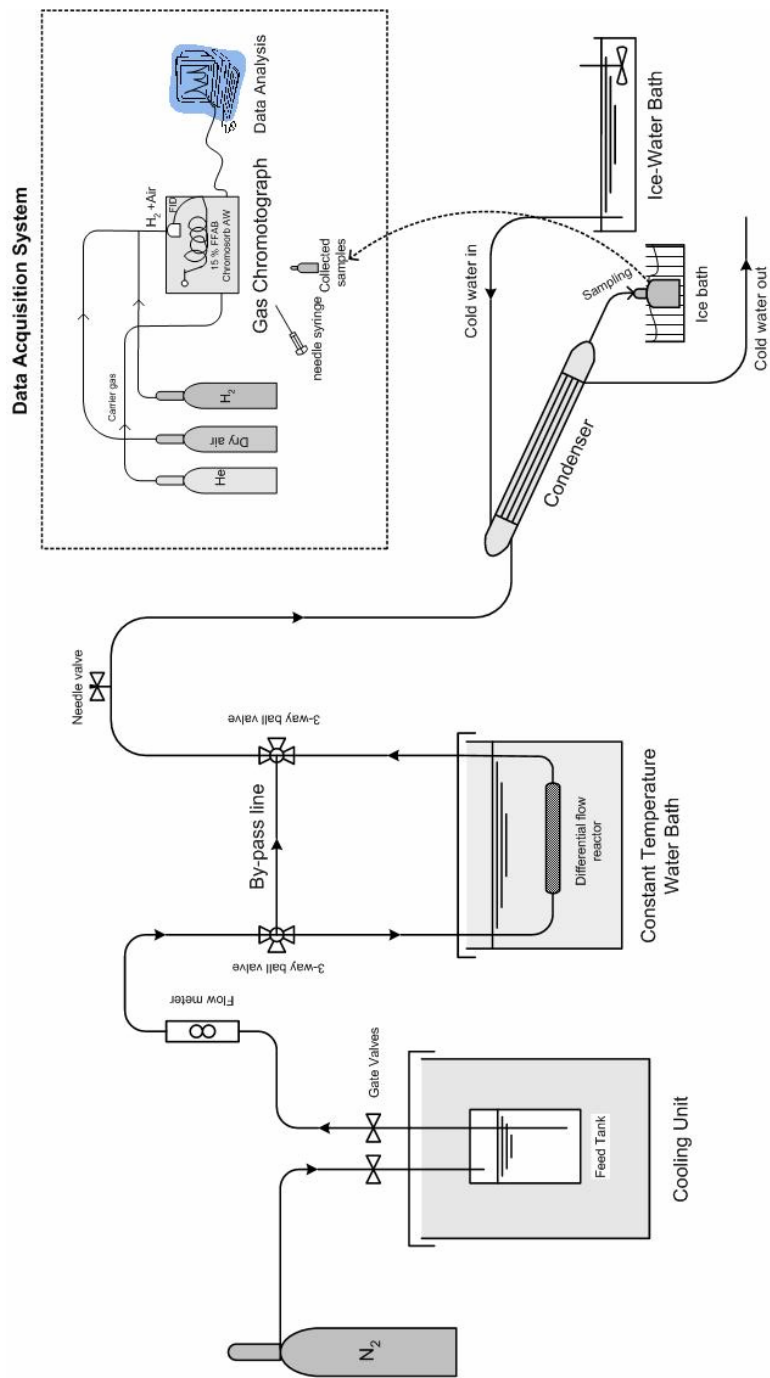
Figure 4.1 Schematic Representation of the Experimental Setup of Liquid Phase Differential Flow Reactor

These experiments were carried out in the presence of excess alcohol (2.7 mol % isoolefin in ethanol) in a temperature range of 333 – 370 K. Pre-dried catalyst particles (about 0.1 g) was placed into a stainless steel tube reactor of 0.46 cm in diameter and 19 cm in length. Catalyst bed was supported by quartz wool from both ends. The reactor was immersed into a constant temperature bath equipped with a temperature controller. The ethanol isoolefin mixture of known composition was put into the feed tank, which was pressurized by nitrogen gas. The flow rate of the reactant mixture was continuously monitored. This mixture was first entered the pre-heater section of the reactor. A bypass line allowed chemical analysis of the feed stream, when desired. The flow rate of the feed stream was 0.0158 cm^3/s.

The reactor effluent stream was passed through a jacketed cooler-condenser. The product was collected in the sample cups which were connected directly to the outlet of the cooler-condenser and immersed in an ice bath to eliminate any loss by evaporation.

4.4.2 Analytical Method

Chemical analysis of the samples from the outlet and inlet streams of the reactor were performed using a Varian Aerograph Gas Chromatograph (GC) equipped with a flame ionization detector (FID), and with a column packed with 15% FFAB on Chromosorb AW. About 5 µl of samples were directly injected to the GC by using a 5 µl Gas Chromatograph syringe.

The column was operated using Helium (He) as the carrier gas. At a constant carrier gas flow rate of 30 cc/min and at a constant column temperature of 100°C. Before starting to analyze the samples, the column was conditioned for 3 hours with the carrier gas. Dry air and hydrogen gases were

fed to system for FID at a flow rate of 300 cc/min and 30 cc/min, respectively. Injector and detector temperatures were also remained constant at 125 and 170°C, respectively. At these conditions, good separation of the reactants and product peaks were achieved.

With the data acquisition system connected to the chromatograph, the response peaks of the samples injected were analyzed with high precision. Before performing the experiments, for each component, chromatograph calibration factors (α) were evaluated which can be found in Appendix B. When the response peaks of experiments were obtained, using the calibration factors, the mole fraction or concentration of the components was found for each sample taken. By this way, the errors due to injection and the probable errors come from the detector were minimized.

In this study, the calibration factors for 2M2B, 2M1B and TAEE were calculated to obtain quantitative results from the Gas Chromatograph trace. The calibration factor of ethanol was taken as unity and the calibration factors of the other species were determined relative to ethanol.

Firstly, 2M2B-EtOH, 2M1B-EtOH, TAME-EtOH mixtures were prepared concerning the composition range of experiments and these mixtures were injected to the column at different amounts (1, 3, 5 µl) and calibration factors of each condition was calculated. According to the results, it is concluded that the differences in concentration and injection amount do not affect the value of calibration factor of those species.

The calibration factors of 2M1B, 2M2B, EtOH and TAEE found from the experiments was given in Table 4.4.

Table 4.4 Calibration Factors for Reactants and Products

Component	Calibration factor, α
2M1B	0.234
Ethanol, EtOH	1.000
Tert Amyl methyl Ether. TAEE	0.235
2M2B	0.237
Ethanol, EtOH	1.000
Tert Amyl methyl Ether. TAEE	0.277

4.5 Physical Properties of Acidic Resin Catalysts

In this study, pore size distributions and surface areas of these catalysts were determined using mercury intrusion porosimetry (Quantachrome 60) and BET sorptometer (Micrometrics ASAP 2000). Hydrogen ion-exchange capacities of these catalysts were evaluated following a direct titration procedure as described by Fisher and Kunin (1955).

In this method, approximately 5 g of resin is placed in a 1 L volumetric flask. A filter paper of medium porosity is used. The sample converted to the hydrogen form with 1 L of 1M HNO_3. The resin is rinsed free of excess acid and drained. A 1.0 g sample of the resin prepared above is precisely weighed into a dry 250 ml Erlenmeyer flask. The remaining sample is used to determine the moisture content by drying at 110°C overnight. Exactly 200 ml of 0.1 N NaOH in 5% (w/w) NaCl is added to the Erlenmeyer flask. The stoppered sample is allowed to stand overnight. Aliquots, 20 ml, of the supernatant liquid are back-titrated to the phenolphthalein end point with 0.1 N HCl. Hydrogen ion-exchange capacity value is calculated from the titer of the sodium hydroxide solution as milliequivalents (meq.) of exchangeable ion (H^+) per dry gram of resin. Hydrogen ion-exchange capacity is calculated by using Eqn.4.1.

$$\text{Hydrogen ion-exchange capacity} = \frac{(200 \text{x} \text{N}_{\text{NaOH}}) - 10 \text{x} (\text{ml.}_{\text{acid}} \text{x} \text{N}_{\text{Acid}})}{\text{samplewt.x} \dfrac{\%\text{Solid}}{100}} \qquad (4.1)$$

Sample calculation of porosimetry data and hydrogen ion-exchange capacity are given in Appendix D.2 and D.3, respectively.

4.6 Diffuse Reflectance Infrared Fourier Transform (DRIFT) Studies

DRIFT measurements using infrared radiation allow many intractable samples to be analyzed with little or no sample preparation. This technique is used mainly for powdered samples, but can also be used successfully for almost any matte surfaced sample such as paper or on cloth products.

In our case, the DRIFT experiments were performed in order to obtain detailed information about the adsorption of reactants (alcohols and isoolefins) and products (ethers) of the etherification reaction on acidic ion-exchange resin catalysts by characterizing the adsorbed species during reaction as well as with single adsorbing species.

4.6.1 Experimental Apparatus

The DRIFT experiments were performed both continuous and batch-wise, depending on the adsorbate. In both of the experiments, first, about 100 mg of pre-dried catalyst (at 90°C) was placed into the heated pan of the DRIFT environmental chamber (Graseby Specac) of the FT-IR instrument (Midac). Catalyst structure was not effected at this temperature. The selector collected total reflectance and the signal from the dedector was monitored on the computer as DRIFT Spectrum. A temperature controller was connected to the chamber in order to adjust the temperature of the chamber to a desired value. A water bath was also used to circulate cold water through the chamber.

An optical diagram of the diffuse reflectance accessory is shown in Figure 4.2. Two Flat mirrors M1 and M2 are used to pass the focused beam to spherical mirror M3. This mirror re-focuses the infrared radiation onto the surface of the sample. The scatter radiation is collected by a second spherical mirror M5 and passed onto the detector optics by flat mirrors M6 and M7. This type of optical geometry is very efficient in that a high percentage of the scattered radiation is collected and analyzed.

In the continuous experiments, adsorption (ethanol, methanol and isobutylene) and vapor phase reaction experiments (methanol-isobutylene and ethanol-isobutylene mixtures) were carried out in the flow reaction chamber (environmental chamber) of the diffuse reflectance FT-IR (DRIFT) cell. These experiments were carried out with Amberlyst-15 (Sigma) as well as with a polystyrene sulfonic acid resin catalyst (cross-linked by divinylbenzene) prepared in our laboratories (Catalyst M).
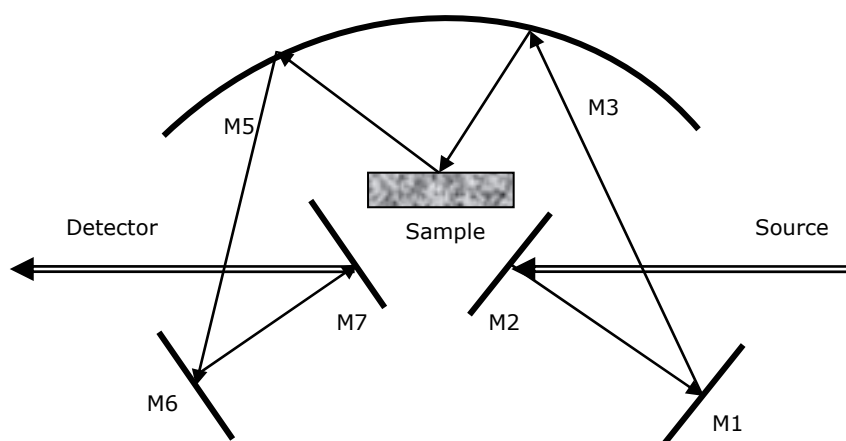
Figure 4.2 Optical diagram of the diffuse reflectance accessory (Nicolet Instrument Corp.)

The physical properties of the two catalysts used in this work are summarised in Table 4.5. Average gel-like micrograin dimensions were obtained

from SEM photographs. Pore size distributions were determined from mercury porosimetry. Catalyst M is also a copolymer of styrene and divinylbenzene sulfonated by chlorosulfonic acid. Details of the preparation of this catalyst were previously explained in Catalyst Preparation and Characterization section. As it was illustrated in our recent presentation (Oktar et al., 1999c), the activity of this catalyst was close to the activity of Amberlyst-15 for the etherification of isoamylenes at low temperatures. However, its activity was much less than Amberlyst-15 at higher temperatures (360 K). Hydrogen ion-exchange capacity (meq. H^+ per unit mass of the catalyst) of this catalyst is less than Amberlyst-15 and it is also less porous (Table 4.5). Consequently, pore diffusion resistance was expected to be more significant in Catalyst M than in Amberlyst-15.

Table 4.5 Physical Properties of the Acidic Resin Catalsysts (Dogu, et al., 2001)

	Amberlyst-15[b]	Catalyst M
surface area,[a] m^2/g (mercury porosimeter)	59.2	13.7
macroporosity,[a] ε_p	0.32	0.08
apparent density, g/cm^3	0.99	1.19
average micrograin diameter, m	8.2×10^{-8}	3.8×10^{-8}
total ion-exchange capacity, mequiv of H^+/g of dry material	5.2	2.9

[a] Surface area and macroporosity (ratio of macropore volume to total catalyst volume) values correspond to pores having diameters greater than 6.7×10^{-9} m.
[b] Oktar et al., 1999a

The adsorbing gas or the reactant mixture was swept by the carrier gas (usually nitrogen) into the reaction chamber. The total flow rate of this gas mixture was 45 ml/min in adsorption experiments and 65 ml/min in reaction experiments. The gas mixture was directly past over the upper surface of the catalyst layer. The pan containing the catalyst directly faces the zinc selenide window of the cell through which IR beam enters and the diffuse reflected beam

leaves. DRIFT spectra thus obtained contain significant information about the surface species during adsorption and reaction experiments. The distance between the catalyst layer and the window is about 7 mm. It was experimentally found out that contribution of the gas phase to the absorption bands of DRIFT spectra were negligibly small in our work. Also, the differences of the spectra obtained with and without the adsorbing/reacting gases were used to eliminate the contributions of the catalyst surface to the DRIFTS bands. Adsorption and reaction experiments were carried out in the temperature range of 313-353 K. In alcohol adsorption experiments, about 10% of the gas mixture constituted alcohols (methanol or ethanol). However, in adsorption of isobutylene higher concentration of hydrocarbon (33% isobutylene in nitrogen) was used considering smaller adsorption equilibrium constants of iso-olefins than alcohols on such resin catalysts (Oktar et al., 1999b). In reaction experiments, the inlet gas mixture contained 30% isobutylene and 7.5% alcohol in nitrogen.

Some of the DRIFT experiments were carried out batchwise by injecting a pulse of tracer (TAME, 2M1B and methanol-2M1B mixture) into the chamber, which was filled with nitrogen gas. Both the inlet and the outlet valves of the chamber were closed to isolate the system.

4.6.2 Analytical Method

Light reflected from a solid surface can be either diffuse, or specular, or both (total reflectance). With the development of diffuse reflectance accessories, diffuse reflectance technique is increasingly becoming the method of choice for analyzing most of the solid samples.

Diffuse reflectance technique was used together with a MIDAC-M Series Fourier Transform Infrared Transform (FT-IR) Spectrometer to acquire complete,

high-resolution spectra. The specifications of the spectrometer can be found in Table 4.6. The diffuse reflectance system (GRASEBY SPECAC, P/N 19930 Series) contained the following parts: In the environmental chamber, the solid samples that had been placed can be analyzed at elevated temperatures up to 500°C and pressures from vacuum to 500 psi. It had a Zinc Selenide window, which gave a good balance between wide mid-IR transmission and mechanical strength. The Selector selectivity collected the total reflectance (diffuse or specular) using its optically optimized off-axis configuration. The Temperature Control Unit was connected to the chamber for controlling the set temperature value.

The operating of the spectrometer was done with a software program called Lab Calc^{TM}. Operating software resides on a hard disk, and data was displayed on monitor. Before taking the spectra, the resolution was set to 2 cm^{-1}, Scan value was set to 1000, and Gain value was set to 4.

Table 4.6 MIDAC M Series FT-IR Spectometer Specifications

Resolution	Step selectable, from 32 cm^{-1} to 2, 1, or 0.5 cm^{-1}
Spectral Range	400 – 6000 cm^{-1} (standard KBr optics)
Accuracy	> 0.01 cm^{-1}
Scan rate	0.125 cm/sec
Infrared Beam	6.4 cm above sample compartment floor, Diameter 0.5 cm at sample
Source	1350 K or 1550 K, air cooled

4.6.3 Experimental Procedure

When FT-IR was turned on, it was waited for 3 hours in order to stabilize it. Before the experiments, the water bath turned on and water flow rate was set to 50 ml/min. For the continuous FT-IR experiments, the chamber was filled with catalyst particles, closed tightly with 8 screws and nitrogen gas together with the adsorbing chemicals (ethanol, methanol, isobutene, or mixture of ethanol-

isobutene and methanol-isobutene) were sent to the chamber. For the batch FT-IR experiments, before closing the chamber, 0.1 ml of one of the adsorbing chemicals (TAME, 2M1B or mixture of methanol-2M1B) was injected to the chamber, on the catalyst particles. The temperature controller was opened and the set value of the temperature is given.

Before taking the spectrum of the catalyst and the adsorbing species, a reference spectrum was taken at every start-up with pure Amberlyst-15 particles and Catalyst M (together with nitrogen gas) by adjusting the type of scan to "reference" in the software program. Before starting to take the spectra, it was waited for 10 minutes so that all the catalyst particles in the chamber were saturated with the gas sent. Then, by adjusting the type of scan to "adsorbance", the actual experimental spectrum was taken.

4.6.4 Data Treatment in DRIFT Studies

The spectra that were collected at many different conditions were analyzed first by using NIST Chemistry Web Book, 1998. Using this Standard Reference Database, a qualitative analysis could be made for each adsorbate-catalyst pair. Then, using the Lab Calc^{TM} software, the areas under the peaks of the spectra were calculated from which quantitative analysis was done.

4.7 TAME and TAEE Production in a Batch Reflux Recycle Reactor

In this study, production of higher ethers (TAME and TAEE) was investigated using isoamylenes-methanol and isoamylenes-ethanol, in the batch Reflux-Recycle-Reactor where Amberlyst-15 was used as the catalyst. The main idea was to propose such a reactor system is that due to lower vapor pressures of product ethers than the reactants, vapor phase reactor inlet stream is always rich in reactants, in this Reflux-Recycle reactor.

4.7.1 Experimental Set-up

The batch Reflux-Recycle-Reactor proposed in this work is composed of three parts, namely a reboiler, vertical vapor phase catalytic reactor section and a condenser used for the liquifaction of reactor effluent stream shown in Figure 4.3. This reactors was constructed by the modification of an available batch distillation apparatus (Armfield Limited UAP 3a). Reactant mixture, which was fed to the boiler, was vaporised into the reactor section and reactor outlet stream was condensed and recycled back to the boiler. In this work, the system was operated batchwise, however it might also be modified for continuous operation. Due to lower vapor pressures of tertiary ethers (TAME and TAEE) than both C_5 reactive olefins and alcohols, vapor phase inlet stream composition of the reactor section was always rich in reactants. Due to short contact times of the reactants with the catalyst (usually a few seconds in our case) very high selectivities could be achieved. Sample calculation of the contact times can be found in details in Appendix D.4.

In the present study, 7 liters of reactant mixture was fed to the boiler. Reactor section was 5 cm in diameter and 36 cm in length containing 60 g of catalyst. Amberlyst-15 acidic resin catalyst particles were packed into small baskets, each containing about 1 g of catalyst. These baskets were uniformly distributed along the column by placing them over 8 perforated plates which were equally spaced (7.5 gr Amberlyst-15/plate). The reboiler, having a volume of 20 liter, was manufactured from corrosion resistant stainless steel and incorporated two electrically heated cartridge type heating elements. Power to the heaters might be continuously varied using a regulator and directly read from the wattmeter calibrated from 0-2 kW.
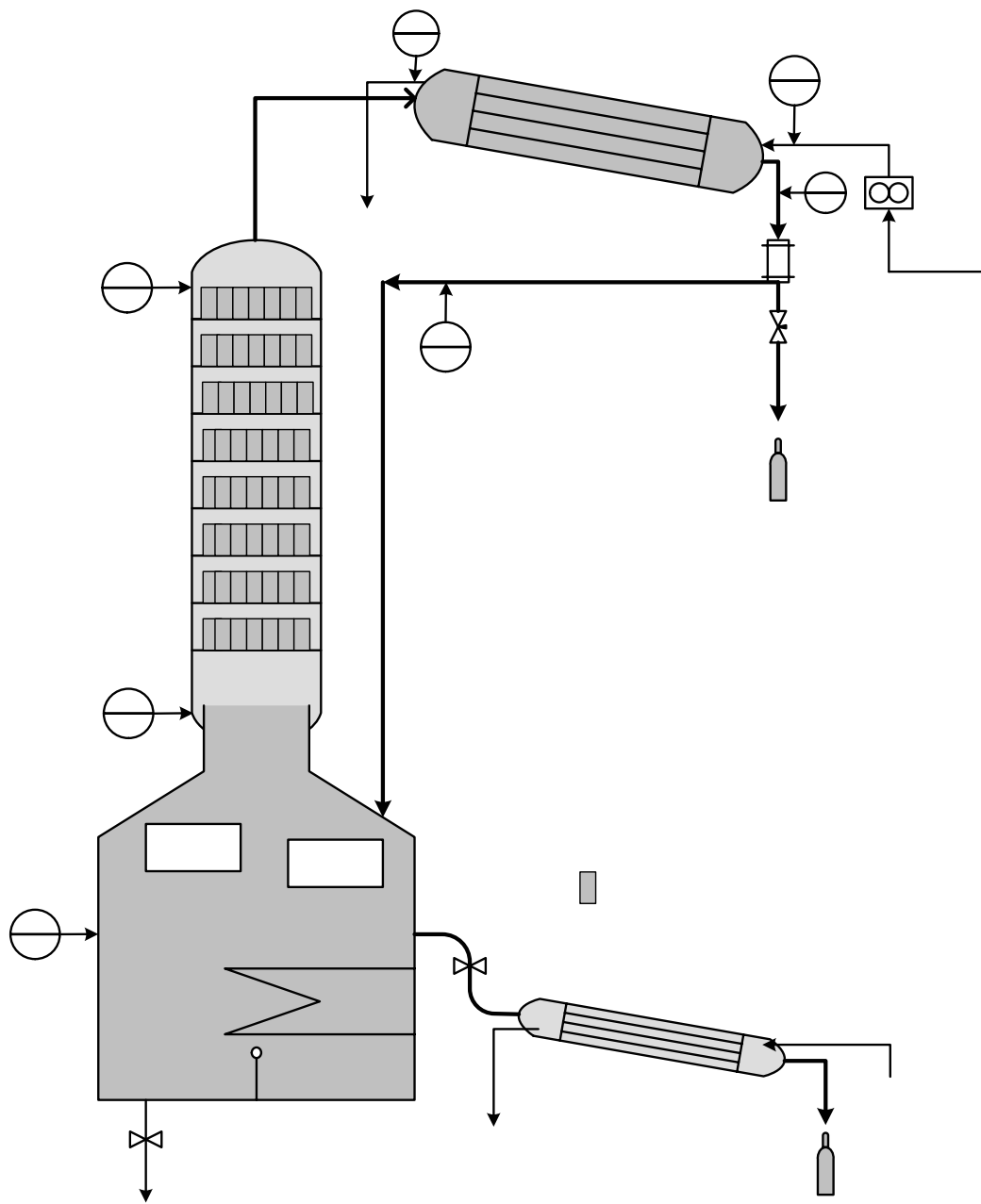
Figure 4.3 Schematic diagram of the experimental set up of the batch T3
Reflux-Recycle-Reactor

At the initial stage of the experimental period, it was set as 1.2 kW, but
after the start of the boiling this value was decreased to control the temperature

of the reboiler easily and to prevent the formation of flooding. A level sensor situated on the top of the feed tank protected the heating elements from overheating. The lower volume limit to be used during the experiment was 5.5 liter and below this value, the controller shut down the system. In our experiments, batch reflux recycle reactor was used indeed system can be operated as a batch and continuous reactive distillation column. The mixture of reactants were prepared in a different container and then poured into the reboiler before starting the process.

Temperatures were measured by 7 thermocouples located at different position on the apparatus (Figure 4.3). Two of them were at the top (T3) and the bottom (T2) of the column. Unfortunately, there were not any thermocouples placed along the column to measure temperatures of each plate. The inlet and outlet temperatures of the cooling water used in condenser (T6 & T7 respectively); the temperatures of the reflux (T5), the condensate (T4) and the reboiler (T1) were also measured by the other thermocouples. In this system, different reflux ratio values could be manually set using two electronic timers, which proportion to the position of the reflux divider. For our experiments, the reflux ratio control was set for total reflux.

The samples were taken from the reflux and the reboiler. A needle valve was used in the reflux section in order to prevent escaping more vapors while taking sample since this situation resulted in a decrease in the pressure of the column. Also, this valve allowed controlling the sample amount, easily, since the pressure inside the column was very high and this pressure resulted to spurt out liquid while taking samples.

Vapor from the top of the column passed to a water-cooled condenser. The volumetric flow rate of cooling water was adjusted by a flow meter. After the

reflux started, the inside pressure of the column could be adjusted by changing the volumetric flow rate of the cooling water. As the volumetric flow rate of cooling water increased, the heat transfer increased and more vapors condensed. This caused decrease in the column pressure. Another condenser was connected to the reboiler valve. Since the temperature of the reboiler was very high comparing to the room temperature, it was necessary to use this condenser to prevent evaporation of the components especially the more volatile ones in the liquid sample. The reboiler, the condenser, and the column was insulated to prevent any heat loses, especially in wintertime.

4.7.2 Experimental Procedure

Experiments were carried out with both methanol-2M2B and ethanol-2M2B mixtures. Experiments were repeated with different feed compositions between 4.6–25 mole % 2M2B in alcohol and also at different boiler temperatures ranging between 72°-104 °C. The reactor section was well insulated. Experiments indicated that temperature variation along the reactor was negligibly small (less than 1°C). The boiler temperature was about 1°C higher than the reactor inlet temperature. In all these experiments, mean residence time of reactants in the reactor section was in the order of magnitude of 5 s, with some variation from experiment to experiment. Physical and chemical properties of the catalyst used (Amberlyst-15) were reported in Table 4.5. Before starting the experiment, Amberlyst-15 particles were dried in a vacuum at 95°C overnight to remove moisture.

Operation of the batch Reflux-Recycle-Reactor proposed in this work involves two distinct time periods. In the first heat-up period, the feed mixture charged to the reboiler was heated to the desired temperature and then heating was continued until condensation of the vapor stream was observed in the

condenser at the exit of the reactor section. It took about 15 minutes (with some variation from experiment to experiment depending upon the composition of the feed mixture) to reach the desired temperature in the reboiler. However, formation of condensate in the condenser was observed about 40 minutes after the start-up of the heating period. During this initial heat-up period, the vapor stream was expected to heat-up the reactor section and condense. Condensed stream within the reactor was refluxed back to the reboiler. Of course, some conversion of the reactants to the product was also observed within the reactor section during this heat-up period.

The second period of the operation of the batch Reflux-Recycle-Reactor proposed in this work started after condensation was observed in the condenser at the exit of the reactor section. In this second time period, temperature was almost constant along the reactor. In this period, the desired reboiler temperature was kept constant by regulating heat input to the reboiler and also by adjusting the flow rate of cooling water used in the condenser. After steady isothermal temperature was reached, heat input to the reboiler was majorly used up for the latent heat of vaporization of the mixture. Our calculations, basing on the heat input to the reboiler, heat taken by the cooling water in the condenser and also basing on the compositions of the condensate and reboiler mixtures, showed that the vapor stream composition in the reactor, was close to the dew point along the reactor. Also, vapor stream flow rates at the inlet and outlet of the reactor section were very close to each other in this second period of the operation. In this period, very little condensation is expected in the reactor section, especially at later times. Some condensation of the product, which has much less volatility than the reactants, is possible within the reactor section at the initial times of the second period. Consequently, in the second period the reactor section may be assumed as a vapor phase reactor.

4.7.3 Analytical Method

Variations of chemical compositions of the mixture in the reboiler and also in the condensed stream which was recycled to the reboiler, were determined by the chemical analysis of samples taken from the reboiler and from the recycle stream, at different times. For this purpose, a gas chromatograph (Varian) equipped with an FID detector, and with a column packed with 15% FFAB on Chromosorb AW was used. Closed sample tubes were kept in an ice-box before gas chromatographic analysis in order not to have any change in the composition due to evaporation.

The samples taken from the reflux and the reboiler were injected to the Varian Aeograph Gas Chromatograph (GC) with a 5 µl Gas Chromatograph syringe. The same GC operating conditions were used previously described in section 4.4.

Three sets of calibration factors calculated in this section depending on components were given in Table 4.7. Details of the calculation were given in Appendix B.

Table 4.7 Calibration Factors for Reactants and Products

Component	Calibration factor, α
2M2B (95 %)	0.256
Ethanol, EtOH (99.8 %)	1.000
Tert Amyl methyl Ether. TAEE	0.318
2M2B (95 %)	0.250
Ethanol, EtOH (%95)	1.000
Tert Amyl methyl Ether. TAEE	0.301
2M2B (95 %)	0.108
methanol, MeOH	1.000
Tert Amyl methyl Ether. TAME	0.136

CHAPTER 5

RESULTS AND DISCUSSIONS

5.1 Effect of Hydrogen ion-exchange capacity on activity of resin catalysts

5.1.1 Heat Treated Amberlyst-15 Catalysts

As it is seen in Table 5.1, significant decrease of hydrogen ion-exchange capacity of Amberlyst-15 was observed with an increase in duration of heat treatment. From macroscopic analysis some shrinking of catalyst particles was also observed. Average macropore diameters, evaluated from the mercury porosimetry, did not show a significant change with heat treatment, however, some increase in porosity was observed. Mercury porosimetry data correspond to pores having diameters greater than 6.7×10^{-9} m.

Table 5.1 Physical properties and hydrogen ion-exchange capacities of heat treated Amberlyst-15 catalysts

Catalyst	Duration of Heat Treatment at 220°C, h	Hydrogen Ion-exchange Capacity, meq. H^+/g.cat.	Porosity ε_a	Average Macropore Diameter, (*) m	Nitrogen Adsorption Surface Area, m^2/g	Average Particle Diameter, m
Amb-15	0	5.1	0.32	2.28×10^{-8}	39.2	7.4×10^{-4}
Amb-15-1	4	3.4	0.39	2.28×10^{-8}	45.0	6.8×10^{-4}
Amb-15-2	24	2.8	0.37	2.37×10^{-8}	48.0	6.6×10^{-4}
Amb-15-3	48	2.7	0.42	2.11×10^{-8}	51.0	6.2×10^{-4}

*Evaluated from mercury porosimeter data.

The differential pore size distributions of catalyst particles which were heat treated at different times (Figure 5.1) also showed that macropore structure of Amberlyst-15 was not significantly altered by the heat treatment procedure used in this work. Pore size distribution became somewhat wider by heat treatment. However, some increase of nitrogen adsorption surface area was observed by heat treatment of Amberlyst-15. This indicated the formation of some micropores (having diameters smaller than 6.7×10^{-9} m), probably within the gel-like micrograins of Amberlyst-15, as a result of heat treatment procedure. Formation of some pores in the pore diameter range of 1×10^{-8} m was also observed in pore size distribution curves (Figure 5.1) by heat treatment.
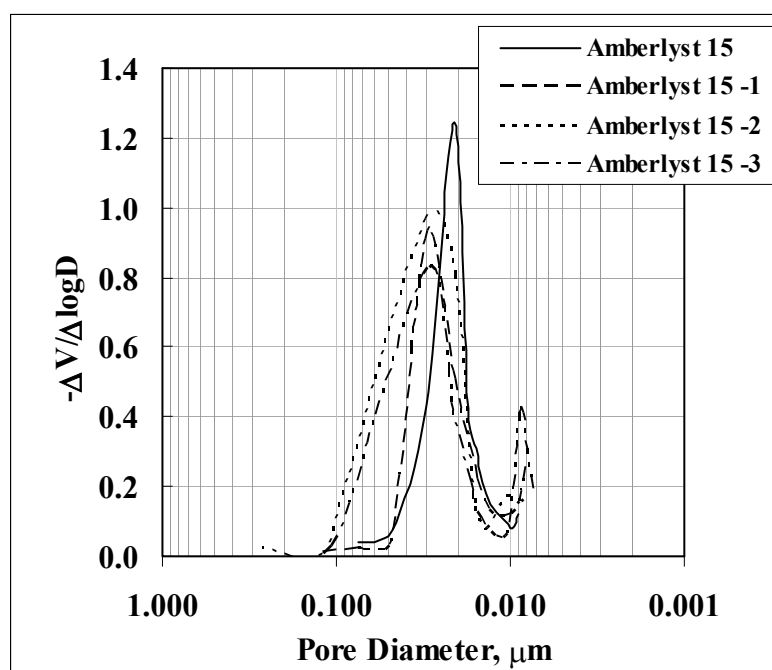
Figure 5.1 Differential pore size distributions of Amberlyst-15 and heat treated Amberlyst-15 catalysts

5.1.2 Synthesized Acidic Resin Catalysts

Physical properties and hydrogen ion-exchange capacities of the synthesized acidic resin catalysts are summarized in Table 5.2. All these synthesized resin catalysts had lower porosities and lower surface areas than

Amberlyst-15. They do not have uniform particle size. From macroscopic analysis, the average particle diameter of these crushed particles was found to be as 6.4×10^{-4} m with a particle size between $(3.3-7.5) \times 10^{-4}$ m. Comparison of hydrogen ion-exchange capacities of catalyst 2A2 and 2A showed that with an increase of sulfonation time from 5 h to 72 h hydrogen ion-exchange capacity increased from 2 meq.H^+/g to 2.8 meq.H^+/g. In fact, catalyst 2A had the highest hydrogen ion-exchange capacity among all the other synthesized catalysts.

Table 5.2 Physical properties and hydrogen ion-exchange capacities of synthesized resin catalysts

Catalyst	Hydrogen Ion-exchange Capacity, meq.H^+/g.cat.	Porosity, ε_a	Average Pore Diameter $\times 10^8$, m	Nitrogen Adsorption Surface Area, m^2/g
2A	2.8	0.13	1.20	15
7A	1.3	0.11	1.30	14
14A	2.0	0.08	0.84	14
12A	2.3	0.09	0.95	15
13A	1.6	0.08	0.81	25
23A	1.7	0.08	0.78	30
2A1	1.9	0.23	2.30	12
2A2	2.0	0.16	2.30	14
2A3	1.8	0.16	1.80	15
2A4	2.0	0.19	3.70	16

Comparison of hydrogen ion-exchange capacities of catalysts 2A1, 2A2, 2A3 and 2A4 indicated that sulfonation temperature did not cause a significant change on hydrogen ion-exchange capacity. The pore size distributions of these catalysts were not also quite different from each other (Figure 5.2). As it was shown in this figure, in addition to the pores in the range of $10^{-7}-10^{-8}$ m, some larger pores having diameters in the range of 10^{-5} m were also observed in these catalysts. An increasing trend was observed in the average macropore diameter of the catalysts with an increase in DVB weight percentages (Table 5.2). In this

evaluate average macropore diameter values were determined from mercury porosimeter data assuming monodisperse pore size distribution.
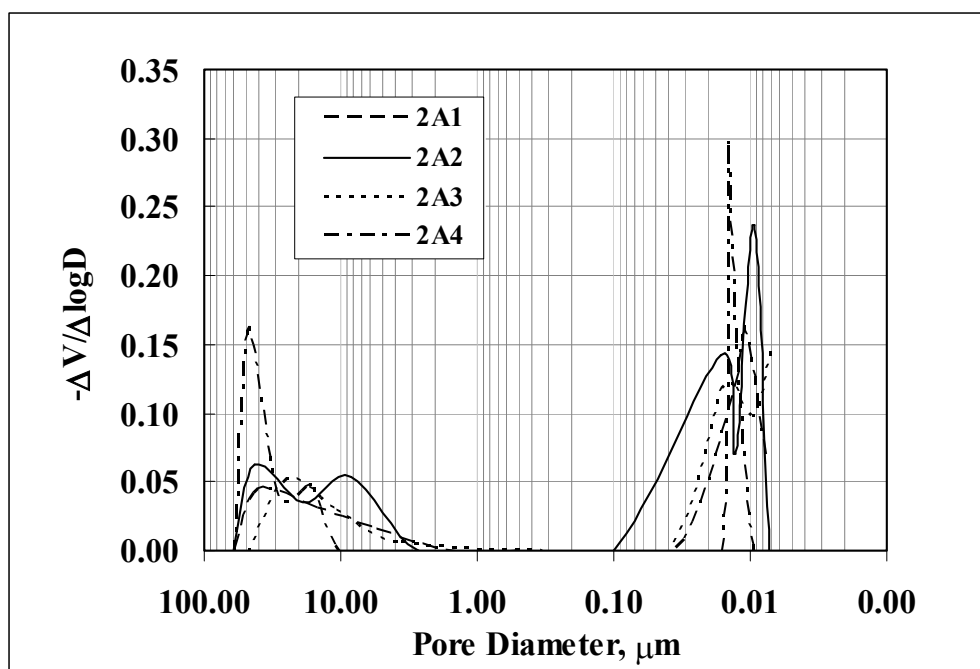
Figure 5.2 Differential pore size distributions of resins catalysts sulfonated at different temperatures

5.1.3 Etherification Reactions

Most important factor, affecting the activity of acidic ion ion-exchange resin catalysts, is the hydrogen ion-exchange capacity. Differences in pore structure of these catalysts might also have some effect on the diffusion resistance and active surface area.

The ion-exchange capacities of the heat treated Amberlyst-15 and the synthesized resin catalysts ranged between 1.3 meq.H^+/g and 5.1 meq.H^+/g. Synthesis of TAEE from 2M2B and 2M1B using all these catalysts was investigated in a fixed bed flow reactor in a temperature range between 333 and 370 K. Fractional conversion values of 2M2B and 2M1B to TAEE are reported in Figures 5.3 and 5.4, respectively.
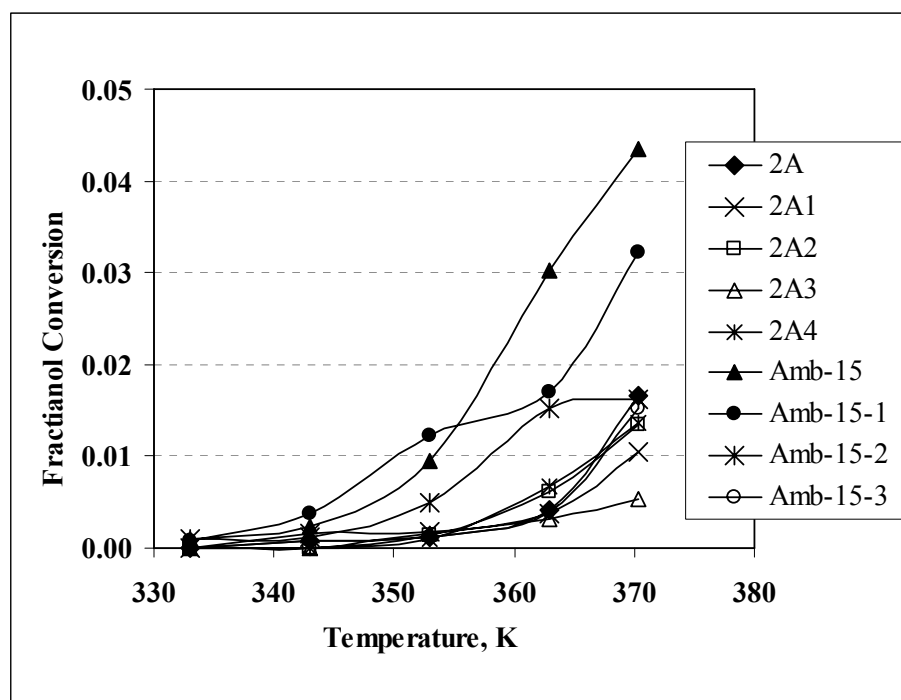
Figure 5.3 Fractional conversions of 2M2B to TAEE using different catalysts in a differential reactor (Inlet concentrations: 2M2B: 2.7 mol%, Ethanol: 97.3 mol%)
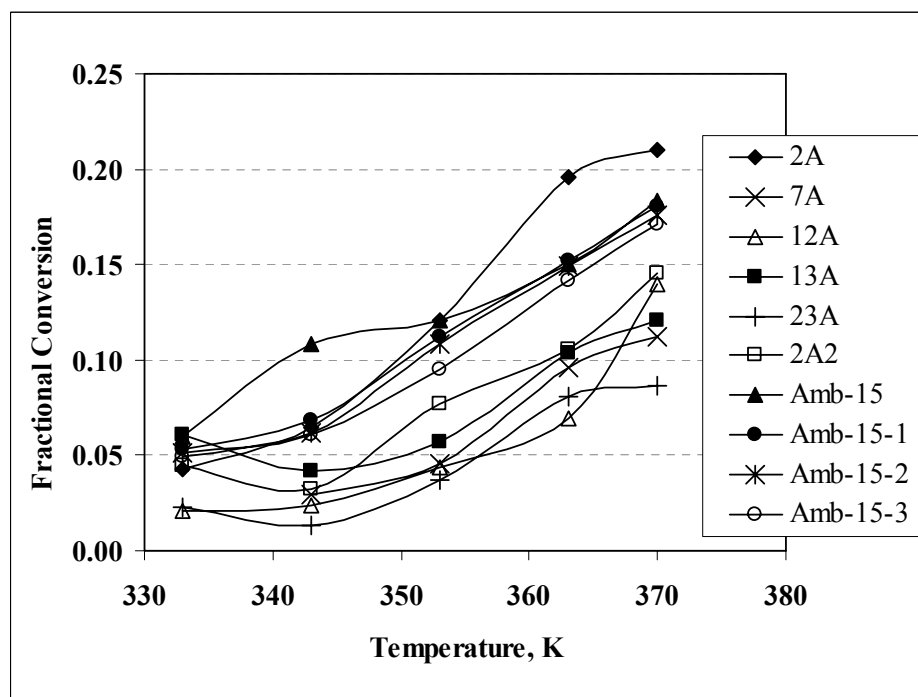
Figure 5.4 Fractional conversions of 2M1B to TAEE using different catalysts in a differential reactor (Inlet concentrations: 2M1B: 2.7 mol%, Ethanol: 97.3 mol%)

There might be some isomerization reaction between 2M1B and 2M2B parallel to the formation of TAEE. However, the conversion values reported in Figures 5.3 and 5.4 correspond to the moles of TAEE produced per mole of isoamylene (2M1B or 2M2B) fed to the reactor. Each point given in these figures actually corresponds to the average of seven data points obtained at the same conditions. The results of repetitive experiments were quite reproducible. Due to differences in structures of different catalysts, some scatter was observed in conversion vs. hydrogen ion-exchange capacity curves. Fractional conversion values of 2M2B were found to be less than 0.045 even at the highest temperatures (370 K) in this fixed bed reactor. However, for 2M1B, fractional conversion values reaching to 0.2 were obtained at the same operating conditions. These results are consistent with the results reported in our recent publication (Oktar et al., 1999a) indicating that 2M1B was much more reactive than 2M2B. In the case of using 2M2B as the reactant, Amberlyst-15 showed the highest activity. Among the synthesized catalysts, 2A gave the highest activity, which had a hydrogen ion-exchange capacity of 2.8 meq.H$^+$/g cat. The activity of this catalyst was found to be even higher than Amberlyst-15 in the etherification of 2M1B to TAEE at 370 K.

Dependence of fractional conversion values of 2M2B and 2M1B to hydrogen ion-exchange capacities of the catalysts obtained at 370 K are illustrated in Figures 5.5 and 5.6, respectively. In these figures, results obtained with heat treated Amberlyst-15 and synthesized acidic resin catalysts were presented together. As it has been shown in Figure 5.5, there is a direct relation between the conversion values and hydrogen ion-exchange capacity of the catalyst, in reaction of 2M2B with ethanol. This relation is close to linear. Amberlyst-15, which had the highest hydrogen ion ion-exchange capacity, also showed the highest activity. However, for the conversion of 2M1B to TAEE, a quite different dependence of conversion to hydrogen ion-exchange capacity of

the catalyst was observed (Figure 5.6). The increasing trend of fractional conversion of 2M1B with hydrogen ion-exchange capacity of the catalysts was observed until a hydrogen ion-exchange capacity of about 2.8 meq.H$^+$/g.
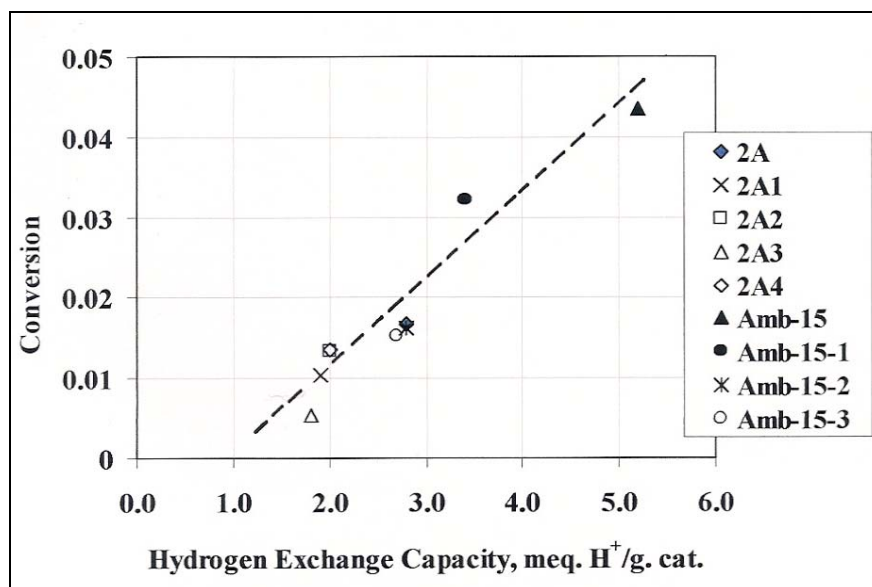
Figure 5.5 Conversion of 2M2B to TAEE at 370 K (Inlet concentrations: 2M2B: 2.7 mol %, Ethanol: 97.3 mol %)
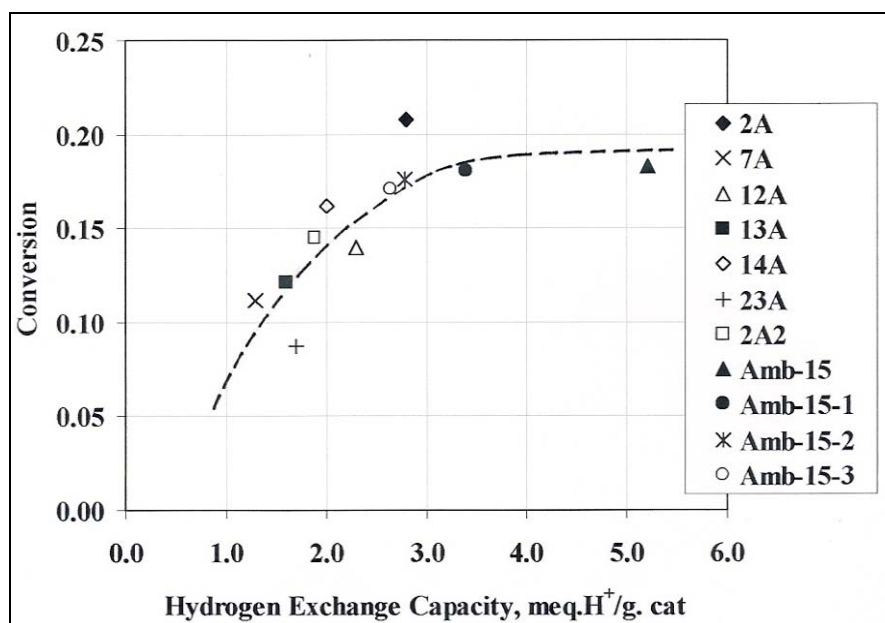
Figure 5.6 Conversion of 2M1B to TAEE at 370 K (Inlet concentrations: 2M1B: 2.7 mol %, Ethanol: 97.3 mol %)

At higher hydrogen ion-exchange capacities, no further increase was observed in the reaction rate. Reactivity of 2M1B was much higher than reactivity of 2M2B. At high surface reaction rates, effects of diffusional resistances on the observed rate were also expected to be more significant. Much less dependence of activity of the catalysts on hydrogen ion-exchange capacity, which was observed in TAEE synthesis from 2M1B at hydrogen ion ion-exchange capacities higher than 2.8 meq.H^+/g, was probably due to the increased significance of diffusion resistance on the observed rate for this reactant. Another possible effect of decrease in hydrogen ion-exchange capacity may be the increase of the distance between the active sites ($-SO_3H$ groups) at the catalyst. This orientation variation of active sites may have a strong influence on the activity since, as it was discussed in Section 5.3, more than one active sites are involved in the reaction mechanism. These results showed that further increase of hydrogen ion ion-exchange capacity of the catalyst over 2.8 meq.H^+/g did not cause any advantage in the formation of TAEE from 2M1B.

The apparent activation energy values of the reaction between isoamylenes and ethanol were evaluated from the data reported in Figures 5 and 6, using both integral and differential methods. As it was reported in the literature, at low concentrations of isoamylenes (excess alcohol) and at low conversions, the reaction rate between isoamylenes and ethanol may be assumed as first order with respect to isoamylene concentration and zero order with respect to alcohol concentration (Tejero et al., 1996; Piccoli and Lovisi, 1995). For this case, the relation between fractional conversion of isoamylene and space time in the reactor (τ) can be expressed as,

$$- \ln(1 - X_{Af}) = k\tau \qquad (5.1)$$

In our experimental work, ethanol is always in excess and fractional conversion values are all less than 0.2. Consequently, Eqn. 5.1 can be used to predict the apparent rate constant k. Space time in the reactor is about 10 seconds. Temperature dependences of apparent rate constants for the reaction of 2M1B and 2M2B with ethanol are shown in Figures 5.7 and 5.8, respectively.
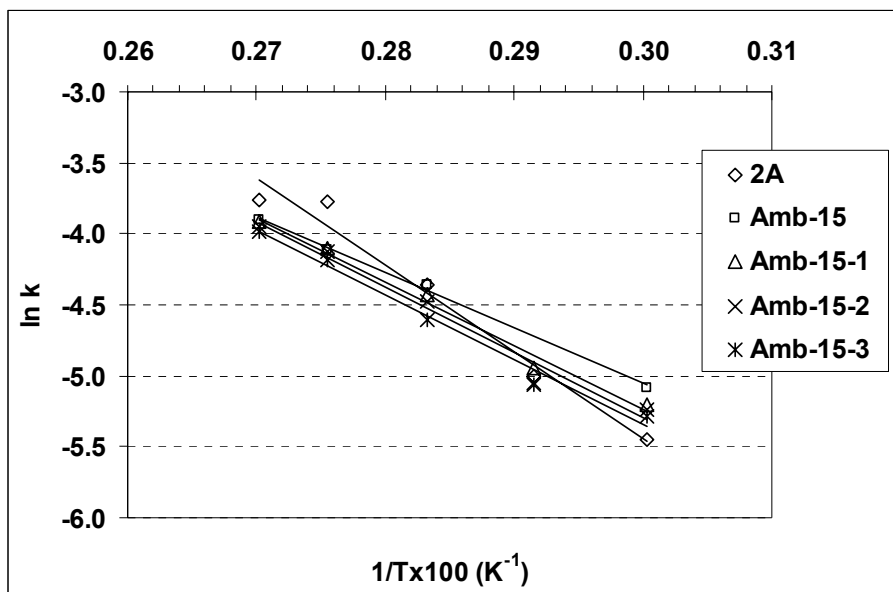
Figure 5.7 Temperature dependence of apparent rate constant of 2M1B+ethanol reaction
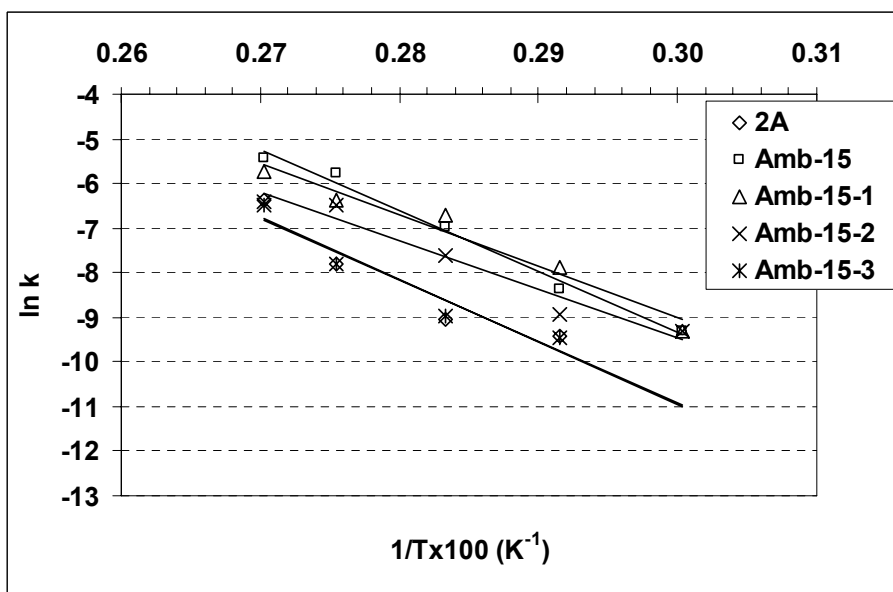
Figure 5.8 Temperature dependence of apparent rate constant of 2M2B+ethanol reaction

The apparent activation energies evaluated from these figures for catalysts Amb-15, Amb-15-1, Amb-15-2, Amb-15-3 and 2A, are reported in Table 5.3.

Table 5.3 Apparent activation energy values evaluated from integral and differential analysis

Catalyst	2M2B+ethanol reaction Ea (kJ/mol)		2M1B+ethanol reaction Ea (kJ/mol)	
	Integral Method	Differential Method	Integral Method	Differential method
2A	117	118	51	48
Amb-15	114	112	33	31
Amb-15-1	96	97	37	38
Amb-15-2	91	91	38	36
Amb-15-3	114	114	38	36

The apparent activation energies were also evaluated from the initial rate values obtained by differential analysis of the data reported in Figures 5.5 and 5.6. In the case of 2M2B+ethanol reaction, conversion values were all smaller than 5% and initial rate analysis was justified. However, in the case of 2M1B+ethanol reaction, conversion values are higher and consequently some error may be expected in the prediction of apparent rates from differential analysis. The activation energy values evaluated from the differential analysis are also reported in Table 5.3. As it is seen in this table, the apparent activation energy values evaluated from the integral and differential methods are very close to each other.

For the reaction of 2M2B with ethanol, apparent activation energy values obtained with Amberlyst-15, heat treated Amberlyst-15 catalysts and synthesized 2A catalyst are all in the range of 91 – 118 kJ/mol. These values are in good agreement with the values reported in the literature (Linnekoski et al., 1997; Paakkonen and Krause, 2003; Rihko and Krause, 1995), where

activation energy values ranging between 93-108 kJ/mol have been reported for the production to TAEE and TAME from 2M2B. Our results showed that activation energy of the reaction did not change much by heat treatment of Amberlyst-15. As a results of heat treatment, some of the −SO$_3$H groups were removed from the catalyst structure causing a decrease in hydrogen ion-exchange capacity but not the activation energy. Decrease of activity of the catalyst as a result of decrease of hydrogen ion-exchange capacity is probably due to decrease of pre-exponential factor of the rate constant which strongly depends upon the number of active sites per gram of catalyst.

The activation energy values evaluated for the reaction of 2M1B with ethanol were much lower than the corresponding values obtained for 2M2B+ethanol reaction. Apparent activation energy values evaluated for Amberlyst-15 and heat treated Amberlyst-15 catalysts are in the range of 33-38 kJ/mol. For the synthesized catalyst 2A, activation energy is 51 kJ/mol. In the literature, a wide range of activation energy values were reported for the reaction of 2M1B with ethanol and methanol. Linnekoski et al. (1997) reported an activation energy value of 90 kJ/mol for TAEE synthesis. In our previous work, an apparent activation energy value of 40.7 kj/mol was reported (Oktar et al., 1999a). In the case of TAME production from 2M1B, activation energy values ranging between 72-95 kJ/mol were reported (Oost and Hoffmann, 1995; Paakkonen and Krause, 2003; Rihko and Krause, 1995). The lower values of apparent activation energies evaluated in our work for 2M1B+ethanol reaction could be partly due to the presence of pore diffusion resistance for this reaction.

5.1.4 Testing of Diffusion Effect on Observed Rates with Amberlyst-15

As it was discussed in our earlier publications (Oktar et al., 1999a and 1999b) that, macropore diffusion resistance was expected to be much more significant than the diffusion resistance in the gel-like micrograins in liquid phase

etherification reactions in the production of TAME and TAEE. The criterion proposed by Doğu and Doğu (1980) (Appendix E.1) was used to test the significance of diffusion resistances on the observed rates obtained in this work. According to this criterion, the following relation should be satisfied for negligible diffusional effects.

$$\left(\frac{(R_A \rho_p)R_o^2}{C_{Ao}D_a} \right)(1 + G) << \frac{3}{4} \tag{5.2}$$

Here, G corresponds to the ratio of diffusion times in the micrograins and macropores,

$$G = \left(\frac{r_o}{R_o} \right)^2 \frac{D_a}{D_i(1 - \varepsilon_a)}. \tag{5.3}$$

The value of effective diffusion coefficients of 2M2B in the macropores may be estimated from the data reported in our recent publication (Dogu et al., 2003). For this catalyst effective diffusivity may be predicted from,

$$D_a = D_M \frac{\varepsilon}{\tau} + \frac{1}{\tau}(\rho_p K)D_s \tag{5.4}$$

The first and second terms on the right hand side of Eqn.5.4 correspond to pore and surface diffusion, respectively. The value of D_M was estimated from the Wilke-Chang model as 1.3×10^{-4} cm^2/s at 370 K. The tortuosity factor was estimated from the well known Wakao and Smith model as $\tau = 1/\varepsilon_a = 3.1$. Using the data reported by Dogu et al. (2003) for D_s and apparent adsorption equilibrium parameters, the value of D_a was estimated from Eqn.5.4 as 1.8×10^{-5} cm^2/s for 2M2B. These calculations showed that surface diffusion contributions to D_a was about 25 % at 370 K. Particle and gel-like micrograin radii of Amberlyst-15 are $R_o = 3.7 \times 10^{-4}$ m and $r_o = 1.14 \times 10^{-8}$ m, respectively. Both Amberlyst-15 particles and gel-like micrograins are expected to swell in the presence of alcohols and water. About 50 % volume swelling of microspheres was obtained in our work. There is no published data for diffusion coefficient (D_i) of 2M2B in

the gel-like micrograins. However, D_i value of isobutylene was reported as 2.6×10^{-12} cm^2/s at 358 K (Oktar et al., 1999b). Somewhat smaller D_i value was expected for 2M2B. By taking the order of magnitude of D_i as 1×10^{-12} cm^2/s, the value of parameter G in Eqn.5.3 was estimated as 2×10^{-2}. This is a clear indication that pore diffusion resistance in the gel-like micrograins is significantly smaller than macropore diffusion resistance in our system and can be neglected.

To test the significance of macropore diffusion resistance on the observed rate, left hand side of the criterion given in Eqn.5.2 was estimated for the conversion of 2M1B and 2M2B to TAEE. The observed initial rates of etherification reactions of 2M1B and 2M2B with ethanol were estimated from the conversion data reported in Figure 5.3 and 5.4 as 1.2×10^{-5} mol/g.s and 3.5×10^{-6} mol/g.s, respectively. Using all these information the left hand side of inequality given in Eqn.5.2 was estimated to be as 2 and 0.6 for reactions of 2M1B and 2M2B with ethanol, respectively. These values showed that for the production of TAEE from 2M1B diffusional effects play significant role on the observed rates. However, in the case of producing TAEE from 2M2B effect of diffusion resistances in the macropores are quite small. Possible effects of external mass transfer resistance on observed rates is also tested by evaluating Biot number

($Bi_m = \dfrac{k_m R_o}{D_a}$) in our system. The mass transfer coefficient, k_m was evaluated

from well known correlation given for fixed beds (Dogu, 1986). The value of Bi_m in our system was found to be in the order of magnitude 30, which indicated that film mass transfer resistance could be neglected as compared to macropore diffusion resistance. As a result of these discussions it was concluded that, the only transport resistance which should be considered in the analysis of the data is macropore diffusion resistance in the production of TAEE from 2M1B and ethanol. However, diffusion resistance was not significant in the production of

TAEE from 2M2B. All these predictions support the discussion given above to explain the behaviour observed in Figures 5.5 and 5.6.

5.2 Diffuse Reflectance Infrared Fourier Transform (DRIFT) Studies

To our knowledge, there are two published DRIFTS study in the literature, related to the synthesis of ethers on acidic catalysts. The first of these studies is of Larsen et al. (1995). In that work, DRIFTS results were reported for ETBE synthesis on a zeolite type catalyst (H-Mordenite). These results showed that ethanol was preferentially adsorbed on the acid sites and also caused an inhibitory effect on the etherification rate at high ethanol concentrations.

Diffuse reflectance FT-IR spectra of methanol, ethanol and isobutylene in adsorption and reaction experiments leading to the formation of MTBE and ETBE were critically investigated on Amberlyst-15 and sysnthesized resin catalyst. The DRIFT experiments were carried out both continuous and batch wise, with Amberlyst-15, and as well as with a polystyrene sulfonic acid resin catalyst (cross-linked by divinylbenzene) prepared in our laboratories (Catalyst M).

5.2.1 Adsorption of Alcohols on Amberlyst-15 and Catalyst M

Typical DRIFT spectra obtained at 353 K in adsorption experiments carried out with methanol and ethanol are given in Figures 5.9 and 5.10, respectively. The contributions of the resin itself to the DRIFT spectra obtained in the presence of adsorbing or reacting gases was found to be rather small. To eliminate any contribution (although it is small) of the catalyst structure to the DRIFT spectra, differences of DRIFT spectra obtained with and without the adsorbing gases were reported in these figures. For comparison, in these figures DRIFT spectra of adsorbed species on Amberlyst-15 and Catalyst M are shown together with reference gas phase IR spectra. Figures 5.9 and 5.10 indicated

that the FT-IR spectra obtained for alcohols on Amberlyst-15 and Catalyst M were very similar.
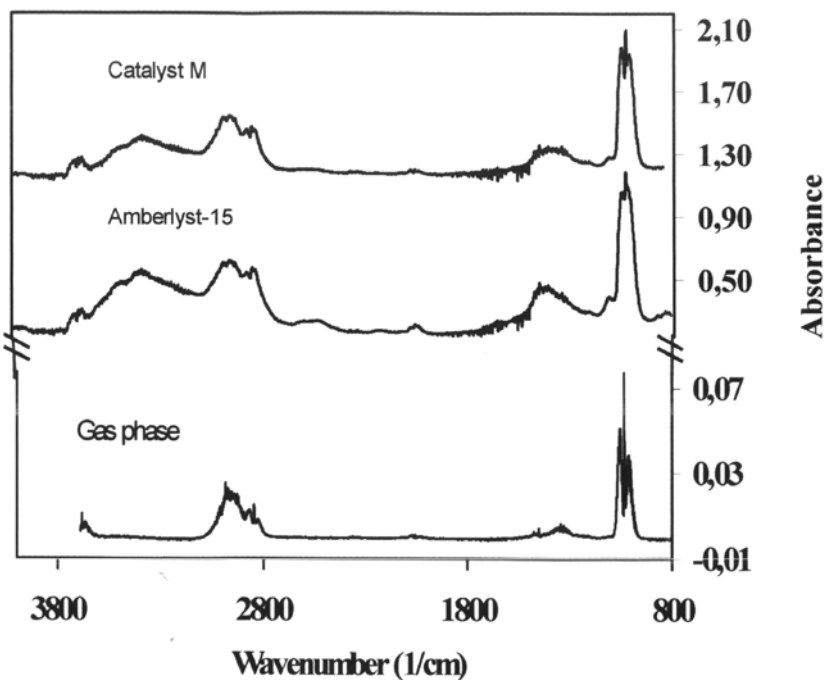
Figure 5.9 DRIFT spectra of methanol on Amberlyst-15 and Catalyst M at 353 K and gas-phase (reference) spectrum
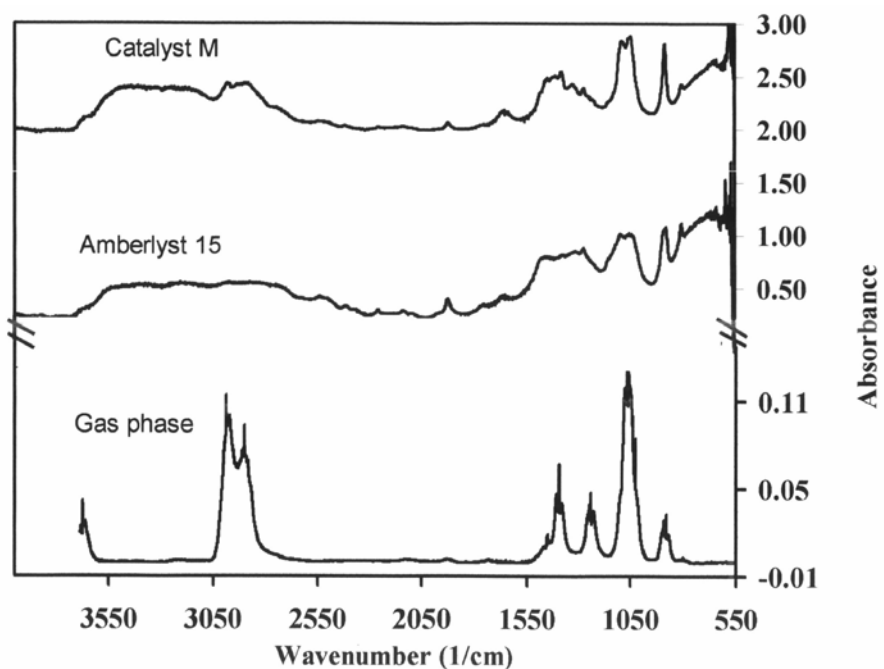
Figure 5.10 DRIFT spectra of ethanol on Amberlyst-15 and Catalyst M at 353 K and gas-phase (reference) spectrum

One of the major differences observed between the gas phase and DRIFT spectra of alcohols is the very broad continuous IR absorption band observed at about 3320 cm^{-1} (between 3080 cm^{-1} and 3630 cm^{-1}) for adsorbed species. This broad band corresponds to the OH stretches of hydrogen bonded network of adsorbed alcohol molecules. The OH groups of alcohols are expected to form hydrogen bridges with the −SO$_3$H groups of the catalyst as well as among themselves. Alcohols are expected to enter between the hydrogen bonded network of −SO$_3$H groups of the catalyst and cause swelling. This broad band observed at 3320 cm^{-1} indicated that adsorbed alcohol molecules showed a liquid-like behavior. Such a broad band was also reported for IR spectra of liquid alcohols (NIST Chemistry Web Book, 1998). In the gas phase spectrum, instead of this broad band a typical OH stretching band was expected at 3681cm^{-1}. The relative intensity of this band is rather small in DRIFT spectra.

The relative intensities of major IR absorption bands shown in Figures 5.9 and 5.10 are summarised in Table 5.4. In the preparation of this table, the peak area of the characteristic CO stretching at 1030 cm^{-1} was taken as unity in each spectrum. As it was shown in Table 5.4, the relative intensity of the broad band observed for ethanol (at 3320 cm^{-1}) is higher than the relative intensity of the corresponding band observed for methanol. This result is in agreement with our previous results on adsorption equilibrium constants on Amberlyst-15 (Oktar et al., 1999b). In that work, it was reported that adsorption equilibrium constant of ethanol was higher than the adsorption equilibrium constant of methanol in the vapor phase. The relative intensity of this band observed with Amberlyst-15 was found to be higher than the corresponding intensity measured with Catalyst M (Table 5.4). This result is in agreement with the higher total exchange capacity of Amberlyst-15 than Catalyst M (Table 4.5).

Table 5.4 Relative Intensities of Major DRIFT Absorption Bands Observed with Methanol[a] and Ethanol[b] at 353 K

	adsorbing molecule	CO stretch (1030 cm^{-1}) (930-1170 cm^{-1})	(1452 cm^{-1}) (1180-1570 cm^{-1})	CH stretch (2943 cm^{-1}) (2700-3080 cm^{-1})	OH stretch (3320 cm^{-1}) (3080-3630 cm^{-1})	(880 cm^{-1})
Amberlyst-15	methanol	1	0.42	1.27	1.37	-
Catalyst M		1	0.28	1.12	0.8	-
Reference (gas)		1	0.14	1.18	-	-
Amberlyst-15	ethanol	1	1.37			0.26
Catalyst M		1	1.07	1.12	1.86	0.21
Reference (gas)		1	0.49	1.5	-	0.12

[a]Other peaks observed with adsorbed methanol: 1090 cm^{-1} (CH_3 rocking), 2042 cm^{-1}, 3664 cm^{-1}.

[b]Other peaks observed with adsorbed ethanol: 808 cm^{-1}, 1923 cm^{-1}, 1660 cm^{-1}, 2251 cm^{-1}, 3664 cm^{-1}.

In the IR spectra, the band observed between 2700 cm^{-1} and 3080 cm^{-1} is majorly due to the CH stretching bands of CH_3 groups of adsorbed species (NIST Chemistry Web Book, 1998). The expected IR absorption bands corresponding to the OH bending (at around 1345 cm^{-1}), to CH_3 s-deform. (at around 1455 cm^{-1}) and to CH_3 d-deform. (at around 1477 cm^{-1}) are found to be over lapped in the DRIFT spectra of adsorbed alcohols giving a broad band at 1452 cm^{-1} (between 1180 cm^{-1}-1570 cm^{-1}). The relative intensity of this band is also higher than the corresponding value for the reference gas phase spectrum (Table 5.4). This is expected to be majorly due to the contribution of OH bending of the hydrogen bridges of the adsorbed alcohol molecules. Same as for the OH stretching band observed at 3320 cm^{-1}, the relative intensity of this band is higher for Amberlyst-15 than Catalyst M. These observations also agree with the previous discussion made for the band observed at 3320 cm^{-1}.

The relative intensity of the absorption band observed at 880 cm^{-1} for ethanol is about twice the corresponding value in the gas phase spectrum (Table 5.4). This peak was expected to be mainly due to CO and C-C stretching with CH_2 rocking (Kuo et al., 1993). Increased significance of this band may be an indication of presence of 2-hydroxyethyl species on the surface. IR absorption bands of •CH_2CH_2OH were reported by Kuo et al. (1993). In addition to this peak, broadening of the bands at 1030 cm^{-1} and at 1452 cm^{-1} (1180-1570 cm^{-1}) may be partly due to the presence of 2-hydroxyethyl species on the surface. For this molecule, IR absorption bands were expected at 1172 cm^{-1} and 1355 cm^{-1} in addition to the bands at 873.9 cm^{-1} and 1040 cm^{-1}.

In the DRIFT spectra of ethanol, another unexpected band was observed at 1660 cm^{-1}. This band is a strong indication of the presence of C=C stretching. Presence of this band together with the small band observed at around 810 cm^{-1}

may be an indication of the presence of ethanol like species in the adsorbed state. In the vapor phase, ethanol was expected to have strong IR bands at 816.6 cm^{-1} (H$_2$C=C OPLA), 1663 cm^{-1} (C=C stretch) and at 3633 cm^{-1} (OH stretch) (Joo et al., 1999). DRIFT experiments carried out at different temperatures showed that by increasing the temperature from 333 K to 353 K, the relative intensity of the band observed at 1660 cm^{-1} increased from 0.08 to 0.11. Similarly, the relative intensity of the band observed at 810 cm^{-1} increased from 0.19 to 0.21 in the same temperature range. These results showed that, besides the hydrogen bonded network structure formed between the adsorbed alcohol molecules and the SO$_3$H sites, some ethanol molecules were chemisorbed to the active sites by dissociation of one or two of the hydrogen atoms. In the chemisorption of an alcohol molecule more than one −SO$_3$H sites might be involved.

5.2.2 DRIFT Results with Isobutylene

To clarify whether isoolefins were also adsorbed on the acidic resin catalysts or not, a set of DRIFT experiments were carried out with isobutylene in the temperature range of 313-353 K. The characteristic and strong IR absorption band observed at 890 cm^{-1} (CH$_2$ wagging), CH$_3$ stretching bands seen between 2840 cm^{-1} and 3030 cm^{-1}, characteristic CH$_2$ asymmetrical stretching at 3086 cm^{-1} and CH$_3$ deformation peaks observed between 1360 cm^{-1} and 1490 cm^{-1} in the DRIFT spectra of isobutylene proved strong adsorption of this molecule on the acidic resin catalysts (Figure 5.11). The qualitative behavior of the DRIFT and the gas phase IR spectra of isobutylene were quite similar. The absorption band observed at 1661 cm^{-1} in the gas phase IR spectrum of isobutylene corresponds to the C=C stretching.

As it is shown in Table 5.5, the relative intensity of this band (with respect to the intensity of CH_2 wagging band observed at 890 cm^{-1}) is around 0.39 in the gas phase spectrum. However, in the adsorbed state, relative intensity of the band at 1661 cm^{-1} is quite less. With an increase of temperature from 313 K to 353 K, relative intensity of this band with respect to the IR band observed at 890 cm^{-1} for CH_2 wagging, decreased significantly (Table 5.5). This result indicated the weakening of the C=C bond of adsorbed isobutylene with an increase of temperature.
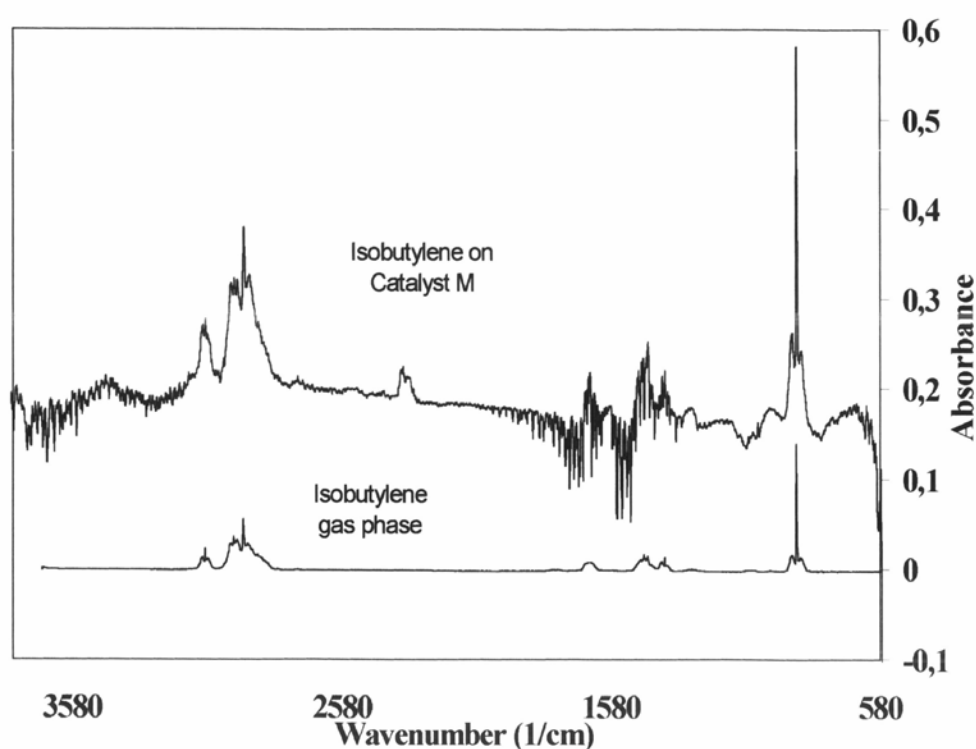
Figure 5.11 DRIFT spectra of isobutylene on Amberlyst-15 and Catalyst M at 353 K and gas-phase (reference) spectrum

Table 5.5 Relative Intensity of C=C Stretching IR Absorption Band with Respect to CH_2 Wagging Band in Isobutylene DRIFT Spectrum

	DRIFT		gas phase spectrum
	313 K	353 K	
C=C stretching (1661 cm^{-1})	0.27	0.03	0.39
CH_2 wagging (890 cm^{-1})	1	1	1

5.2.3 DRIFT Experiments under Reaction Conditions

DRIFT spectra obtained in the reaction experiments conducted with a gas stream containing 30% isobutylene and 7.5% alcohol (in nitrogen) on Amberlyst-15 and on Catalyst M proved the presence of adsorbed ether molecules formed as a result of surface reaction. DRIFT spectra of methanol-isobutylene mixture obtained at 353K are shown in Figure 5.12. In the same figure, DRIFT spectra of methanol and isobutylene obtained in separate adsorption experiments are also shown. Major peaks observed in the DRIFT spectra obtained in the reaction experiments conducted with the methanol-isobutylene mixtures and the expected relative contributions of isobutylene, methanol and MTBE to these bands are summarised in Table 5.6. IR spectrum of MTBE is available in the NIST Chemistry Web Book (1998).
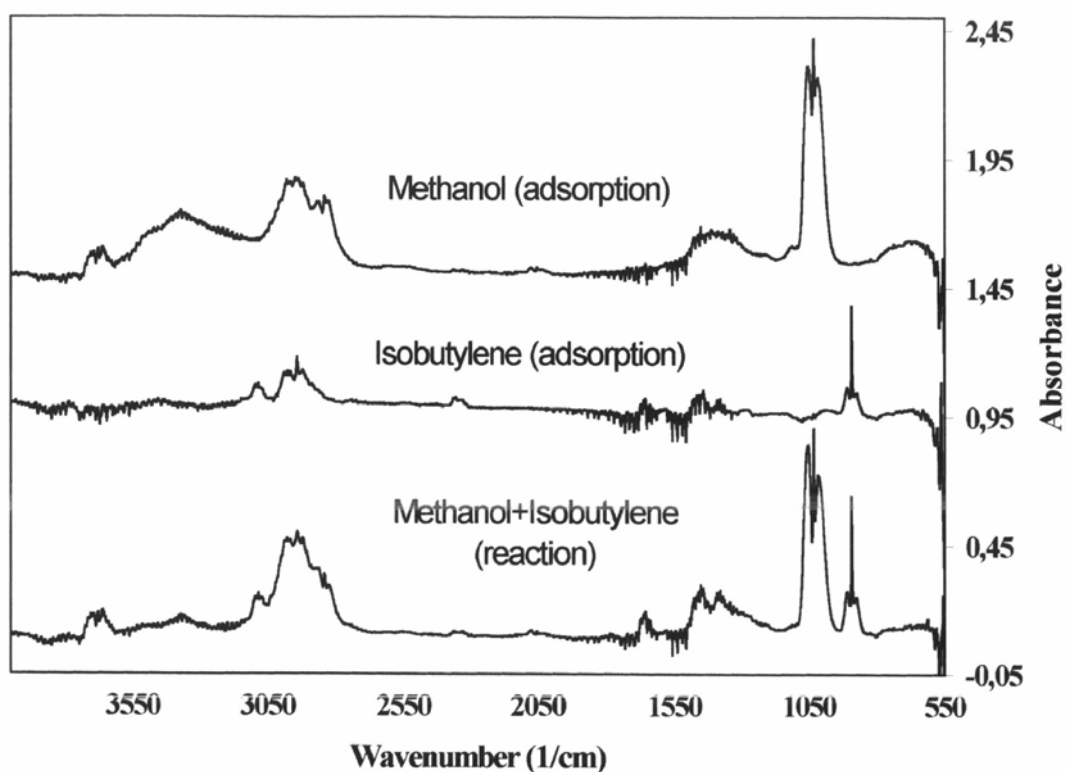
Figure 5.12 DRIFT spectra of methanol and isobutylene in adsorption and reaction experiments on Catalyst M at 353 K

Table 5.6 Major Peaks Observed in the DRIFT Spectra Obtained in the Reaction Experiments with Methanol-Isobutylene Mixture and the Relative Contributions of Isobutylene, Methanol, and MTBE to those Peaks

observed bands	possible contributions	isobutylene	methanol	MTBE
890 cm^{-1}	CH$_2$ wag	high	-	low
930-1170 cm^{-1}	1030cm^{-1}(CO-stretch)	-	high	-
	1085cm^{-1}(C-O-C)	-	-	high
1180-1570 cm^{-1}	1282 cm^{-1}(C-C stretch) 1345 cm^{-1}(OH bend) 1381 cm^{-1}(CH$_3$ s-deform) 1458 cm^{-1}(CH$_3$ d-deform)	medium	high	medium
1661 cm^{-1}	C=C stretch	high	-	-
2700-3070 cm^{-1}	2890 cm^{-1} (CH$_3$ s-str.) 2980 cm^{-1} (CH$_3$ d-str.)	high	high	high
3086 cm^{-1}	CH$_2$ a-stretch	high	-	-
3080-3630 cm^{-1} 3680 cm^{-1}	OH stretch liquid OH stretch gas	-	high	-

The strong IR absorption band observed between 930 and 1170 cm^{-1} is due to the adsorbed alcohol, as well as the reaction product MTBE. The characteristic CO stretching of methanol was expected to be at 1030 cm^{-1}. However, a characteristic band of an aliphatic ether (C-O-C) was expected at around 1085 cm^{-1}. By the formation of MTBE, a shift of the wide band observed between 930 and 1170 cm^{-1} to higher wave numbers and an increase in intensity were expected.

As it was illustrated in Table 5.7, with increasing temperature, the relative intensity of this band [with respect to the CH$_3$ stretching bands at 2943 cm^{-1} (2700-3070 cm^{-1})] increased, with a corresponding decrease in the intensity of CH$_2$ wagging band observed at 890 cm^{-1}. These observations indicate the formation of adsorbed ether molecules on the surface. The bands at 890 cm^{-1} (CH$_2$ wag), 3086 cm^{-1} (CH$_2$ a-stretch), and 1661 cm^{-1} (C=C stretch) correspond primarily to isobutylene. The decreasing trends of intensity of these three bands, together with the increased of intensity of the band observed between 930 cm^{-1} and 1170 cm^{-1}, indicate the increased conversion of isobutylene to MTBE with an increase in temperature. The intensity of the broad band observed at 3320 cm^{-1} (between 3080 and 3630 cm^{-1}) for adsorbed methanol (OH stretch of hydrogen bonded network of adsorbed alcohol molecules) showed a decrease in the reaction experiments. Also, some decrease of the wide band between 1180 and 1570 cm^{-1} was observed with an increase of the temperature in the reaction experiments. This wide band is primarily due to the contributions of OH bending and CH$_3$ deformation. All three species (methanol, isobutylene and MTBE) are expected to contribute to this wide band observed between 1180 and 1570 cm^{-1}. However, the contribution of alcohol is expected to be more significant. The decrease in intensity of this band with temperature together with the increase in

intensity of the band observed at 1030 cm^{-1} (930-1170 cm^{-1}), also support our conclusion about the formation of MTBE species on the surface.

Table 5.7 Relative Intensities of Major DRIFT Bands Observed in Methanol-Isobutylene Reaction on Catalyst M

temperature (K)	890 cm^{-1}	1030 cm^{-1} (930-1170 cm^{-1})	1452 cm^{-1} (1180-1570 cm^{-1})	1661 cm^{-1}	2943 cm^{-1} (2700-3070 cm^{-1})	3086 cm^{-1}
313	0.37	0.90	0.77	0.13	1	0.19
333	0.33	1.01	0.73	0.11	1	0.15
353	0.21	1.13	0.59	0.08	1	0.07

Another very important conclusion reached from DRIFT spectra obtained in experiments conducted with isobutylene only and with isobutylene-methanol mixtures is the significant increase of the characteristic IR absorption bands of isobutylene (CH$_2$ wag at 890 cm^{-1} and CH$_2$ asymmetrical stretch at 3086 cm^{-1}) in the presence of alcohols (Table 5.8).

Table 5.8 Comparison of intensity ratios in reaction and adsorption experiments for isobutylene

temperature (K)	CH$_2$ wagging 890 cm^{-1}	CH$_2$ a-stretch 3085 cm^{-1}
313	3.9	3.9
333	3.2	2.6
353	1.5	1.3

(*) These numbers correspond to the ratios of intensities of the bands observed in the reaction and absorption experiments

This result is in agreement with our previous results (Oktar et al., 1999b) reported for adsorption of isoamylenes in the presence of alcohols on Amberlyst-15. In that work, higher adsorption equilibrium constants of C_5 iso-olefins were obtained in the presence of alcohols.

We propose a bridged structure of adsorbed isobutylene between the $-SO_3H$ sites of the catalyst and the adsorbed alcohol molecules (Figure 5.13). By the formation of this bridged structure of adsorbed isobutylene molecules on the surface and by weakening of the C=C bond with an increase of temperature, adsorbed ether molecules are formed on the surface. During this etherification step, involvement of hydrogen from the $-SO_3H$ sites is also expected.
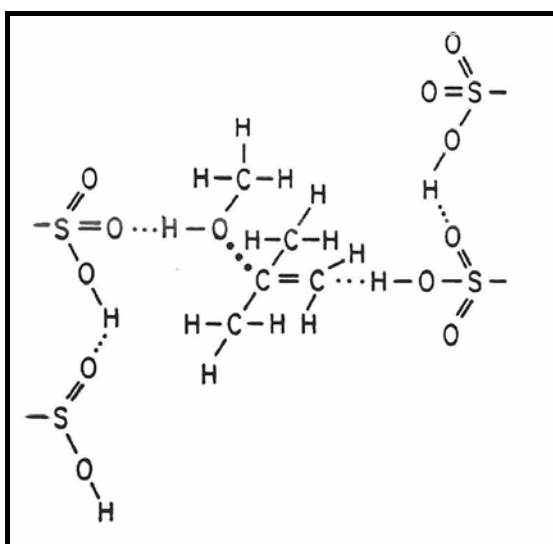
Figure 5.13 Schematic representations of methanol and isobutylene adsorbed on SO_3H sites

All of these results indicate that the formation of ether molecules involves adsorbed alcohol and adsorbed iso-olefin molecules in the concentration range studied in this work. As reported in our previous publication (Oktar et al., 1999b), the adsorption equilibrium constants of alcohols are more than an order of magnitude greater than the adsorption equilibrium constants of iso-olefins. Consequently, at high concentrations of alcohols, most of the active sites are

expected to be covered by alcohol molecules. For high values of alcohol-to-isobutylene ratios, the availability of the empty sites for isobutylene adsorption is expected to decrease, and consequently, a decrease in the reaction rate with an increase in alcohol concentration is expected. In fact, such a decrease was reported in the literature (Subramaniam and Bhatia, 1987) for methanol/isobutylene mole ratios greater than 0.1. In our DRIFT experiments, this ratio was 0.25. Our results indicate that ether molecules are also formed in the adsorbed state. All of these results suggest a Langmuir-Hinshelwood type reaction model involving adsorbed isobutylene and adsorbed alcohol molecules.

Similar conclusions can be reached from the analysis of DRIFT spectra of ethanol-isobutylene mixtures obtained with Amberlyst-15 and Catalyst M (Figure 5.14).
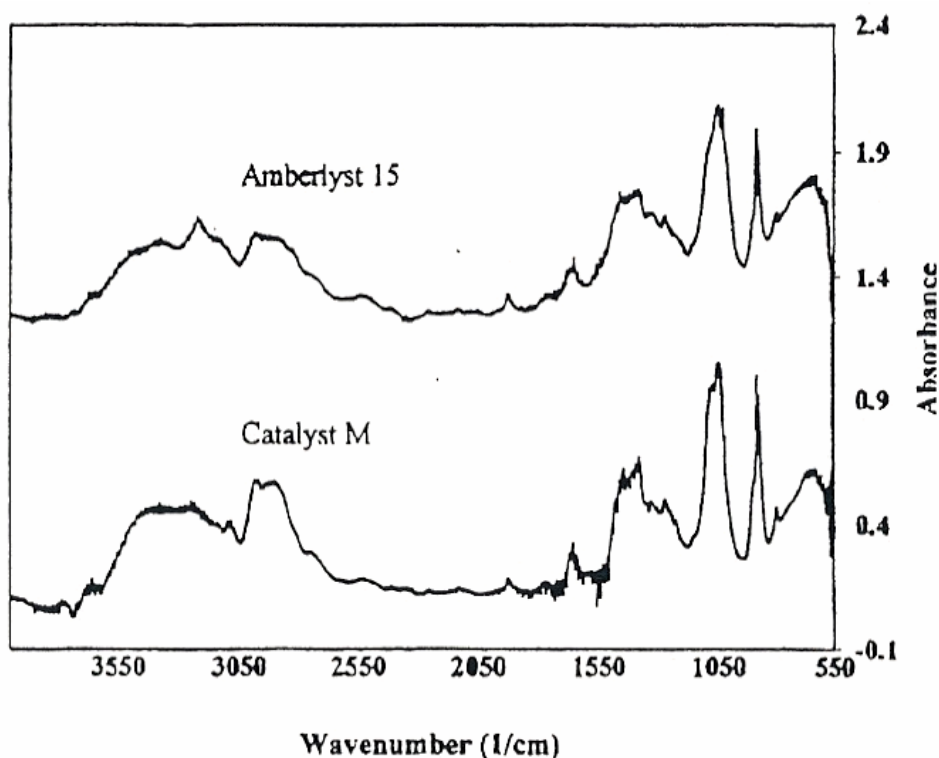
Figure 5.14 DRIFT spectra obtained in reaction experiments carried out with ethanol-isobutylene mixtures with Amberlyst-15 and Catalyst M at 353 K

In Figure 5.15, DRIFT spectra obtained with ethanol-isobutylene mixture in the vapor-phase reaction experiment and DRIFT spectra of ethanol and isobutylene obtained in separate adsorption experiments are displayed. In the case of ethanol-isobutylene reaction experiments, the IR absorption band observed at 890 cm^{-1} is due to both isobutylene and ethanol. The wide band observed at 1030 cm^{-1} is due to both ethanol and ETBE. The interaction of IR absorption bands is much more complex in ETBE synthesis than in MTBE synthesis. Nevertheless, similar conclusions can be reached in this case as in the case of the methanol-isobutylene DRIFT spectra.
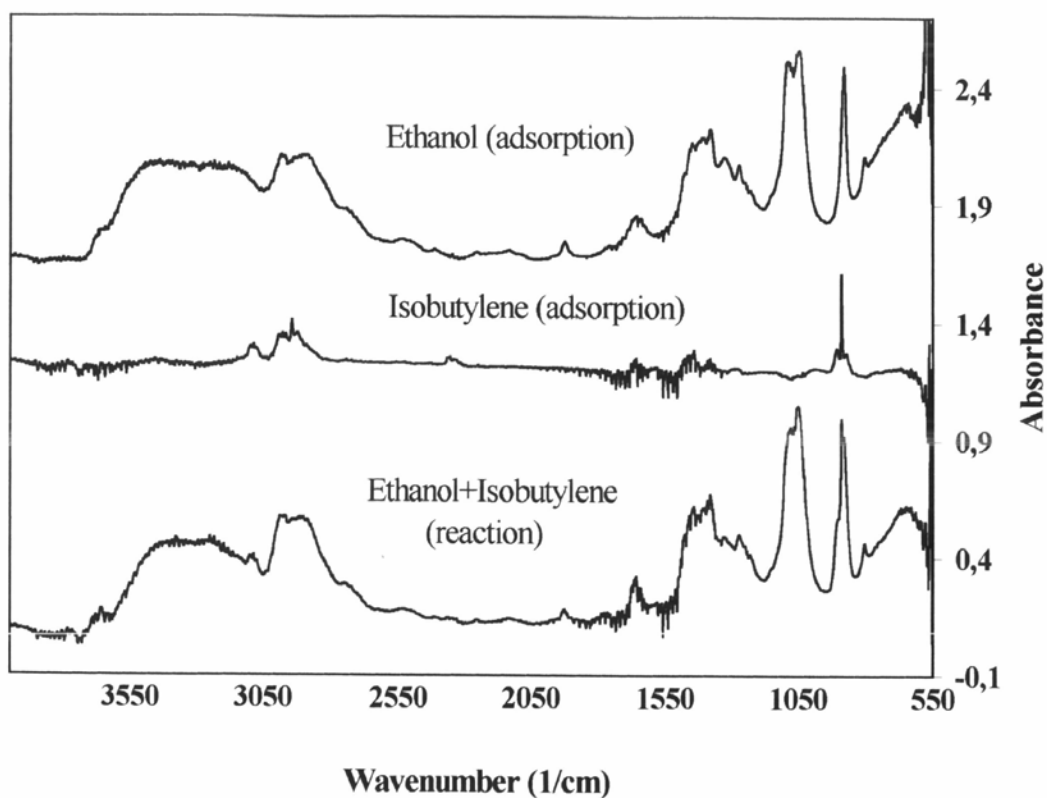
Figure 5.15 DRIFT spectra of ethanol and isobutylene in adsorption and reaction experiments on Catalyst M at 353 K

As shown in Table 5.9, the relative intensities of 1661 cm^{-1} (C=C stretch) and 890 cm^{-1} bands (with respect to the IR band observed at 2943 cm^{-1} for CH_3

stretch) show a decreasing trend with temperature, whereas the band observed at 1030 cm^{-1} slightly increased. These results are in agreement with the formation of the ether molecules on the surface.

Table 5.9 Relative Intensities of Some Major DRIFT Bands Observed during Ethanol-Isobutylene Reaction on Catalyst M

temperature		CO stretch	C=C stretch	CH$_3$ stretch
(K)	890 cm^{-1}	1030 cm^{-1}	1661 cm^{-1}	2943 cm^{-1}
333	0.24	0.55	0.07	1
353	0.19	0.58	0.03	1

5.2.4 DRIFT Results of 2M1B, Methanol and 2M1B-Methanol Mixtures

DRIFTS results obtained with 2-methyl-1-butene (2M1B) at temperatures of 313, 333 and 353 K are shown in Figure 5.16.

Strong IR absorption bands observed between 2800 cm^{-1} and 3040 cm^{-1} corresponds to the CH$_3$ stretching bands. The sharp CH$_2$ wag-band observed at 890 cm^{-1} and the small CH$_2$ asym. stretching (vinyl proton) band observed at 3085 cm^{-1} are characteristic bands for isoamyl species. Qualitative behavior of DRIFT spectrum is quite similar to the IR spectrum of gas phase 2M1B. In the gas phase spectrum, CH$_2$ wag-band was expected at a higher wave number (at 940 cm^{-1}) (NIST Chemistry Web Book, 1998). The shift of this band in the DRIFT spectrum is an indication that, CH$_2$ group of 2M1B was involved in the adsorption of 2M1B to the $-$SO$_3$H sites of the catalyst. For the other bands observed at 1384 cm^{-1} (CH$_3$ s-deform) and at 1457 cm^{-1} (CH$_3$ d-deform), no significant shift of the

band position was observed as compared to the corresponding values reported for gas phase IR spectra.
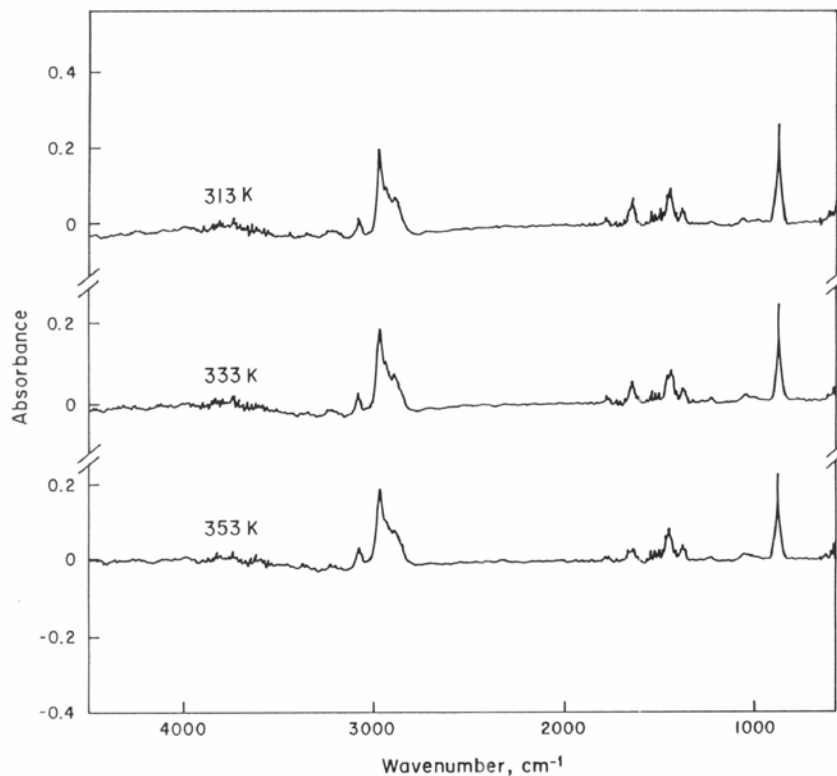
Figure 5.16 DRIFTS results of 2M1B obtained in adsorption experiments on Amberlyst-15 (Differences of spectra obtained with and without adsorbing species)

The band observed at 1651 cm^{-1} corresponds to the C = C stretching. In the gas phase, this band was expected at about 1660 cm^{-1}. The relative intensity of this band with respect to the CH$_3$ stretching bands observed between 2800 cm^{-1} and 3040 cm^{-1} (the ratio of peak area of C = C stretching band at 1651 cm^{-1} to the peak area of CH$_3$ stretching band) showed a decreasing trend with an increase in temperature (Table 5.10). This decreasing trend indicated weakening of the C = C bond of adsorbed species with an increase in temperature. A similar result was reported for adsorption of isobutylene on Amberlyst-15 in our previous publication (Dogu et al., 2001).

Table 5.10 Relative Intensity Values C=C Stretching Band with Respect to the Intensity of CH_3 Stretching Band in Adsorption of 2M1B on Amberlyst-15

T (K)	CH_3 stretching 2975 cm^{-1} (2800 cm^{-1} – 3040 cm^{-1})	C=C stretching 1651 cm^{-1} (1590 cm^{-1} – 1703 cm^{-1})
313	1	0.140
333	1	0.129
353	1	0.118

In Figure 5.17, DRIFTS results obtained with TAME at different temperature on Amberlyst-15 are shown (Aydın, 1999). Similar to the spectra obtained with 2M1B, characteristic CH_3 stretching bands (between 2730 cm^{-1} and 3040 cm^{-1}) and CH_3 deformation bands (CH_3-deform at 1457 cm^{-1} and CH_3 d-deform at 1380 cm^{-1}) were also detected with TAME. The major difference of the spectrum of TAME from the spectrum of 2M1B is the sharp band observed at 1085 cm^{-1}. This band is the characteristic band of aliphatic ethers (C-O-C).

As it was shown in Figure 5.17, the relative intensity of this band, with respect to the bands observed for CH_3 stretching or deformation, decreased with an increase in temperature accompanied with an increase of the sharp band observed at 1030 cm^{-1}.

The intensity of the band observed at 1030 cm^{-1} was very small at 313 K. However, its intensity became highly significant at 363 K. This band is very characteristic for the CO stretching of methanol (Dogu et al., 2001 and NIST Web Book, 1998). The ratio of the IR absorption peak heights of 1085 cm^{-1} and 1030 cm^{-1} bands decreased from 3.0 to 0.9 with an increase of temperature from 313 K to 363 K (Table 5.11).
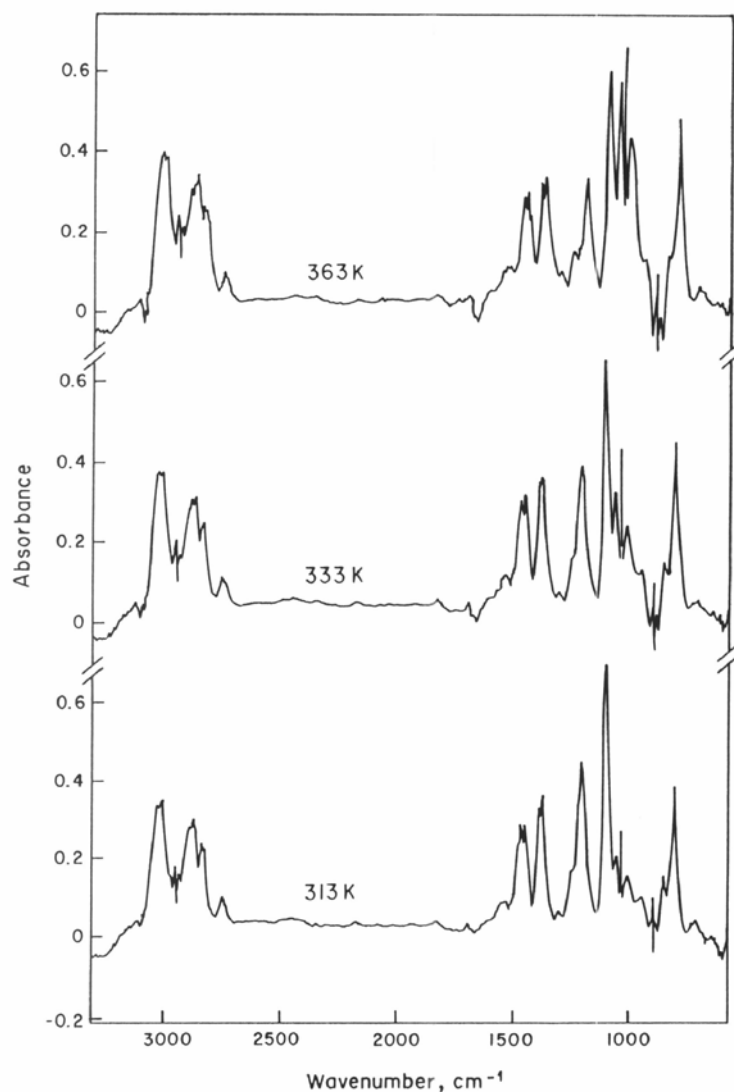
Figure 5.15 DRIFTS results of TAME obtained in adsorption experiments on Amberlyst-15 at different temperatures (Aydin, 1999)

Table 5.11 The Intensity Ratio Values of IR Absorption Bands of 1085 Cm^{-1} (C-O-C Band of TAME) and 1030 cm^{-1} (CO stretching of Methanol) in Adsorption of TAME on Amberlyst-15

temperature (K)	Intensity Ratio (band height of 1085 cm^{-1} / band height of 1030 cm^{-1})
313	3.0
333	1.5
363	0.9

Decrease of the intensity of the band at 1085 cm^{-1} together with an increase of the intensity of the band observed at 1030 cm^{-1} indicated the decomposition of the adsorbed TAME molecules, forming adsorbed methanol by the association of the hydrogen from at –SO$_3$H sites of the catalyst. This is schematically illustrated in Figure 5.18. The increase of the CH$_2$ wag-band observed at 810 cm^{-1} for adsorbed TAME with an increase in temperature is also in agreement with these conclusions.
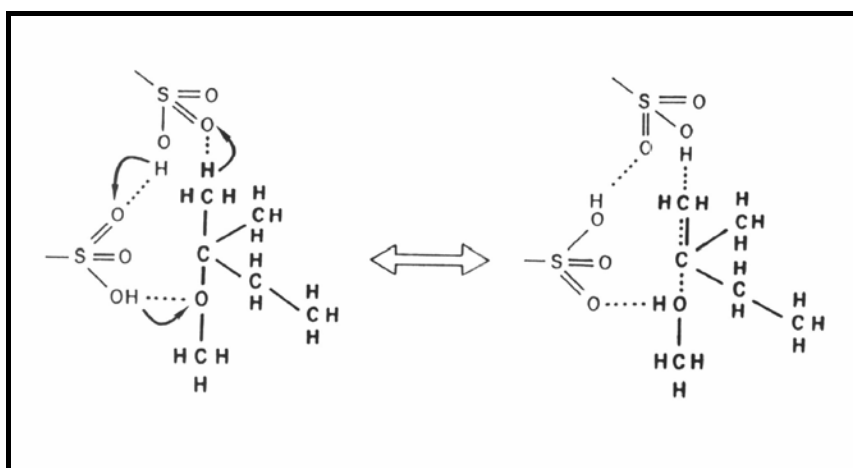
Figure 5.18 Schematic representation of TAME adsorption

DRIFT spectra of 2M1B and an equimolar mixture of 2M1B-methanol obtained at 353 K are shown in Figure 5.19 The IR absorbtion band observed between 930 cm^{-1} and 1170 cm^{-1} with the 2M1B-methanol mixture (reaction experiments) is due to the contributions of CO stretching of methanol (which was expected at 1030 cm^{-1}) and C-O-C IR absorbtion band of reaction product TAME (at around 1085 cm^{-1}). An increase of the relative intensity of this band with respect to the relative intensity of the OH stretching observed between 3080 cm^{-1} and 3630 cm^{-1} was expected by the formation of TAME on the surface. In fact, the relative intensity ratio of these two bands increased from 0.11 to 0.16 by increasing the temperature from 313 K to 353 K (Table 5.12). In the same temperature range,

relative intensity of C=C stretching band observed at 1651 cm^{-1} with respect to the relative intensity of the CH$_3$ stretching (between 2700 cm^{-1} and 3080 cm^{-1}) decreased from 0.072 to 0.060. These results supported the formation of TAME molecules on the surface. These results clearly showed that both alcohol and 2M1B molecules were adsorbed on the surface and TAME was produced following a Langmuir-Hinshelwood type reaction mechanism.
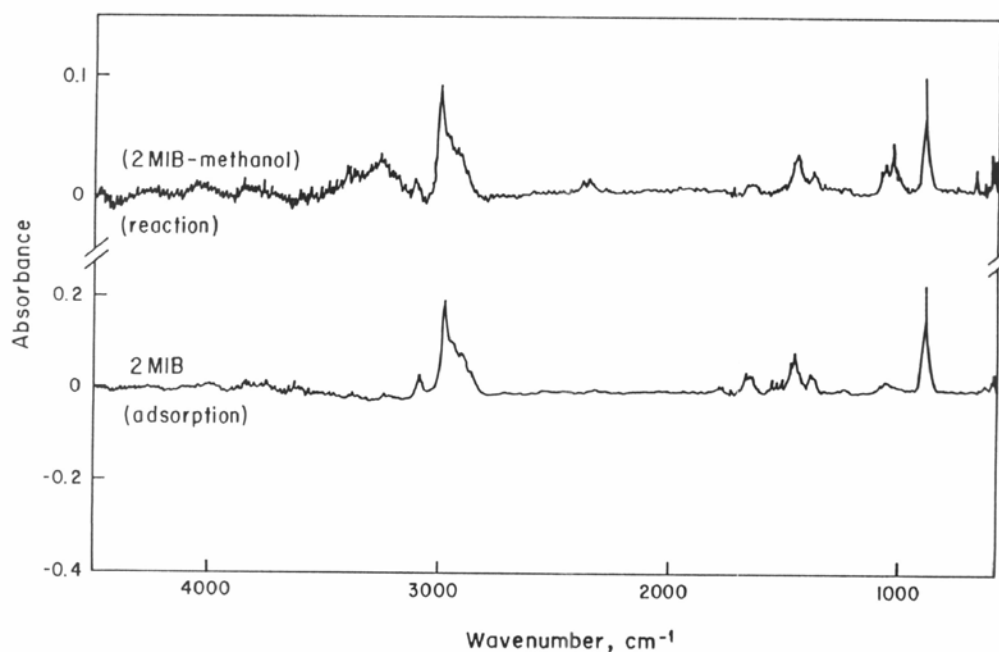
Figure 5.19 DRIFTS results of 2M1B, methanol and equimolar 2M1B-methanol mixture obtained at 353 K on Amberlyst-15

Table 5.12 Relative Intensity Values of the Band Observed Between 930 cm^{-1} and 1170 cm^{-1} with Respect to the Relative Intensity of the Band between 3080 cm^{-1} and 3630 cm^{-1}, in Reaction Experiments

Temperature (K)	OH stretching (3080 cm^{-1} – 3630 cm^{-1})	(C-O-C ether) and (CO methanol) (930 cm^{-1} – 1170 cm^{-1})
313	1	0.11
333	1	0.15
353	1	0.16

5.3 Analysis of Proposed Mechanism

Basing on the DRIFTS results, following reaction mechanism was proposed for the formation of TAME or TAEE over Amberlyst-15.

$$A \text{ (methanol or ethanol)} + \underline{S} \xrightleftharpoons{K_A} \underline{AS} \tag{5.5}$$

$$B \text{ (isoamylene)} + \underline{AS} + \underline{S} \xrightleftharpoons{K_I} \underline{ABSS} \tag{5.6}$$

$$\underline{ABSS} \xrightleftharpoons[k_{-3}]{k_3} \underline{ESS} \qquad \text{(rate determining step)} \tag{5.7}$$

$$\underline{ESS} \xrightleftharpoons{K_E} E \text{ (TAME or TAEE)} + \underline{2S} \tag{5.8}$$
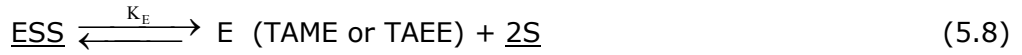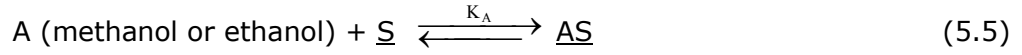
The rate expression derived basing on this reaction mechanism is given by Eqn. 5.9.

$$r = k\left(a_A a_B - \frac{a_E}{K}\right) \left[\frac{\left[(1 + K_A a_A)^2 + k''\left(a_A a_B + \frac{K_E}{K_A K_B} a_E\right)\right]^{\frac{1}{2}} - (1 + K_A a_A)}{(K_A K_B a_A a_B + K_E a_E)} \right]^2 \tag{5.9}$$

Considering the non-idealities of the alcohol–isoamylene–tert-ether mixtures, activities are used in Eqn. 5.9. The equilibrium constant K of etherification reaction for the synthesis of TAEE is given by Kitchaiya and Datta (1994).

$$\ln K = 26.779 + \frac{2078.6}{T} - 6.5925 \ln T + 0.0231T - 1.126 \times 10^{-5} T^2 - 1.414 \times 10^{-8} T^3 \tag{5.10}$$

As it was reported in the literature (Oktar et al., 1999b), the adsorption equilibrium constants of alcohols are more than two orders of magnitude greater than the adsorption equilibrium constants of i-olefins (i-butylene, 2M1B, 2M2B) and tert-ethers. Consequently, the orders of magnitude of the terms containing the adsorption equilibrium constant of tert–ether (K_E) in Eqn. 5.9 are expected to be rather small.

For the synthesis of TAEE, initial rate data were reported in our previous publications (Oktar et al., 1999a; Boz et al., 2004a) and also in other published work (Linnekoski et al., 1997; 1999). In the analysis of the initial rate data, the terms containing activity of ether (a_E) become negligible in Eqn. 5.9 and the rate expression reduces to

$$r = k'\left(\frac{a_A}{a_B}\right)\left\{\left[\left(\frac{1}{a_A} + K_A\right)^2 + k''\left(\frac{a_B}{a_A}\right)\right]^{1/2} - \left(\frac{1}{a_A} + K_A\right)\right\}^2 \quad \text{(initial rate)} \quad (5.11)$$

Here, the combined rate constants k' and k'' are

$$k' = (kS_o)/(16K_A(K_BS_o)); \qquad k'' = 8(K_BS_o)K_A, \qquad (5.12)$$

where S_o is the total number of sites per unit mass of catalyst (mol/g).

The initial rate data obtained in our studies and also published in the literature (Oktar et al., 1999a; Linnekoski et al., 1997;1999; Boz et al., 2004a) at different temperatures were analyzed using Eqn. 5.11 and the rate parameters were determined using a Quasi-Newton regression procedure. Eqn. 5.11 contains three parameters, namely k', k'' and K_A. Regression results became highly dependent an initial estimates, if all three of these parameters were left as adjustable. The adsorption equilibrium constants of ethanol (K_A) obtained from independent adsorption experiments were reported in our earlier publication (Doğu et al., 2001). As it was discussed in the earlier publications (Doğu et al., 2001; 2003; Oktar et al., 1999b), adsorption equilibrium constant of liquid ethanol shows an unexpected increasing trend with an increase in temperature at temperatures greater than about 330 K. This behavior was explained by the

chemisorption of some of the ethanol molecules by dissociation of one or two hydrogen atoms on Amberlyst-15. Also, due to swelling of gel-like polymer structure of Amberlyst-15, higher penetration of alcohol molecules into the polymer structure and a corresponding increase in availability of active sites was reported at higher temperatures. The adsorption equilibrium constants reported by Doğu et al. (2001) were based on fluid phase concentrations. However, the adsorption equilibrium constants which appear in Eqns. 5.9 and 5.11 are in terms of activities (K_A= [AS] / [S] a_A). Knowing the temperature, pressure and compositions of the mixtures, activity coefficients of ethanol were evaluated using the UNIFAC program (Orbey and Sandler, 1998) and adsorption equilibrium constants based on activities were estimated from the experimental adsorption equilibrium constants reported in the literature. The temperature dependence of K_A, thus evaluated is illustrated in Table 5.13. The adsorption equilibrium constants of ethanol evaluated from this analysis are substituted into Eqn. 5.11 and the rate parameters k' and k'' were evaluated by regression analysis of the initial rate data. In this analysis, UNIFAC program was again used for the estimation of activity coefficients. In this analysis, data reported for the reaction of ethanol with 2M1B and also with an isoamylene mixture, which constituted majorly 2M2B (95 % 2M2B, rest being majorly 2M1B), were used. Analysis of the data available in the literature at 333, 343, 353 and 360 K were analyzed to obtain the rate parameters. The rate parameters k' and k'' which were evaluated from this analysis are also reported in Table 5.13.

The agreement of the proposed rate expression with the data published in the literature was found to be quite good. Typical experimental results and model predictions of the initial rate of TAEE formation from 2M1B and 2M2B are illustrated in Figures 5.20 a-d.

Table 5.13 Temperature dependence of rate and adsorption equilibrium parameters of the model (Eqn. 5.9)

2M1B	2M2B
ln k' = − 6199.3 (1/T) + 16.7 (mol/g.s)	ln k' = − 4961.1 (1/T) + 13.1 (mol/g.s)
ln k″ = − 7463.3 (1/T) + 20.8	ln k″ = − 5490.2 (1/T) + 15.0
ln (k_3S_o) = − 13663 (1/T) + 38.3	ln (k_3S_o) = − 10451 (1/T) + 28.8
ln (K_BS_o) = 1901.4 (1/T) − 11.2	ln (K_BS_o) = 3874.5 (1/T) − 17.01
ln K_A = − 9364.7(1/T) + 29.9 (ethanol)	
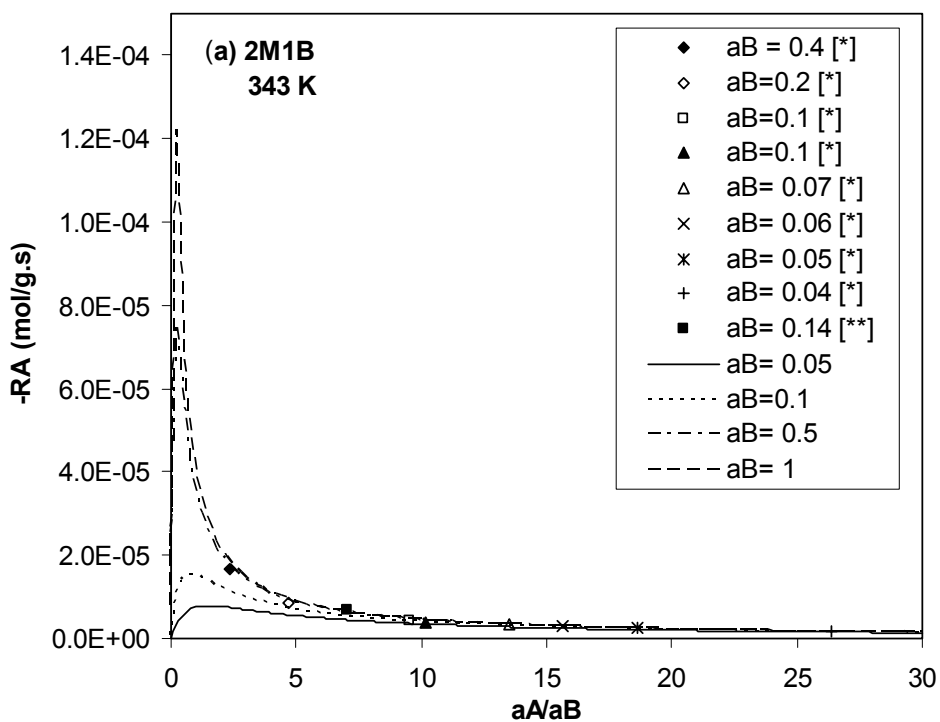
Figure 5.20a Rate of TAEE formation using 2M1B at 343 K
([*]=Oktar et al., 1999a; [**]=This work)
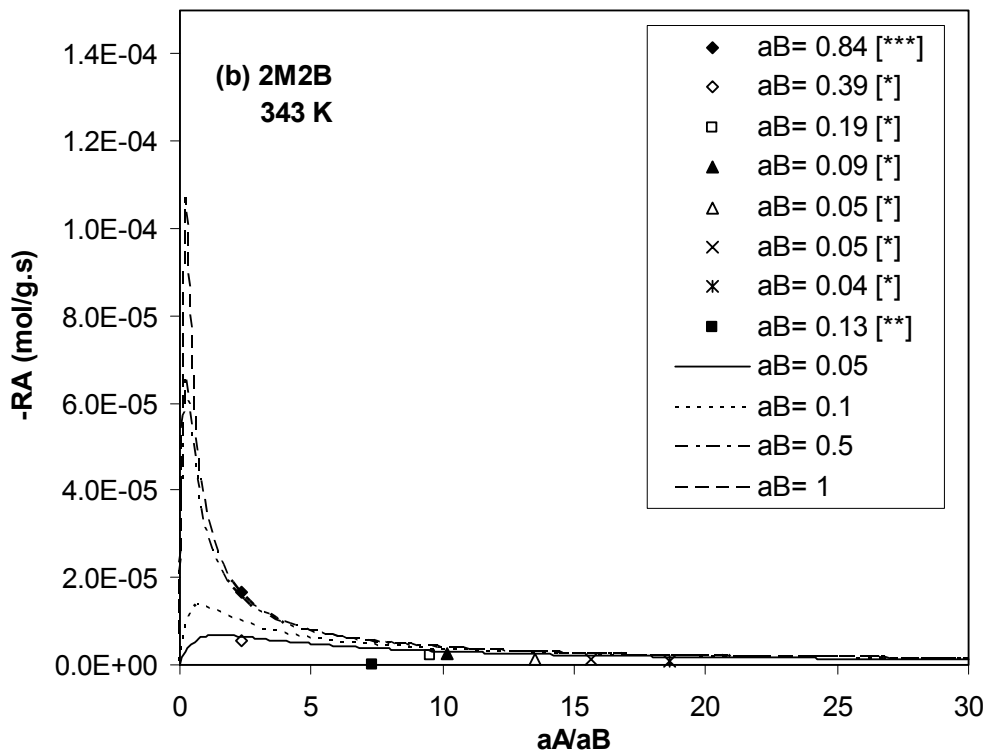
Figure 5.20b Rate of TAEE formation using 2M2B at 343 K

([*]=Oktar et al., 1999a; [**]=This work; [***]=Linnekoski et al., 1997)
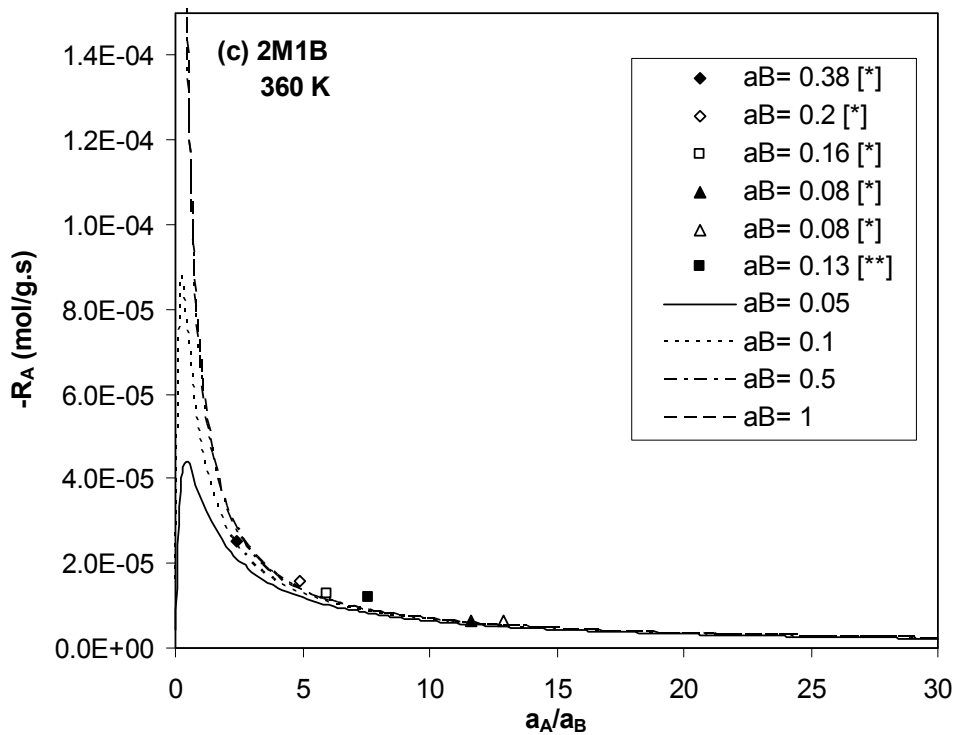
Figure 5.20c Rate of TAEE formation using 2M1B at 360 K

([*]=Oktar et al., 1999a; [**]=This work)
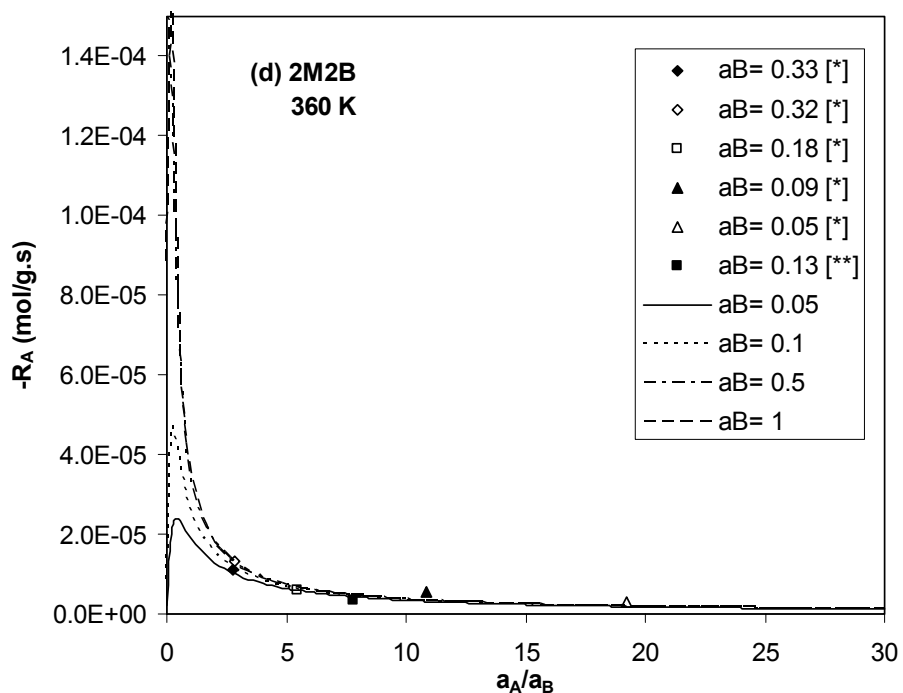
Figure 5.20d Rate of TAEE formation using 2M2B at 360 K
([*]=Oktar et al., 1999a; [**] =This work)

As it is seen in these figures the rate values pass through a sharp maximum as the ratio of activity of ethanol to isoamylene (a_A / a_B) increases. This maximum is also clearly seen in Figure 5.21, where the predicted rate values are plotted as a function of activity of ethanol (a_A) (activity of isoamylene (a_B) being the parameter). In the presence of alcohols, most of the surface is expected to be covered by alcohol molecules.

As a result of this, number of available sites involved in the adsorption of i-olefins is drastically decreased with an increase in alcohol concentration. At sufficiently high alcohol activities, reaction rate becomes almost zero order with respect to alcohol activity. However, reaction order with respect to i-olefins is close to one. This behavior of the rate expression is also consistent with the conclusions of Tejero et al. (1996) reported for liquid phase synthesis of MTBE.
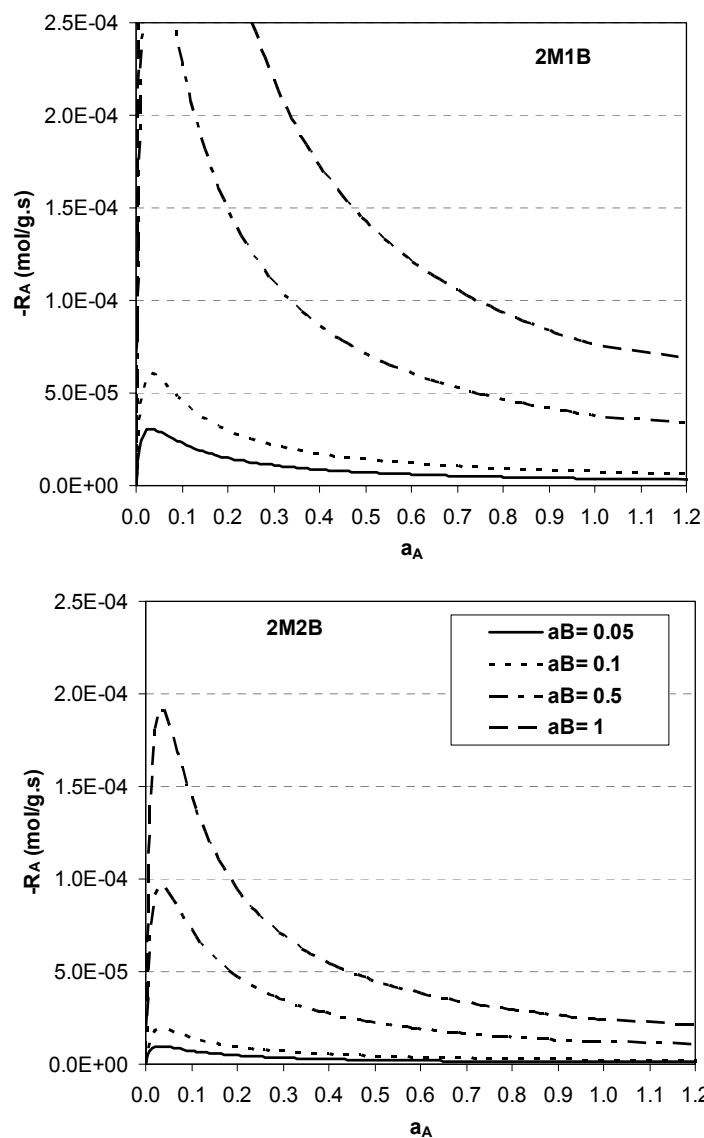
Figure 5.21 Dependence of initial rate of TAEE formation on activities of ethanol (a_A) and isoamylenes (a_B) at 353 K

The temperature dependence of the rate constants k' and k'' obtained for 2M1B+ethanol and 2M2B+ethanol reactions are illustrated in Figure 5.22. As it seen in Figures 5.20 and 5.21, the reactivity of 2M1B is higher than the reactivity of isoamylene mixture, which constituted majorly 2M2B. This activity difference becomes more significant at higher temperatures. Activation energies of the rate constants (k' and k'') of 2M1B+ethanol reaction are also higher than the corresponding values of 2M2B+ethanol reaction.

Knowing the k', k'' and K_A values, adsorption equilibrium constant of isoamylenes (2M1B and 2M2B) and the rate constant of the rate determining step of the mechanism (Eqn. 5.7) are determined using the definitions of k' and k'' (Eqn. 5.12). Temperature dependence of these parameters is also given in Table 5.13.
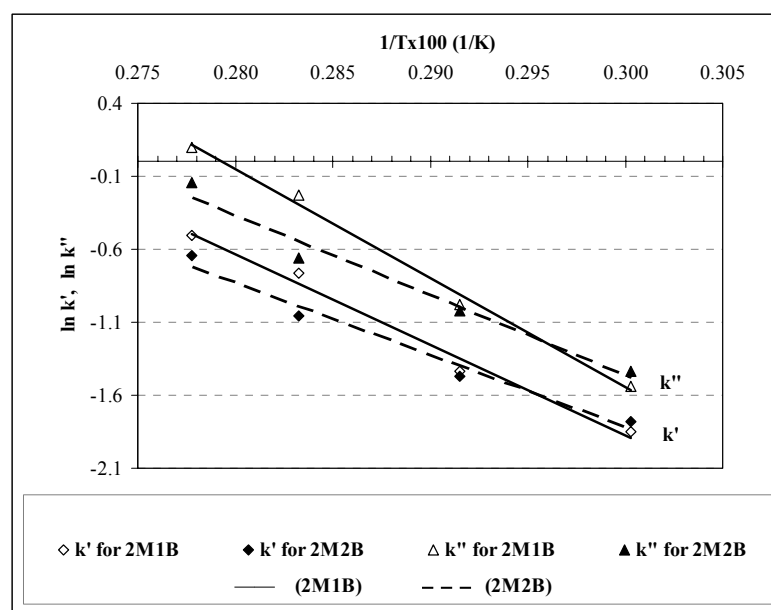
Figure 5.22 Temperature dependence of rate constants (Boz et al., 2004c)

5.4 Diffusion Resistances and Contribution of Surface Diffusion in TAME and TAEE Production Using Amberlyst-15

Gas chromatographic techniques have been frequently used for the evaluation of effective diffusivities and adsorption equilibrium constants in porous solids. Applications of packed bed moment technique to porous catalysts having bidisperse pore structures were introduced in the early papers of Haynes and Sarma (1973) and Hashimoto and Smith (1974). More recently, Oktar et al. (1999b) illustrated the use of such a technique to evaluate adsorption equilibrium constants in macroreticular resin catalysts.

Batch adsorbers containing porous catalysts may be used to analyze the concentration decay curves of an adsorbate in an inert solvent, for the evaluation of effective diffusivities. In the present study, this idea, which was originally introduced in the early work of Furusawa and Suzuki (1975), was used for the derivation of moment expressions corresponding to catalysts having bimodal pore size distributions.

Species conservation equation in the macropores of a spherical porous catalyst may be expressed as,

$$\frac{D_a}{R^2} \frac{\partial}{\partial r}\left(R^2 \frac{\partial C_A}{\partial R}\right) - \left(\frac{3}{r_o}\right)\rho_p D_i \frac{\partial q}{\partial r}\bigg|_{r=r_o} = \varepsilon_a \frac{\partial C_A}{\partial t} \qquad (5.13)$$

Derivation of equations are given in Appendix. In macroreticular resin catalysts, diffusing species within the macropores adsorb on the external surface of micrograins and then adsorbed species penetrate into the gel-like micrograins by diffusion (Oktar et al., 1999b). Significant interaction of diffusing species and the solid phase was expected during the diffusion process within the hydrogen bonded dense structure of micrograins. For this model, species conservation equation for the micrograins becomes

$$\frac{D_i}{r^2} \frac{\partial}{\partial r}\left(r^2 \frac{\partial q}{\partial r}\right) = \frac{\partial q}{\partial t} \qquad (5.14)$$

where, $q\big|_{r=r_o} = K C_A$. $\qquad (5.15)$

For a perfectly mixed batch adsorber, the mass conservation equation for the adsorbate in the liquid phase and the definition of n'th moment (μ_n) may be written as,

$$\frac{dC}{dt} = -\left(\frac{m_s}{\rho_P}\right)\left(\frac{3}{R_o}\right)D_a \left.\frac{\partial C_A}{\partial R}\right|_{R=R_o} \tag{5.16}$$

$$\mu_n = \int_o^\infty \left(\frac{C - C_e}{C_o - C_e}\right)t^n dt \tag{5.17}$$

The zeroth moment expression derived for the bidisperse system described by Eqns. 5.13-5.16 becomes

$$\mu_o = \frac{\rho_p K}{15\left(1 + \dfrac{m_s}{\rho_p}\rho_p K\right)}\left(\frac{R_o^2}{D_a} + \frac{r_o^2}{D_i'}\right) \tag{5.18}$$

fo $\rho_p K \gg \varepsilon_a$. Here, effective micrograin diffusivity D_i' is defined as,

$$D_i' = D_i \rho_p K \tag{5.19}$$

The ratio of diffusion resistances within the macropores and in the gel-like micrograins was characterized by a dimensionless parameter α, which was defined as,

$$\alpha = (R_o / r_o)^2 (D_i' / D_a) \tag{5.20}$$

For α values much greater than unity, micropore diffusion resistance may be neglected. For a catalyst with negligible micropore diffusion resistance, (monodispersed catalyst), diffusion and adsorption processes may be modeled by two different approaches; namely by considering diffusion and adsorption

terms separately within the porous catalyst (Model MB) or by assuming adsorption at the external surface of the catalyst followed by diffusion of adsorbed species into the pellet (Model MA). Model equations and the corresponding zeroth moment expressions for these two approaches are given in Table 5.14. Details of moment expression derivations are given in Appendix E.1.

Table 5.14 Model equations and zeroth moment expressions for a spherical monodisperse catalyst pellet.

MODEL MB	MODEL MA
$$\frac{D_a}{R^2}\frac{\partial}{\partial R}\left(R^2\frac{\partial C_A}{\partial R}\right)=\left(\varepsilon_a+\rho_pK\right)\frac{\partial C_A}{\partial t} \quad (5.21)$$	$$\frac{D_a}{R^2}\frac{\partial}{\partial R}\left(R^2\frac{\partial q}{\partial R}\right)=\frac{\partial q}{\partial t} \quad (5.24)$$
$C_A=C$ at $R=R_o$ (5.22)	$q=KC$ at $R=R_o$ (5.25)
$$\mu_o=\frac{R_o^2\left(\rho_pK+\varepsilon_a\right)}{15D_a\left(1+\frac{m_s}{\rho_p}\left(\varepsilon_a+\rho_pK\right)\right)} \quad (5.23)$$	$$\mu_o=\frac{R_o^2}{15D_a\left(1+\frac{m_s}{\rho_p}\left(\rho_pK\right)\right)} \quad (5.26)$$

The major limitation of using moment analysis for the evaluation of the adsorption and diffusion parameters is the assumption of linear adsorption isotherm used in the derivation. The nonlinear equilibrium relation $q=F(C)$ between the adsorbed concentration q and the fluid phase concentration C, may be expanded in Taylor series and following approximation may be made,

$$q-q_e=F'(C_e)(C-C_e)\ . \tag{5.27}$$

Derivation of moment expressions with such a linearization procedure yields similar moment expressions as given in Equations 5.18, 5.23 and 5.26 with K values, being the apparent adsorption equilibrium constants, evaluated

from the derivative of the adsorption isotherm at the concentration of interest. For a Langmuir adsorption isotherm of the form

$$q/q_m = K_A C/(1+K_A C), \tag{5.28}$$

apparent adsorption equilibrium constant may be found from,

$$K = K_A q_m/(1+K_A C_e)^2 \tag{5.29}$$

By using small amounts of catalyst in the batch adsorber, C_o and C_e values become sufficiently close and the use of constant apparent adsorption equilibrium constant may safely be justified. Experimental values of zeroth moment were evaluated from the concentration decay curves by the numerical integration of Eqn.5.17 and they were used for the evaluation of effective diffusivities from Eqns. 5.18, 5.23 and 5.26. In these analysis experimental data reported by Aydın (1999) are used. In these calculations, apparent adsorption equilibrium constant (K) values evaluated from Eqn. 5.29 were used. Some typical values of effective diffusivities and apparent K values obtained at different concentrations are summarized in Table 5.15.

The effective diffusivity values evaluated from the monodisperse models were found to be in the orders of magnitude of 10^{-5} cm^2/s and 10^{-7} cm^2/s for Models MB and MA, respectively. For large values of adsorption equilibrium constants, the relation between the effective diffusion coefficients of these two models can be expressed as,

$$D_{a, \text{(Model B)}} = D_{a, \text{(Model A)}} (\rho_p K) \tag{5.30}$$

Table 5.15 Diffusivities of Methanol, Ethanol and 2M2B in Amberlyst 15 (Doğu et al., 2003)

Species	C_e mmol/ml	μ_o , s	K,ml/g (Eq.17)	D_a , cm^2/s Model MA	D_a ,cm^2/s Model MB	D_s ,cm^2/s Model MB
Methanol (47° C)	0.038	86.4	66.8	8.0×10^{-7}	5.3×10^{-5}	2.10×10^{-6}
	0.024	76.8	109.2	7.8×10^{-7}	8.5×10^{-5}	2.18×10^{-6}
	0.010	63.1	221.8	7.0×10^{-7}	15.5×10^{-5}	2.06×10^{-6}
	0.006	55.7	268.4	7.2×10^{-7}	19.1×10^{-5}	2.17×10^{-6}
Ethanol (47° C)	0.088	80.0	28.2	10.1×10^{-7}	2.8×10^{-5}	2.44×10^{-6}
	0.056	82.5	45.9	9.1×10^{-7}	4.2×10^{-5}	2.40×10^{-6}
	0.033	82.4	71.3	8.3×10^{-7}	5.9×10^{-5}	2.29×10^{-6}
	0.024	83.4	87.4	7.7×10^{-7}	6.7×10^{-5}	2.17×10^{-6}
2M2B (24° C)	0.0100	56.5	86.5	12.4×10^{-7}	10.6×10^{-5}	3.72×10^{-6}
	0.0060	56.4	108.1	11.7×10^{-7}	12.5×10^{-5}	3.52×10^{-6}
	0.0047	56.1	116.9	11.5×10^{-7}	13.3×10^{-5}	3.48×10^{-6}
	0.0031	55.4	129.2	11.3×10^{-7}	14.5×10^{-5}	3.43×10^{-6}

As it is seen in Table 5.15, diffusivity (D_a) values obtained from Model MB are highly concentration dependent. Higher D_a values were obtained for higher values of apparent adsorption equilibrium constants. This is an indication of significance of surface diffusion in the macropores. Besides that, the D_a values found from this model were about in the same order of magnitude and even higher than the corresponding liquid phase molecular diffusion coefficients (D_M = 6.2×10^{-5} cm^2/s for ethanol, and 8.2×10^{-5} cm^2/s for methanol at 47°C; and 3.2×10^{-5} cm^2/s for 2M2B at 24° C) which were estimated from the Wilke-Chang model. This is another indication of significant contribution of surface diffusion. A similar conclusion was reached in the early work of Furusawa and Smith (1974)

for diffusion of benzaldehyde in liquid filled pores of Amberlite. In a macroporous particle, diffusivity may be expressed as,

$$D_a = D_M \frac{\varepsilon_a}{\tau} + \frac{1}{\tau}(\rho_p K)D_s \qquad (5.31)$$

Here, the first term corresponds to the effective molecular diffusivity within the macropores and the second term corresponds to the surface diffusion contribution. $\rho_p K$, which appears in the second term comes from the gradient of surface concentration using the adsorption isotherm . The tortuosity factor τ was approximated from the well known Wakao and Smith model as ($\tau = 1/\varepsilon_a$) as 3.1 in our system. The surface diffusivities (D_s) evaluated using Eqn. 5.31 were found to be constant (independent of concentration) for both alcohols and also for 2M2B (Table 5.15). Due to the significant contribution of surface diffusion, Model MA could also be considered to be a good representation of this system. The diffusion coefficients evaluated for Model MA were also found to be almost independent of concentration (Table 5.15).

The increase of adsorbed concentration of alcohols with an increase in temperature (especially over 320 K for liquid phase adsorption) was explained by the increased availability of active sites for adsorption, as a result of swelling of the catalyst and higher penetration of alcohol molecules into the gel-like structure of polymer at higher temperatures and also due to chemisorption of some of the alcohol molecules on the $-SO_3H$ sites of the catalyst.

Observed K and D_a values (Table 5.16) obtained from Model MB decreased, while D_s values were increased, with an increase in temperature, for 2M2B. Temperature dependence of D_a was strongly affected by the significance

of surface diffusion contribution. Surface diffusion coefficient D_s was expected to increase with temperature. However, the decrease of $\rho_p K$ with an increase of temperature was much more significant than increase of D_s for 2M2B. This resulted a decrease of D_a with temperature.

Table 5.16 Temperature effect on 2M2B diffusivities ($C_o = 0.0088$ mmol/ml)

T, K	K_A ml/mmol	C_e mmol/ml	K, ml/g	D_a, cm^2/s Model MA	D_a, cm^2/s Model MB	D_s, cm^2/s Model MB
297	35.8	0.0060	108.1	11.7×10^{-7}	12.5×10^{-5}	3.52×10^{-6}
306	11.8	0.0075	44.0	22.4×10^{-7}	9.9×10^{-5}	6.78×10^{-6}
309	6.5	0.0080	26.1	34.4×10^{-7}	8.4×10^{-5}	9.63×10^{-6}

However, for methanol, an increasing trend was observed for μ_o and for the corresponding D_a values evaluated from model MB (Table 5.17). Significance of surface diffusion was also apparent for alcohols. Contribution of surface diffusion term (second term on the right hand side of Eqn. 5.31) to effective macropore diffusivity, D_a, was higher than 85 % at all temperatures. Temperature dependence of μ_o obtained for ethanol showed a similar trend as methanol (Table 5.18). D_a values obtained from Model MA for both methanol and ethanol showed a slight decreasing trend with temperature. The unexpectedly high value of D_a found for ethanol at 334 K from Model MB is due to the high value of apparent K value estimated from Eqn. 5.31 using the adsorption equilibrium parameters reported by Oktar (2001).

Table 5.17 Temperature effect on methanol diffusivities (C_o=0.035 mmol/ml) (Doğu et al., 2003)

Temperature, K	C_e mmol/ml	μ_o s	D_a cm^2/s Model MA	D_a cm^2/s Model MB
306	0.022	66.6	9.7x10^{-7}	8.4x10^{-5}
317	0.020	69.1	8.8x10^{-7}	9.2x10^{-5}
329	0.019	70.2	8.2x10^{-7}	10.0x10^{-5}
339	0.016	76.4	6.6x10^{-7}	11.2x10^{-5}

Table 5.18 Temperature effect on ethanol diffusivities (C_o=0.12 mmol/ml) (Doğu et al., 2003)

Temperature, K	C_e mmol/ml	μ_o s	D_a cm^2/s Model MA	D_a cm^2/s Model MB
306	0.094	82.0	10.4x10^{-7}	1.6x10^{-5}
320	0.088	80.0	10.1x10^{-7}	2.8x10^{-5}
334	0.080	88.6	8.4x10^{-7}	4.1x10^{-5}
347	0.076	92.5	8.5x10^{-7}	2.9x10^{-5}

5.5 TAME and TAEE Production in a Batch Reflux-Recycle Reactor

Chemical analysis of the samples taken from the reboiler at different times showed that the only products observed in the reaction of isoamylene with methanol or ethanol is TAME or TAEE, respectively. No side products were observed in gas chromatographic analysis. Such very high selectivity values approaching to unity were obtained due to very short contact times (per pass) of reactants with the catalyst bed in the proposed batch reflux recycle reactor. Instantaneous values of fractional conversion of isoamylene to the respective ether were evaluated from the reboiler compositions. At any instant, conversion of 2M2B (ξ_{IA}) in the reboiler was evaluated from

$$\xi_{IA} = \frac{X_E}{X_E + X_{IA}} \tag{5.32}$$

Here, X_E and X_{IA} are the mole fractions of ether (TAME or TAEE) and isoamylene in the reboiler, respectively.

5.5.1 Batch Reflux-Recycle-Reactor Results for TAME Production and Model Predictions

The initial values of vapor phase IA concentrations (in methanol) and the bubble point pressures corresponding to each liquid phase concentration used in experiments conducted at 94°C reboiler temperature, are summarized in Table 5.19. As it is seen in Table 5.19, a liquid phase IA mole fraction of 0.25 corresponds to a vapor phase IA mole fraction of about 0.55 at 94 °C. Similarly, vapor phase reactor inlet IA mole fractions and the bubble point pressures corresponding to different reboiler temperatures for a liquid phase containing 6 mole % IA (in methanol) are given in Table 5.20. Vapor phase compositions were calculated using the experimental liquid mole fractions. In these calculations, the program WSMMAIN was used (Orbey and Sandler, 1995, 1998). This program calculated multicomponent VLE using the PRSV EOS and the Wong-Sandler mixing rule. Also, NRTL excess free-energy model was used with this mixing rule.

Table 5.19 Initial values of liquid and reactor inlet vapor compositions in IA-methanol reaction at 94°C

Liquid mole fraction of 2M2B in the reboiler	0.046	0.060	0.100	0.250
Reactor inlet vapor mole fraction of 2M2B	0.27	0.31	0.41	0.55
Bubble point pressure, bar	3.7	3.9	4.5	5.5

Table 5.20 Initial values of reactor inlet vapor compositions in IA-methanol
reaction at a liquid feed composition of 6 mole % IA in methanol

Reboiler Temperature, °C	72	82	94	104
Reactor inlet vapor mole fraction of 2M2B	0.38	0.35	0.31	0.29
Bubble point pressure, bar	2.1	2.8	3.9	5.2

Time dependence of experimental conversion values of 2M2B to TAME, obtained at 94°C with different feed compositions is shown in Figure 5.23.
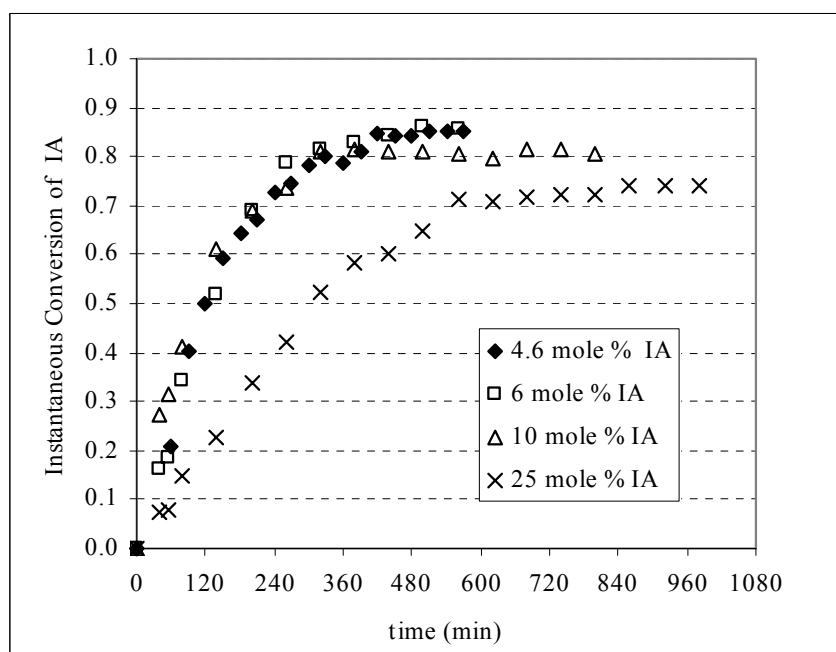
Figure 5.23. Time dependence of instantaneous conversion of 2M2B to TAME (evaluated at the reboiler) at different feed compositions (T=94°C)

In order to predict the variation of the composition of the species and the instantaneous conversion of IA in the reboiler, conservation equations were written for both the reactor and the reboiler sections in the second isothermal

119

period of operation of the batch Reflux-Recycle-Reactor. Major assumptions of the model include plug flow in the reactor section, perfect mixing in the reboiler and vapor-liquid equilibrium between the liquid in the reboiler and reactor inlet stream. Considering very short residence times of molecules in the reactor section (couple of seconds per pass) as compared to the time scale of concentration variations measured in the reboiler (couple of hours), a pseudo-steady state assumption was made for the reactor section, after the preheat period. Also, vapor stream flow rate, Q, was assumed as constant along the reactor (in this second period of operation), which was justified by calculations based on energy and material balances around the reboiler, condenser and the reactor.

$$QC_{IA,o}^{V} \frac{d\xi_{IA}^{V}}{dW} + R_{IA} = 0 \qquad \text{(Reactor section)} \qquad (5.33)$$

$$QC_{IA,o}^{V}\left(1 - \xi_{IA,f}^{V}\right) - QC_{IA,o}^{V} = V \frac{dC_{IA}^{L}}{dt} \qquad \text{(Reboiler)} \qquad (5.34)$$

There are number of mechanisms, which are explained previously, including Langmuir-Hinshelwood and Rideal-Eley type rate models, proposed in the literature for such etherification reactions (Subramaniam and Bhatia, 1987; Parra et al., 1994; Oost and Hoffmann, 1996; Rihko and Krause, 1996; Linnekoski et al., 1997; de Lasa et al., 1999). From the Diffuse Reflectance FTIR studies reported in Section 5.2, it was shown that adsorbed alcohols and adsorbed isoolefin molecules both participate in the reaction mechanism in vapor phase etherification reactions. However, the adsorption equilibrium constants of alcohols are much higher than the adsorption equilibrium constants of isoolefins. In fact, the adsorption equilibrium constants of ethanol and methanol on Amberlyst-15 were reported to be at least 2 orders of magnitude greater than

the adsorption equilibrium constants of isoamylenes (Oktar et al, 1999b). As a result of this difference, most of the surface was expected to be covered by alcohol molecules and zero order dependence of the rate on alcohol concentration was expected at sufficiently high alcohol concentrations. In fact, this zero order dependence of the rate on alcohol concentration was also reported by Tejero et al. (1996) for MTBE synthesis for alcohol/isoolefin mole ratios greater than 0.59. A similar conclusion was reached by Piccoli and Lovisi (1995) for synthesis of TAME. For all of the experiments conducted in this work, alcohol concentration in the vapor phase reactor section may be assumed as excess. With these considerations and basing on the proposals reported in the literature, a simple reversible rate expression with apparent forward reaction rate orders of one and zero for isoamylene and alcohol, respectively, was assumed to obtain model predictions.

$$- R_{IA} = k_1 \left(C_{IA}^V - C_E^V / (K^{(V)} C_M^V) \right)$$ (5.35)

Our earlier studies on TAEE synthesis over Amberlyst-15 had also shown an apparent first order dependence of reaction rate on isoamylene concentration in systems where alcohol concentration was in excess (Oktar et al., 1999a). Our experimental results also indicated small variation of alcohol concentration along the reactor. Consequently, constant alcohol concentration assumption in the reactor section is not expected to bring major error to the analysis.

With these considerations, a first order reversible reaction rate model was assumed and following expression was obtained for conversion per pass at the reactor outlet.

$$\xi_{IA,f}^{V} = \xi_{IA,e}^{V}\left[1 - \exp\left(-\frac{(M+1)}{(M+\xi_{IA,e}^{V})}\frac{k_1 W}{Q}\right)\right].$$ (5.36)

Here, $\xi_{IA,e}^{V}$ is the vapor phase equilibrium conversion that could be achieved at the outlet of the reactor section and M is the ratio of concentrations of the product ether and isoamylene at the reactor inlet, $M = C_{E,o}^{V} / C_{IA,o}^{V}$.

Combining Eqns.5.34 and 5.36, following expression may be written for the rate of change of concentration of IA in the reboiler as a function of time.

$$\frac{dC_{IA}^{L}}{dt} = -\frac{QK_{IA}}{V}\xi_{IA,e}^{V}\left[1 - \exp\left(-\frac{(M+1)}{(M+\xi_{IA,e}^{V})}\frac{k_1 W}{Q}\right)\right]C_{IA}^{L}$$ (5.37)

Here K_{IA} is the vapor liquid equilibrium constant of isoamylene evaluated at the reboiler composition, temperature and pressure.

$$C_{IA,o}^{V} = K_{IA}C_{IA}^{L}$$ (5.38)

The system under consideration is highly nonideal. Due to variations in the composition of the mixture in the reboiler, K_{IA}, $\xi_{IA,e}^{V}$ and M are expected to change as a function of time. Consequently, instead of using the analytically integrated form of Eqn. 5.37 in checking the experimental data, differential analysis was preferred.

Experimental values of $\left(-\dfrac{dC_{IA}^{L}}{dt}\right)$ were evaluated by differential analysis of the concentration data obtained for isoamylene (C_{IA}^{L}) in the reboiler. At each

data point corresponding to different times, $\dfrac{dC_{IA}^{L}}{dt}$, M, Q, K_{IA} and $\xi_{IA,e}^{V}$ values were evaluated and substituted into Eqn. 5.37 to calculate forward apparent rate constant, k_1 (see Appendix D5 for sample calculation). The values of M were determined from the experimental values of ether and isoamylene mole fractions in the reboiler using the VLE calculations. The vapor flow rate (Q) values in the reactor were estimated from the heat input rate to the reboiler by making adiabatic reboiler assumption. In this estimation procedure heat input from the electrical heater was equated to the summation of heat of vaporization of the reboiler mixture and sensible energy required to increase the temperature of the condensed recycled stream to the reboiler temperature.

In most of the experiments, reported in Figure 5.23, the average value of vapor flow rate within the reactor was kept in the range of 200-265 cm^3/sec. However, at high olefin concentrations, some decrease in heat input to the reboiler was necessary, because of experimental difficulties to control the system pressure and temperature at the desired values in these experiments. This was especially correct in experiments conducted with 25% isoamylene. For this case, the average value of vapor flow rate within the reactor was about 62 cm^3/min. This is the major reason of obtaining lower instantaneous conversions (as evaluated from the reboiler compositions) in the set of experiments conducted with that composition (Figure 5.23).

Vapor-liquid equilibrium constant values (K_{IA}) were estimated using WSNMAIN program (Orbey and Sandler, 1995, 1998). In this estimation procedure, experimental reboiler compositions, temperature and pressure values were used at each data point.

The vapor phase equilibrium conversion value of isoamylene ($\xi_{IA,e}^{V}$) at the exit of the reactor section was estimated from the corresponding equilibrium constants. Equilibrium constants for liquid phase reactions R1 and R2 are reported by Rihko and Krause, (1995) and Kitchaiya and Datta, (1995).

For the same reactions, vapor phase chemical equilibrium constants were estimated from the liquid phase equilibrium constants, following the procedure reported by Jensen and Datta (1995). In this procedure, free energy of reaction values for the vapor phase reaction were estimated from the free energy of reaction in the liquid phase. Vapor phase equilibrium constants for these two reactions evaluated at different temperatures are given in Table 5.21.

Table 5.21 Estimated vapor phase equilibrium constants

Temperature, K	$K^{(V)}$ for TAME reaction (R1)	$K^{(V)}$ for TAEE reaction (R2)
345	0.471	0.165
355	0.313	0.110
367	0.200	0.071
377	0.141	0.046

Using the equilibrium constants reported in Table 5.21, equilibrium conversions of isoamylene were evaluated at each data point using the following expression

$$K^{(V)} = \frac{1}{P} \frac{(M + \xi_{IA,e}^{V})(1 - y_{IA,o}\xi_{IA,e}^{V})}{(1 - \xi_{IA,e}^{V})(y_{M,o} - y_{IA,o}\xi_{IA,e}^{V})} \tag{5.39}$$

A set of results obtained at 94°C with an initial reboiler composition of 10 % isoamylene in methanol are reported in Table 5.22. As it is seen in this table, variation of K_{IA} value with respect to time was quite small. However, M values

and the corresponding C_E^L / C_{IA}^L values in the reboiler increased significantly (as expected) with an increase in conversion. Equilibrium conversion of IA ($\xi_{IA,e}^V$), as evaluated from Eqn. 5.39, showed a significant decrease as time was increased. At very long times, reactor inlet composition may approach to chemical reaction equilibrium in vapor phase at the corresponding temperature and $\xi_{IA,e}^V$ value is expected to reach zero. The value of rate constant, k_1, obtained at different data points from differential analysis, is almost constant (Table 5.22).

Table 5.22 Parameters evaluated at some data points corresponding to an initial IA-methanol mixture of 10% IA. (T=94°C)

Time (min)	$\xi_{IA,e}^V$	K_{IA}	C_M^V	$M = \dfrac{C_{E,o}^V}{C_{IA,o}^V}$ (Reactor inlet)	$\dfrac{C_E^L}{C_{IA}^L}$ (Reboiler)	k_1 (m³/g.s)
40	0.358	0.0314	0.713	0.024	0.38	0.207
80	0.332	0.0295	0.721	0.047	0.70	0.206
320	0.205	0.0336	0.859	0.295	4.25	0.237
500	0.183	0.0316	0.841	0.307	4.26	0.225
680	0.185	0.0321	0.847	0.308	4.31	0.234

Similar results are obtained with different initial feed compositions at 94°C. As it is seen in Table 5.23, k_1 values did not also change much by changing feed composition. These results showed that the pseudo first order rate assumption used in the derivation of Eqn. 5.35 was quite acceptable. An important conclusion reached from this analysis is related to the very high experimental conversion values obtained in this work. As it is seen in Table 5.22, even the initial value of vapor phase equilibrium conversion that could be reached at the exit of the reactor section was less than 0.36. However, the experimental instantaneous conversion values obtained from the reboiler compositions, reached values close to 0.90 at 94°C (Figure 5.23). These results

showed one of the advantages of the proposed batch Reflux-Recycle-Reactor as compared to a single pass vapor phase fixed bed catalytic reactor.

Table 5.23 Calculated apparent rate constants for IA-methanol reaction carried out at different initial feed compositions (94°C).

Initial feed composition of IA	k_1,average cm^3/g.s	$\xi_{IA,e}^V$ (range)
4.6	0.221	0.365- 0.164
6	0.230	0.359 - 0.152
10	0.224	0.369 - 0.200
25	0.212	0.341 - 0.190

As it was mentioned before, in the experiments conducted with 25% isoamylene in methanol, vapor flow rate in the reactor (Q) was much lower than the other experiments. This is the major reason of obtaining lower instantaneous conversion values at that composition (Figure 5.23). However, the rate constant, k_1, obtained at that composition was about the same as the corresponding values obtained at other compositions (Table 5.23). This result justified that, even at that composition pseudo-first order dependence of the reaction rate on isoamylene concentration and pseudo-zero order dependence on alcohol concentration did not bring significant error to the analysis procedure.

5.5.2 Temperature Dependence of Rate Constant for TAME Production

Figure 5.24 illustrates the time dependence of 2M2B conversion values obtained at different temperatures at a liquid stream composition of 6 mole % 2M2B in methanol. Initial vapor phase mole fractions of IA, as estimated from the corresponding liquid phase compositions are given in Table 5.20. Changes in reaction temperature are expected to change the equilibrium conversion at the reactor outlet ($\xi_{IA,e}^V$) and K_{IA} values as well as the apparent rate constant, k_1. A

decrease in $\xi_{IA,e}^{V}$ values is expected with an increase in temperature. Vapor liquid equilibrium constants of isoamylene (K_{IA}) evaluated from WSNMAIN program showed about 45% increase with an increase in temperature from 72°C to 104°C.
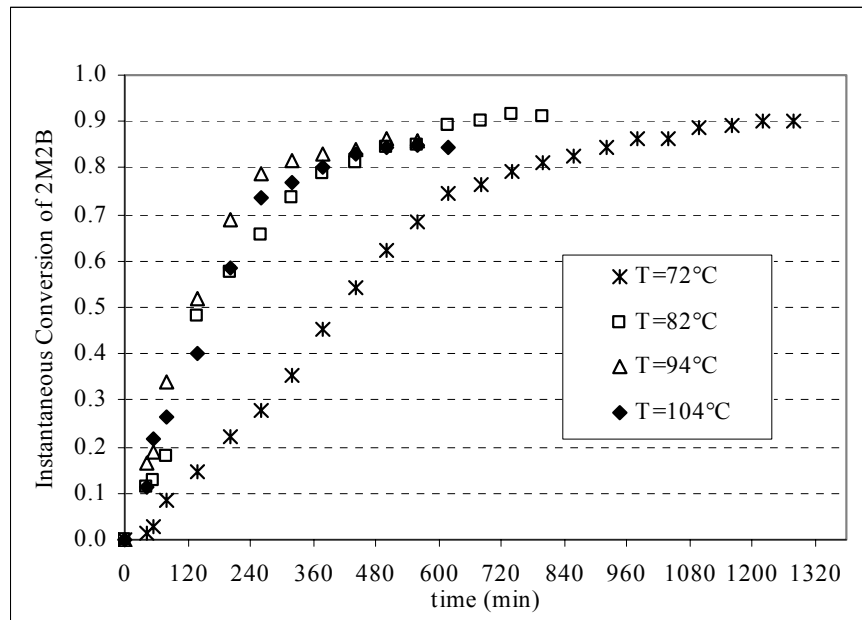
Figure 5.24 Time dependence of instantaneous conversion of 2M2B to TAME (evaluated at the reboiler) at different temperatures (feed compositions: 6 mole % mixture of 2M2B in methanol)

The value of vapor flow rate in the reaction section (Q) was around 240 cm^3/s at 94°C and 104°C. Due to experimental difficulties in control of system pressure, somewhat lower initial Q values were used at lower temperatures and especially at 72°C. The reaction rate constant, k_1, was then evaluated at each data point following the differential analysis procedure. Results showed that fluctuations of k_1 values, evaluated from different data points of experiments obtained at the same temperature, were quite small. Average values of apparent rate constant evaluated at each temperature are reported in Table 5.24. At lower temperatures, reaction rate is rather low and consequently much longer times are necessary to reach conversion values over 0.90 (Figure 5.24).

Table 5.24 Apparent rate constants and vapor phase equilibrium conversion ranges in each set of IA-methanol reaction at different temperatures (Initial composition: 6 mole% IA in methanol)

T (°C)	k_1,average (cm^3/g.s)	$\xi_{IA,e}^V$ (range)
72	0.158	0.463 - 0.1834
82	0.184	0.394 - 0.054
94	0.230	0.354 - 0.151
104	0.332	0.309 - 0.363

Experimental values of maximum conversions obtained at longer times, are plotted as a function of temperature in Figure 5.25. In the same figure, vapor phase equilibrium conversions that could be reached at the same temperature and with feed compositions corresponding to the initial compositions of the reboiler mixture are also shown. As it is clearly seen in this figure, conversions obtained in this work are more than twice the corresponding equilibrium conversion values calculated with these assumptions.
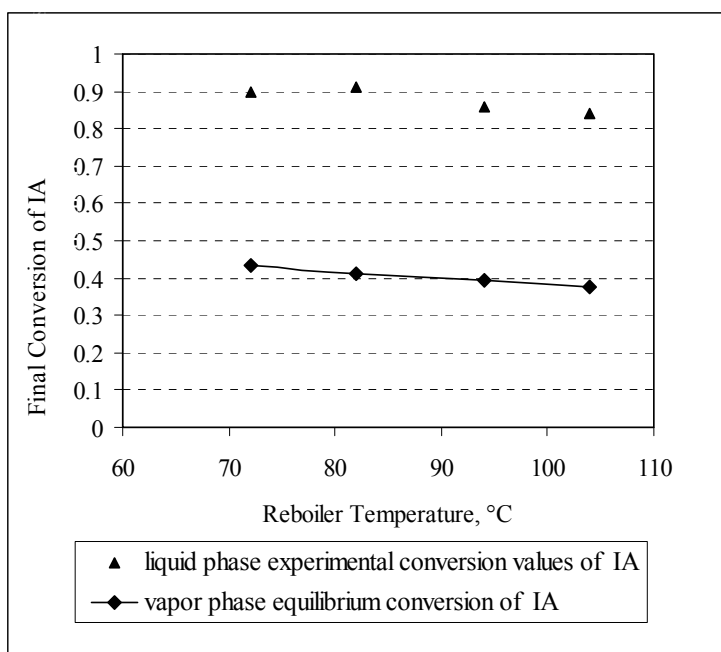
Figure 5.25 Comparison of maximum conversions of IA (at the reboiler) obtained in TAME synthesis at different temperatures with the corresponding vapor phase equilibrium conversions (corresponding to the initial reboiler compositions)

Temperature dependence of reaction rate constants, k_1, is shown in Figure 5.26. The apparent activation energy of k_1 was evaluated as 24.8 kJ $(mol)^{-1}$. To our knowledge there is no activation energy value reported in the literature for vapor phase synthesis of TAME. However, the liquid phase activation energy values reported in the literature for etherification reactions of 2M1B and 2M2B with methanol are in the range of 72-94 $kJ(mol)^{-1}$ (Subramaniam and Bhatia, 1987; Hwang and Wu, 1994; Piccoli and Lovisi, 1995; Rihko et al., 1997; Kiviranta-Paakkonen et al., 1998; Paakkonen et al., 2003). This low value of activation energy obtained in this work for vapor phase synthesis of TAME is expected to be majorly due to significance of transport resistance in our system.
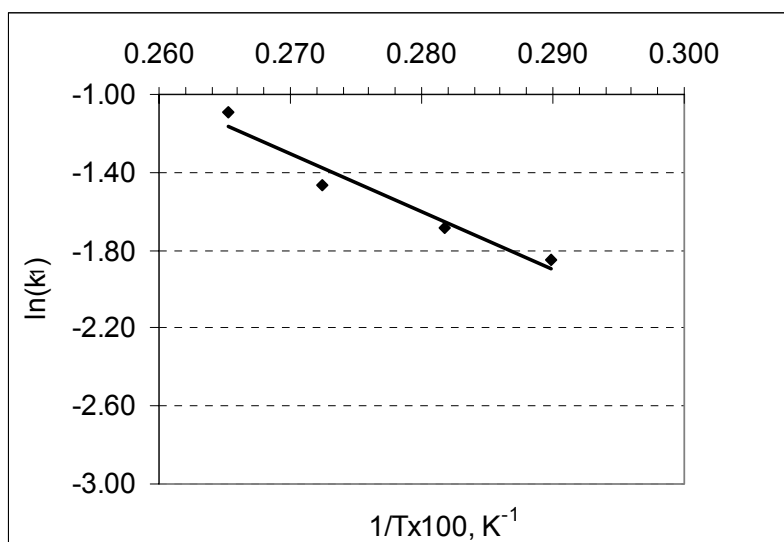
Figure 5.26 Temperatures dependence of the apparent rate constants of IA etherification reaction with methanol.

As it was discussed above, a thin liquid film is expected to form over the catalyst particles in the batch Reflux-Recycle-Reactor, due to condensation of the product, especially during the heat up period and also at the initial times of the isothermal operation period of the reactor. Macropores of the Amberlyst-15 were also expected to be filled with liquid, which was expected to be majorly

composed of product ether, and reactant alcohol. In fact, the catalyst particles taken out from the reactor at the end of the experiments were found to be wet and swelled. It is well known that Amberlyst-15 particles are swelled in the presence of polar molecules, like alcohols. In this system three transport resistances may effect the observed rate. These resistances are transport resistance of IA from vapor phase to the catalyst surface through the thin liquid film covering the external catalyst surface, diffusion resistance in the macropores and diffusion resistance in the gel-like micrograins of Amberlyst-15. Effects of diffusion resistances in the macropores and also in the gel-like micrograins of Amberlyst-15, may be tested using the criterion proposed in the literature (Dogu and Dogu, 1980; Dogu, 1998).

The value of effective diffusion coefficient of 2M2B in the macropores of Amberlyst-15 catalyst was estimated as 1.8×10^{-5} cm^3/s at 370 K from the data reported in Section 5.4. Particle and gel-like micrograin radii of Amberlyst-15 are $R_o = 3.7 \times 10^{-4}$ m and $r_o = 1.14 \times 10^{-8}$ m, respectively (Dogu et al., 2003). There is no published data for diffusion coefficient (D_i) of 2M2B in the gel-like micrograins. However, D_i value of isobutylene was reported as 2.6×10^{-12} cm^2/s at 358 K (Oktar et al., 1999b). Somewhat smaller D_i value was expected for 2M2B. By taking the order of magnitude of D_i as 1×10^{-12} cm^2/s, the value of parameter G (Eqn. 5.2) was estimated as 2×10^{-2}. This is a clear indication that diffusion resistance in the gel-like micrograins is significantly smaller than macropore diffusion resistance in our system and can be neglected. Knowing the observed reaction rate constants (Tables 5.25 and 5.26), observed rates were estimated and the order of magnitude of the dimensionless group which appear on left hand side of criterion given in Eqn. 5.2 was estimated to be greater than 15. This is a clear indication of significance of macropore diffusion resistance on the observed rate. In this system, diffusion resistance through the liquid film

covering the catalyst particles is also expected to have some effect on the observed rate. Due to such contributions of transport resistances, lower observed activation energies are expected in our system.

Table 5.25 Calculated apparent rate constants for IA-methanol reaction carried out at different initial feed compositions (94°C)

Initial feed composition of IA	k_1,average cm^3/g.s
4.6	0.22
6	0.23
10	0.23
25	0.22

Table 5.26 Apparent rate constants and vapor phase equilibrium conversion ranges in each set of IA-methanol reaction at different temperatures (Initial composition: 6 mole % IA in methanol)

T (°C)	k_1,average (cm^3/g.s)
72	0.16
82	0.19
94	0.23
104	0.34

5.5.3 Results Obtained for TAEE Synthesis

Similar experiments were also carried out with ethanol-IA mixtures to produce TAEE. Initial values of reactor inlet vapor compositions of experiments conducted at 94°C using IA-ethanol mixtures are reported in Table 5.27.

Table 5.27 Initial values of reactor inlet vapor compositions in IA-ethanol reaction at 94°C

Liquid mole fraction of 2M2B in the reboiler	0.04	0.10
Reactor inlet vapor mole fraction of 2M2B	0.19	0.35
Bubble point pressure, bar	2.2	2.7

As it is seen in Figures 5.27 and 5.28, lower conversion values of IA to TAEE were observed as compared to conversion values obtained in TAME synthesis. This is majorly due to less reactivity of ethanol as compared to methanol.
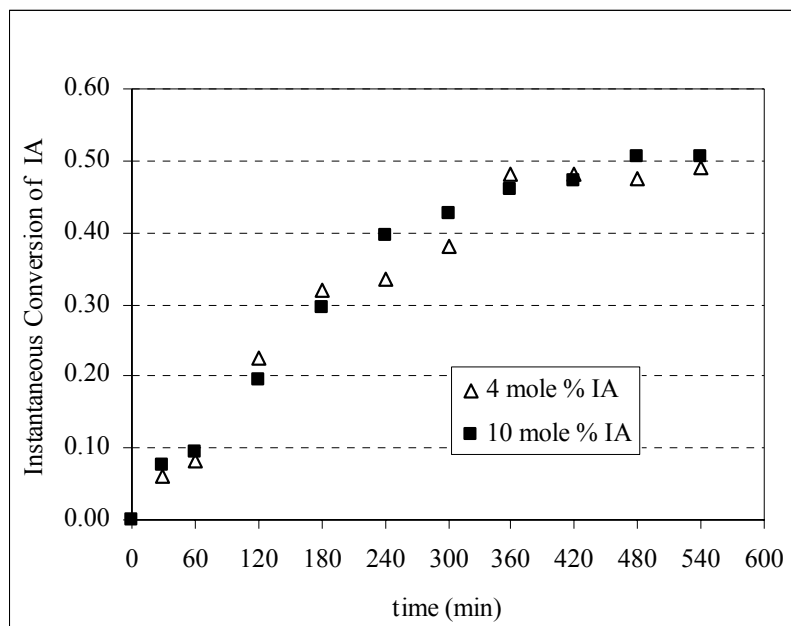
Figure 5.27. Time dependence of instantaneous conversion of IA to TAEE (evaluated at the reboiler) at different feed compositions (T=94°C)
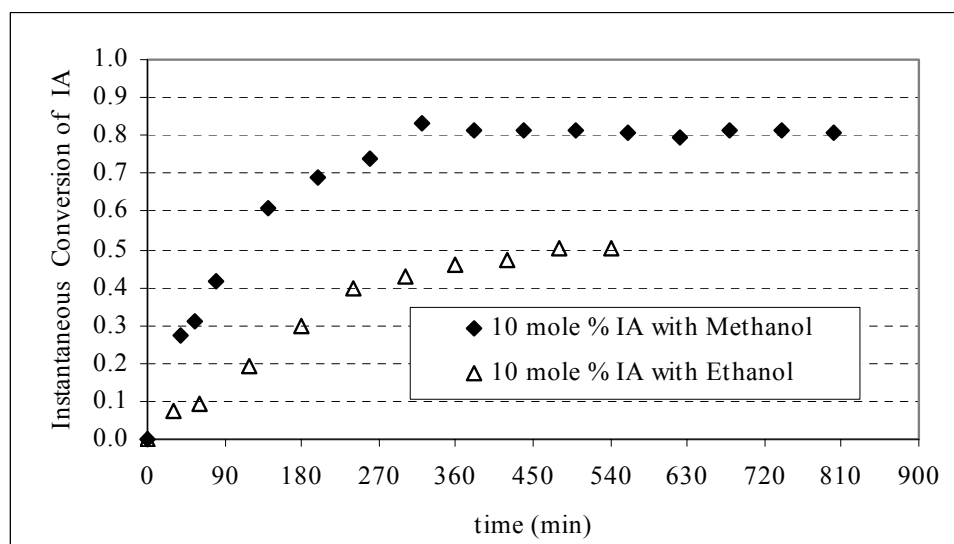
Figure 5.28. Comparison of conversions of IA in reactions with methanol and ethanol (T= 94°C)

A similar differential analysis was applied to calculate forward apparent

rate constant, k_1, by substituting $\dfrac{dC_{IA}^{L}}{dt}$, M, Q, K_{IA} and $\xi_{IA,e}^{V}$ values in Eqn.5.37.

To illustrate the results of these calculations, a set of results obtained at some

data points obtained with an initial reboiler composition of 10 mole % IA in

ethanol are reported in Table 5.28 (at 94°C). As it is seen in Table 5.28, the

value of rate constant, k_1, obtained at different data points from differential

analysis, is almost constant.

Table 5.28 Parameters evaluated at some data points corresponding to an initial
IA-ethanol mixture of 10 mole % IA (T=94°C)

Time (min)	$\xi_{IA,e}^{V}$	K_{IA}	$M = \dfrac{C_{E,o}^{V}}{C_{IA,o}^{V}}$ (Reactor inlet)	$\dfrac{C_{E}^{L}}{C_{IA}^{L}}$ (Reboiler)	k_1 (m^3/g.s)
60	0.122	0.0449	0.005	0.11	0.062
120	0.117	0.0454	0.012	0.25	0.061
240	0.109	0.0494	0.032	0.65	0.056
420	0.091	0.0461	0.045	0.90	0.059
540	0.084	0.0454	0.051	1.03	0.059

Similar results were obtained with 4 mole % IA in ethanol at an initial

feed composition of 94°C. As it is seen in Table 5.29, k_1 values did not also

change much by changing feed composition. For IA-ethanol system, much longer

times were needed to reach high conversions, as compared to IA-methanol

system. As it was illustrated in Figure 5.28, conversion values obtained with

ethanol (using 10 mole % IA in the liquid feed) were much lower than the

corresponding values obtained with methanol. This result agreed well with the

literature indicating that methanol was more reactive than ethanol in

etherification reactions using Amberlyst-15.

Table 5.29 Calculated apparent rate constants for IA-ethanol reaction carried out at different initial feed compositions (94°C)

Initial feed composition of IA	k_1,average cm^3/g.s
4	0.060
10	0.059

CHAPTER 6

CONCLUSIONS AND RECOMMENDATIONS

In this study, kinetic studies and reaction mechanism for the production of tertiary ethers used as gasoline additives were investigated in details. Major conclusions are summarized;

1. Hydrogen ion-exchange capacity of acidic resin catalysts was a major factor on the activity in the etherification reactions of isoamylenes with ethanol. For 2M1B, which was much more reactive than 2M2B, hydrogen ion-exchange capacity of the catalyst becomes insignificant over a hydrogen ion-exchange capacity of 2.8 meq.H^+/g. This was concluded to be majorly due to the increased significance of diffusion resistance on the observed rate.

2. DRIFT spectra obtained with alcohols (ethanol and methanol) and isobutylene on acidic ion–exchange resin catalysts showed that alcohols and isobutylene were both adsorbed on the $-SO_3H$ sites of the catalyst during etherification reactions. Adsorbed alcohol molecules were bridged by hydrogen bonds to each other and also to the $-SO_3H$ sites of the catalyst. It was also concluded that, in addition to the hydrogen bonded adsorbed species, some alcohol molecules were strongly

chemisorbed to the active sites by dissociation of one or two of the carbon bonded hydrogen atoms. Isobutylene was found to be more adsorbed in the presence of alcohols. A bridged structure of adsorbed isobutylene between the adsorbed alcohols and the $-SO_3H$ sites was proposed to explain this behavior. By the increase of temperature, C=C bond was weakened both in the adsorption and reaction experiments. It was concluded that the ether molecules (MTBE and ETBE) are formed on the catalyst surface in adsorbed state. All these results supported a Langmuir-Hinshelwood type reaction mechanism involving adsorbed alcohol and isobutylene molecules in the synthesis of MTBE and ETBE on acidic ion-exchange resin catalysts.

3. DRIFTS results obtained with 2M1B, methanol and TAME in adsorption and reaction experiments proved that all three of these species were adsorbed on Amberlyst 15 and supported a Langmuir-Hinshelwood type reaction mechanism. Adsorbed TAME molecules were found to dissociate on the catalyst surface with an increase of temperature, forming methanol and adsorbed t-amyl species. It was concluded that 2M1B was adsorbed forming a bridged structure between the $-SO_3H$ sties and adsorbed alcohol molecules.

4. Basing on the DRIFTS results obtained with TAME at different temperatures and also with isoamylenes, ethanol, methanol, isoamylene–alcohol mixtures a Langmuir-Hinshelwood type reaction mechanism explains the synthesis of TAME and TAEE over Amberlyst-15. Since the adsorption equilibrium constants of alcohols are about two orders of magnitude greater than the adsorption equilibrium constants of isoamylenes and tert-ethers, number of available sites are

drastically decreased with an increase in alcohol activities. Consequently, a sharp maximum was observed in the rate of tert-ether formation when plotted as a function of activity ratio of alcohol to isoamylene.

5. Effective diffusion coefficients evaluated from batch adsorption experiments of methanol, ethanol and 2M2B showed that surface diffusion had significant contribution to the total diffusion flux into a macroreticular resin catalyst, namely Amberlyst-15. In liquid filled pores, macropore diffusion resistance was found to be much more significant than diffusion resistance inside the gel-like micrograins. It was also shown that, moment analysis of concentration decay curves obtained in batch adsorption experiments can be used for the evaluation of effective diffusivities.

6. The batch Reflux-Recycle reactor proposed here was shown to give high yields and selectivities and recommended for equilibrium limited reactions in which relative volatilities of reactants were much higher than products. Conversion values over 0.91 were achieved in TAME synthesis with no formation of side products. The apparent activation energy of k_1 was evaluated as 24.8 kJ $(mol)^{-1}$ in TAME synthesis. This low value of activation energy for TAME synthesis is concluded to be majorly due to significance of transport resistances in the batch Reflux-Recycle-Reactor. Pore diffusion resistance in the gel-like micrograins is significantly smaller than macropore diffusion resistance in our system and can be neglected. However, significant transport resistances are expected in the macropores and also through the thin liquid film covering the catalyst particles. It was also concluded that, reactivity of

methanol was higher than ethanol in the etherification reaction of isoamylenes, over Amberlyst-15.

7. As a result of catalyst development, characterization, kinetic and reactor development studies carried out in this study, it was concluded that tert-amyl-ethyl-ether (TAEE) could be effectively produced and used as a gasoline blending oxygenate.

REFERENCES

Ahmed, F.E., 2001, "Toxicology and human health effects following exposure to oxygenated or reformulated gasoline", Toxicology Letters, Vol. 121, pp.89-113.

Aiouache, F. and Goto, S., 2003, "Sorption effects on kinetics of etherification of *tert*-amyl alcohol and ethanol", ", Chem. Eng. Science,Vol.58, pp. 2065-2077.

Ali, A. and Bhatia, S., 1990, "Methyl tertiary butyl ether formation in a catalytic bed reactor-kinetic and modeling study", Chem. Eng. J., Vol. 44, pp. 97-106.

Al-Jarallah, A. M., Siddiqui, M.A.B., Lee, A.K.K., 1988, "Kinetics of Methyl Tertiary Butyl Ether Synthesis Catalyzed by Ion Exchange Resin", Can. J. Chem. Eng., Vol. 66, pp. 802-806.

Ancillotti, F. and Fattore, V., 1998, "Oxygenate fuels: Market and expansion and catalytic aspect of synthesis", Fuel Processing Technology, 57, pp. 163–194.

Ancillotti, F., Mauri M.M., Pescarollo, E., and Romagnoni, L., 1978, "Mechanisms in the reaction between olefins and alcohols catalyzed by ion exchange", Journal of Molecular Catalysis, Vol. 4, pp. 37-48.

Aydın, E., 1999, "Adsorption Studies for Alcohols, Iso-olefins and Corresponding Ethers (ETBE, TAME) on Amberlyst-15", MS Thesis, Middle East Technical University, Ankara.

Baur, R., Krishna, R., 2002, "Hardware selection and design aspects for reactive distillation columns. A case study on synthesis of TAME", Chemical Engineering and Processing, Vol. 41, pp. 445-462.

Baur, R., Taylor, R., Krishna, R., 2003, "Bifurcation analysis for tame synthesis in a reactive distillation colunm: comparison of pseudo-homogeneous and heterogenous reaction kinetics models", Chemical Engineering and Processing, Vol. 42, pp. 211-221.

139

Brown, S.L., 1997 , Atmospheric and potable water exposures to methyl *tert*-butyl ether (MTBE). Reg. Toxicol. Pharmacol., 25, pp. 256–276.

Caprino, L. and Tonga, G.I, 1998, "Potential health effects of gasoline and its constituents: a review of current literature (1990–1997) on toxicology data", Environ. Health Perspect*., Vol. 106, pp. 115–125.

Çersu, F., 1995, "Kinetics of Vapor Phase Production of ETBE", MS Thesis, Middle East Technical University, Ankara.

Chu, P., and Kühl, G.H., 1987, "Preparation of Methyl tert-Butyl Ether (MTBE) over Zeolite Catalysis", Ind. Eng. Chem. Res., Vol. 26, pp. 365-369.

Colombo, F., Cori, L. , Dalloro, L., and Delogu, P., 1983, "Equilibrium Constant for the Methyl tert-Butyl Ether Liquid-Phase Synthesis by use of UNIFAC", Ind. Eng. Chem. Res., Vol. 22, pp. 219-223.

Cunill, F., Vila, M., Izquierdo, J.F., Iborra, M., Tejero, J., 1993, "Effect of Water Presence on Methyl tert-Butyl Ether and Ethyl tert- butyl Ether liquid Phase Synthesis", Ind. Eng. Chem. Res., Vol. 32, pp. 564-569.

De Lasa, H., Fournier, P., Prakash, A., Tarek, E. S., 1999, "MTBE Synthesis in a Novel Riser Simulator", Can. J. Chem. Eng., Vol. 77, pp. 413-419.

Dekant, W., Bernauer, U., Rosner, E., and Amberg, A., 2001, "Toxicokinetics of ethers used as fuel oxygenates", Toxicology Letters, Vol. 124, pp. 37-45.

Dogu G and Dogu T. A general criterion to test the importance of diffusion limitations in bidisperse porous catalysts. AIChE Journal. 1980; 26 (2): 287-288.

Dogu T. Diffusion and reaction in catalyst pellets with bidisperse pore size distribution. Ind. Eng. Chem. Res. 1998; 37: 2158-2171.

Dogu, G.,1986, Handbook of Heat and Mass Transfer, Vol.2, Mass Transfer and Reactor Design, Gulf Publ. Co., Houston, p. 434.

Dourson, M.,L., and Felter, S.P., 1997, "Route-to-route extrapolation of the toxic potency of MTBE", Risk Anal., Vol. 17, pp. 717–725.

EPA (Environmental Protection Agency), 1999. Achieving Clean Air and Clean Water. The Report of the Blue Ribbon Panel on Oxygenates in Gasoline. US EPA 420-R-99-021. Washington, DC.

Fite, C., Iborra, M., Tejero, J., Izquierdo, J.F. and Cunill, F., 1994, Kinetics of the liquid-phase synthesis of ETBE, Ind. Eng. Chem. Res., Vol. 33, pp. 581-591.

Gates, B.C. and Rodriguez, W., 1973, "General and specific acid catalysis in sulfonic acid resin", J. Catal., Vol. 31, pp. 27-31.

Gicquel, A., and Torck, B., 1983, "Synthesis of MTBE Catalyzed by Ion-Exchange Resin. Influence of Methanol Concentration and temperature", Journal of Catalysis, Vol. 83, pp. 9-18.

Gonderten, I., 1997, "Production of Additives for Environmentally Benign Gasoline", MS Thesis, Middle East Technical University, Ankara.

González, J.C. and Fair, J.R., 1997, "Preparation of Tertiary Amyl Alcohol in a Reactive Distillation Column. 1. Reaction Kinetics, Chemical Equilibrium, and Mass-Transfer Issues", Ind. Eng. Chem. Res., Vol. 36, pp. 3833-3844.

Iborra, M., Izquierdo J.F., Tejero J., Cunill F., 1992, "Application of the response surface methodology to the kinetic study of the gas phase addition of ethanol to isobutene on a sulfonated styrene divinyl benzene resin", Ind. Eng. Chem. Res., Vol. 31, 1840-1848.

Ignatius, J., Järvelin, H., and Lindqvist, P., 1995, "Use TAME and heavier ethers to improve gasoline properties", Hydrocarbon Processing, February, pp. 51-53.

Izquierdo, J.F., Cunill, F., Vila, M., Iborra, M., and Tejero, J., 1994, "Equilibrium constants for methyl tert-butyl ether and ethyl tert-butyl ether liquid-phase syntheses using C_4 olefinic cut", Ind. Eng. Chem. Res., Vol. 33, pp. 2830-2835.

Izumi, Y., Hasebe, R., and Urabe, K., 1983, "Catalysis by Heterogeneous Supported Heteropoly Acid", Journal of Catalysis, Vol. 84, pp. 402-409.

Jayadeokar, S.S and Sharma, M.M., 1993, "Simultaneous hydration and etherification of isoamylene using sub-azeotropic ethanol: Use of ion exchange resins as catalyst", React. Polym. Vol.19, pp. 169–179.

Jensen, K.L., and Datta, R., 1995, "Ethers from ethanol. 1. Equilibrium thermodynamic analysis of the liquid-phase ethyl tert-butyl ether reacion", Ind. Eng. Chem. Res., vol. 34, pp. 392-399.

Kitchaiya, P., and Datta, R., 1995, "Ethers from ethanol. 2. Reaction equilibria of simultaneous tert-amyl ethyl ether synthesis and isoamylene isomerization", Ind. Eng. Chem. Res., Vol. 34, pp. 1092-1101.

Kiviranta-Paakkonen PK, Struckmann LK, Linnekoski JA, Krause AOI. Comparison of the various kinetic models of TAME formation by simulation and parameters estimation. Ind. Eng. Chem. Res. 1998; 37(1): 18-24.

Knifton, J.F., Edwards, J.C., 1999, "Methyl tert-butyl ether synthesis from tert-butanol via inorganic solid acid catalysis", Applied Catalysis A: General, Vol. 183, pp.1 13.

Krause, A.O.I., and Hammarstróm, 1987, "Etherification of isoamylenes with methanol", Applied Catalysis, Vol.30. pp. 313-324.

Linnekoski, J.A., Krause, A.O.I., Struckmann, L.K., 1997, "Kinetics of heterogeneously catalyzed formation of *tert*-amyl ethyl ether.", Ind. Eng. Chem. Res., Vol. 36, pp. 310-316.

Linnekoski, J.A., Krause, A.O.I., Struckmann, L.K., 1998, "Etherfication and Hydration of Isoamylenes with Ion Exchange Resin", Applied Catalysis A: General, 170, pp. 117-126.

Linnekoski, J.A., P.K. Paakkönen, A.O.I Krause, Ind. Eng. Chem. Res., 38 (1999) 4563.

Noeres, C., Kenig, E.Y., Górak, A., 2003, "Modelling of Reactive Separation Processes: reactive Absorption and Reactive Distillation", Chemical Engineering and Processing, Vol. 42, pp. 157-178.

Obalı, Z., 2003, "Heteropolyacid Catalysts for Etherification of Isoolefins", MS. Thesis, Middle East Technical University, Ankara.

Oktar, N., 2001, "Kinetics for the Production of Tertiary Ethers Used As Gasoline Additives", Ph.D. Thesis, Gazi University Institute of Science and Technology, Ankara.

Oktar, N., Murtezaoglu, K., Dogu, G., Gonderten, I., and Dogu, T., 1999a, "Etherification Rates of 2-Methyl-2-Butene and 2-methyl-1-Butene with Ethanol for Environmentally Clean Gasoline Production", Journal of Chemical Technology and Biotechnology, Vol. 74, pp. 155-161.

Oktar, N., Murtezaoglu, K., Dogu, T. and Dogu, G., 1999b, "Dynamic Analysis of Adsorption Equilibrium Parameters of Reactants and Products in MTBE, ETBE and TAME", The Canadian Journal of Chemical Engineering, Vol. 77, pp. 406-412.

Oost, C. and Hoffmann, U., "The Synthesis of Tertiary Amyl Methyl Ether (TAME): Microkinetics of the Reaction", 1996, Chem. Eng. Sci., Vol. 51, pp. 329-340.

Orbey, H., Sandler, S.I., 1995, "Reformulation of Wong-Sandler Mixing Rule for Cubic Equations of State", AIChE Journal, Vol.41, No.3, pp.683-690.

Orbey, H., Sandler, S.I., Modeling Vapor-Liquid Equilibria. New York: Cambridge University Press, 1998.

Panneman, H.J., Beenackers, A.A.C.M., 1995, "Synthesis of Methyl tert-Butyl Ether Catalyzed by Acidic Ion Exchange Resins.Influence of the Proton Activity", Ind. Eng. Chem.Res., Vol.34, pp. 4318-4325.

Parra, D., Tejero, J., Cunill, F., Iborra, M., Izquierdo, F., 1994, "Kinetic Study of MTBE Liquid Phase Synthesis Using C$_4$ Olefinic Cut", Chem. Eng. Sci., Vol. 49, 4563-4578.

Pescarollo, E., Trotta, R., and Sarathy, P.R., 1993, Etherify light gasolines, Hydrocarbon Processing, February. pp. 53-60.

Piccoli RL, Lovisi HR. Kinetic and thermodynamic study of the liquid-phase etherification of isoamylenes with methanol. Ind. Eng. Chem. Res. 1995; 34: 510-515.

Rehfinger, A. and Hoffmann, U., 1990, "Kinetics of methyl tertiary butyl ether liquid phase synthesis catalyzed by ion exchange resin-I. Intrinsic rate expression in liquid phase activities", Chem. Eng. Science, Vol. 45, pp. 1605-1617.

Rihko, L.K., and Krause, A.O.I., 1993, "Reactivity of isoamylenes with ethanol", Applied Catalysis A: General, Vol. 101, pp. 283-295.

Rihko., L.K. and Krause, A.O.I., 1995, "Kinetics of heterogeneously catalyzed tert-amyl methyl ether reactions in the liquid phase", Ind. Eng. Chem. Res., Vol. 34, pp. 1172-1180.

Rihko., L.K. and Krause, A.O.I., 1996, "Etherification of FCC light gasoline with methanol", Ind. Eng. Chem. Res., Vol. 35, pp. 2500-2507.

Rihko., L.K., Linnekoski, J.A. and Krause, A.O.I., 1994, "Reaction equilibria in the synthesis of 2-methoxy-2-methyl butane and 2-ethoxy-2-methyl butane in the liquid phase", Journal of Chem. Eng. Data, Vol. 39, pp. 700-704.

Rosenkranz, H.S., and Klopman, G., 1991, "Prediction of the lack of genotoxicity and carcinogenicity in rodents after two gasoline additives: methyl- and ethyl-*t*-butyl ethers". In Vivo Toxicol. Vol. **4**, pp. 49–54.

S. Fisher, s., and Kunin, R., 1955, "Routine Exchange Capacity Determinations of Ion Exchange Resins" Analytical Chemistry Vol.27 (7) pp.1191-1194.

Schipper, P.H., Sapre, A.V. and Q.N.Le, 1990, "Chemical Apects of Clean Fuels Production", Chem.Eng.Sci., Vol. 45, pp. 1605-1617.

Shikata, S., Okuhara, T., Misono, M., 1995, "Catalysis by heteropoly compounds. Part XXVI. Gas phase synthesis of methyl tert-butyl ether over heteropolyacids", Journal of Molecular Catalysis A: Chemical 100, pp:49-59.

Sneesby, M.G., Tadé, M.O., Datta, R. and Smith,T.N., 1997, " ETBE synthesis via reactive distillation 1. Steady-state simulation and design aspects", Ind. Eng. Chem. Res. Vol. 36, pp. 1855–1869.

Sola, L., Pericas,M.A., Cunill, F., Izquierdo, J.F., 1997, "A Comperative Thermodynamic and Kinetic Study of Reaction Between Olefins and Light

Alcohols Leading to Branched Ethers", Ind. Eng. Chem. Res., Vol. 36, pp. 2012-2018.

Stern, B.R. and Kneiss, J.J., 1997, "Methyl tertiary butyl ether (MTBE): use as an oxygenate in fuels", J. Anal. Toxicol. Vol.17, pp. S1–S2.

Subramaniam, C. and Bhatia, S., 1987, "Liquid Phase Synthesis of Methyl Tert-Butyl Ether Catalyzed by Ion-exchange Resin", Can. J. Chem. Eng., Vol. 65, pp. 615-622.

Sundmacher, K. and Hoffmann, U., 1995. Oscillatory vapor–liquid transport phenomena in a packed reactive distillation column for fuel ether production. *Chemical Engineering Journal* 47, pp. 219–228.

Tau, L., and Davis, B.H., 1989, "Acid catalyzed formation of ethyl tertiary butyl ether (ETBE)", Applied Catalysis, Vol.53, pp. 263-271.

Tejero J., Cunill, F., Izquierdo, F., and Izquierdo, J.F., 1989, " " Ind. Eng. Chem. Res., Vol. 28, 1269-

Tejero, J., Cunill, F., .Izquierdo, F. Iborra, M.; Parra, D., 1996, "Scope and Limitations of Mechanistic Inferences from Kinetic Studies on Acidic Macroporous Resins. The MTBE Liquid-Phase Synthesis Case", Appl. Catal. A: General, Vol. 134, pp. 21-36.

Thornton, R., Gates, B. C., 1974, "Catalysis by Matrix-Bound Sulfonic Acid Groups: Olefin and Paraffin Formation from Butyl Alcohols", J. Catal., Vol. 34, pp. 275.

Vainiotalo, S., Y. Peltonen, A. Ruonakangas and P. Pfaffli , 1999, "Customer exposure to MTBE, TAME, C6 alkyl methyl ethers, and benzene during gasoline refueling" Environ. Health Perspect. 107 , pp. 133–140.

Varışlı, D., "The Simultaneous Production of Tert-Amyl Alcohol and Tert-Amyl Ethyl Ether in a Reactive Distillation Column", MS. Thesis, 2003, Middle East Technical University, Ankara.

World Health Organization of the United Nations, 1998. Environmental Health Criteria 206: Methyl *Tertiary*-Butyl Ether. WHO, Geneva, Switzerland.

Zhang, T. and Datta, R., 1995, "Integral analysis of methyl tert-butyl ether synthesis kinetics", Ind. Eng. Chem. Res., Vol. 34, pp. 730.

Zundel. G., Hydration and Intermolecular Interaction. Infrared Investigations with Polyelectrolyte Membranes, Academic Press, New York, 1969.

APPENDIX A

GAS CHROMATOGRAPH CALIBRATION FACTORS

During the analysis of reactants and products, to evaluate the peak read from the computer that is connected to the gas chromatography or integrator, and to calculate concentrations of the species using these peaks, it is necessary to calculate the calibration factors for gas chromatography. By this way, the errors due to injection and the probable errors come from the detector can be eliminated.

In this study, the calibration factors for 2M2B, TAA and TAME were calculated to obtain quantitative results from the GC trace. The calibration factor of ethanol was taken as a unit and the ratio between each of these species and ethanol were found.

Firstly, 2M2B-EtOH, TAEE-EtOH; 2M1B-MeOH and TAME-MeOH mixtures were prepared concerning the composition range of experiments and these mixtures were injected to the column at different amounts. According to the results, it is concluded that the differences in concentration and injection amount do not affect the value of calibration factor of that species.

A.1 Sample calculation for finding calibration factor:

To find out the calibration factor, for each species, mixtures of different volume fraction were prepared, and different amounts of samples from these mixtures were injected to the gas chromatograph. The calculation procedure for calibration factor was given in the following.

A_A : Area belongs to C_5 reactive olefin, 2M2B

A_B : Area belongs to EtOH

A_C : Area belongs to TAME

y_i : Volume fraction belongs to i'th component

x_i : Molar fraction belongs to i'th component

α_i : Relative calibration factor belongs to i'th component

$$A_A \beta_A + A_B \beta_B = 1$$

$$x_A = \frac{A_A \beta_A}{A_A \beta_A + A_B \beta_B} = \frac{\dfrac{A_A \beta_A}{A_B \beta_B}}{\dfrac{A_A \beta_A}{A_B \beta_B} + \dfrac{A_B \beta_B}{A_B \beta_B}} \quad \text{and} \quad \alpha_i = \frac{\beta_A}{\beta_B}$$

$$x_A = \frac{\dfrac{A_A}{A_B} \alpha_A}{\dfrac{A_A}{A_B} \alpha_A + 1} \quad \text{and} \quad \alpha_A = \frac{x_A}{\dfrac{A_A}{A_B}(1 - x_A)}$$

$$\frac{x_A}{x_B} = \frac{y_A}{y_B} \times \frac{\dfrac{\rho_A}{M_A}}{\dfrac{\rho_B}{M_B}} \qquad x_A + x_B = 1.0$$

Solving these equations simultaneously, calibration factor for species A can be found. Results of calibration experiments using 2M2B-EtOH mixtures and EtOH-TAEE mixtures were given in Table A.1 and A.2, respectively.

The calibration factors for 2M2B-MeOH-TAME system were also calculated in the same way.

Table A.1 The evaluation of calibration factor α of 2M2B

Injection amount,μl	y_A / y_B	AA	AB	AA/AB	x_B	x_A	α
1	0.10	241	1223	0.19706	0.94858	0.05142	0.275
1	0.10	244	1269	0.19228	0.94858	0.05142	0.282
3	0.10	752	3517	0.21382	0.94858	0.05142	0.254
3	0.10	742	3486	0.21285	0.94858	0.05142	0.255
5	0.10	1295	5681	0.22795	0.94858	0.05142	0.238
5	0.10	1226	5512	0.22242	0.94858	0.05142	0.244
1	0.20	481	1167	0.41217	0.89988	0.10012	0.270
1	0.20	489	1163	0.42046	0.89988	0.10012	0.265
3	0.20	1489	3301	0.45108	0.89988	0.10012	0.247
3	0.20	1349	3082	0.43770	0.89988	0.10012	0.254
5	0.20	2463	5177	0.47576	0.89988	0.10012	0.234
5	0.20	2401	5004	0.47982	0.89988	0.10012	0.232
1	0.46	882	963	0.91589	0.80004	0.19996	0.273
1	0.46	846	936	0.90385	0.80004	0.19996	0.277
3	0.46	2742	2771	0.98953	0.80004	0.19996	0.253
3	0.46	2632	2656	0.99096	0.80004	0.19996	0.252
5	0.46	4326	4328	0.99954	0.80004	0.19996	0.250
5	0.46	4276	4467	0.95724	0.80004	0.19996	0.261
						$\alpha_{2M2B.avg}$:	0.256

Table A.2 The evaluation of calibration factor α of TAEE

Injection amount,μl	y_C/y_B	AC	AB	AC/AB	x_B	x_C	α
1	0.12	201.2	1215	0.16560	0.95006	0.04994	0.317
1	0.12	194.3	1259	0.15433	0.95006	0.04994	0.341
3	0.12	588	3326	0.17679	0.95006	0.04994	0.297
3	0.12	555	3300	0.16818	0.95006	0.04994	0.313
5	0.12	748	4884	0.15315	0.95006	0.04994	0.343
5	0.12	780	4835	0.16132	0.95006	0.04994	0.326
1	0.25	357	975	0.36615	0.90024	0.09976	0.303
1	0.25	393	1080	0.36389	0.90024	0.09976	0.305
3	0.25	1061	3077	0.34482	0.90024	0.09976	0.321
3	0.25	1058	3039	0.34814	0.90024	0.09976	0.318
5	0.25	1541	4283	0.35979	0.90024	0.09976	0.308
5	0.25	1543	4453	0.34651	0.90024	0.09976	0.320
						$\alpha_{2M2B.avg}$:	0.318

A.2 Sample Calculation for finding Concentration from GC

The mole fraction of components was calculated by using the following method.

$$A_A \beta_A + A_B \beta_B + A_C \beta_C = 1.0$$

$$x_{A'} = \frac{A_A \beta_A}{A_A \beta_A + A_B \beta_B + A_C \beta_C}$$

$$x_{A'} = \frac{\dfrac{A_A \beta_A}{A_B \beta_B}}{\dfrac{A_A \beta_A}{A_B \beta_B} + \dfrac{A_B \beta_B}{A_B \beta_B} + \dfrac{A_C \beta_C}{A_B \beta_B}} \quad \text{and defining,} \quad \alpha_i = \frac{\beta_i}{\beta_B}$$

$$X_{A'} = \frac{\left(\dfrac{A_A}{A_B}\right) \times \alpha_A}{\left(\dfrac{A_A}{A_B} \times \alpha_A + 1 + \dfrac{A_C}{A_B} \times \alpha_C\right)}$$

The mole fraction of other components is calculated in the same way. The final form of these equations is given in the following:

$$X_{B'} = \frac{1}{\left(\dfrac{A_A}{A_B} \times \alpha_A + 1 + \dfrac{A_C}{A_B} \times \alpha_C\right)}$$

$$X_{C'} = \frac{\left(\dfrac{A_C}{A_B}\right) \times \alpha_C}{\left(\dfrac{A_A}{A_B} \times \alpha_A + 1 + \dfrac{A_C}{A_B} \times \alpha_C\right)}$$

APPENDIX B

PROPERTIES OF CHEMICALS

Table B.1 Properties of components

Components	Formula	MOL WT	$T_b(K)$	$T_c(K)$	P_c (Bar)	OMEGA
Methanol	CH_3OH	32.042	64.60	512.60	80.90	0.565
Ethanol	C_2H_5OH	46.069	78.30	516.20	63.80	0.649
2M2B	C_5H_{10}	70.135	38.50	470.00	38.60	0.339
2M1B	C_5H_{10}	70.135	31.10	465.00	34.50	0.237
TAA	$C_5H_{12}O$	88.15	102.0	545.0	39.5	0.478
TBA	$C_4H_{10}O$	74.123	82.4	506.2	39.7	0.613
TAME	$C_6H_{14}O$	102.177	359.0	531.5	31.1	0.322
TAEE	$C_7H_{16}O$	116.177	375.2	552.7	28.0	0.303

APPENDIX C

EXPERIMENTAL DATA

C.1 Etherification Reactions

Etherification reactions were performed by using differential flow reactor to test the activity of heat treatment and synthesized polymeric catalysts. Before each experiment, by-pass data were taken in order to calculate initial feed concentrations (experimental) and in all other calculations these experimental feed concentrations were used.

Table C.1.1 Experimental Data of Synthesized Catalyst for 2M1B+Ethanol Mixture (C_{A0}: 16.36 M, C_{B0}: 0.45 M)

Conversion Values For Different Catalysts, X_{Af}								
T,K	2A	7A	12A	13A	14A	21A	23A	2A2
333	0.042	–	0.0208	0.0612	0.0308	0.0500	0.0227	0.0450
343	0.065	0.0290	0.0233	0.0419	0.0519	0.0604	0.0134	0.0323
353	0.120	0.0458	0.0439	0.0567	0.1007	0.0799	0.0374	0.0768
363	0.205	0.0958	0.069	0.1040	0.1043	0.1183	0.0804	0.1060
370	0.208	0.1122	0.1398	0.1211	0.1622	0.1850	0.0868	0.1457
Reaction Rate Values, $-R_A \times 10^6$ (mol/g cat.s)								
T,K	2A	7A	12A	13A	14A	21A	23A	2A2
333	2.67	–	1.31	3.86	1.92	3.16	1.43	2.92
343	4.07	1.80	1.47	2.65	3.22	3.82	0.85	2.09
353	7.58	2.84	2.77	3.58	6.25	5.05	2.36	4.97
363	12.90	5.95	4.35	6.57	6.47	7.47	5.08	6.86
370	13.10	6.96	9.20	7.65	10.07	11.68	5.48	9.43

Table C.1.2 Experimental Data of Heat Treated Amberlyst-15 Catalysts for 2M1B+Ethanol Mixture (C_{A0}: 16.36 M, C_{B0}: 0.45 M)

Conversion Values For Different Catalysts, X_{Af}				
T,K	Amb-15	Amb-15-1	Amb-15-2	Amb-15-3
333	0.0601	0.0535	0.0515	0.0495
343	0.1086	0.0685	0.0622	0.0612
353	0.1204	0.1120	0.1079	0.0947
363	0.1506	0.1519	0.1489	0.1418
370	0.1834	0.1802	0.1762	0.1706
Reaction Rate Values, $-R_A \times 10^6$ (mol/g cat.s)				
T,K	Amb-15	Amb-15-1	Amb-15-2	Amb-15-3
333	3.89	3.48	3.35	3.22
343	7.03	4.45	4.04	3.98
353	7.80	7.28	7.01	6.15
363	9.75	9.87	9.67	9.21
370	11.87	11.70	11.44	11.08

Table C.1.3 Experimental Data for Synthesized Catalyst for 2M2B+Ethanol Mixture (C_{A0}: 16.36 M, C_{B0}: 0.45 M)

Conversion Values For Different Catalysts, X_{Af}					
T, K	2A	2A1	2A2	2A3	2A4
333	0.0000	0.0000	0.0000	0.0000	0.0000
343	0.0008	0.0017	0.0000	0.0000	0.0000
353	0.0012	0.0018	0.0013	0.0015	0.0010
363	0.0041	0.0037	0.0061	0.0032	0.0066
370	0.0167	0.0104	0.0134	0.0053	0.0136
Reaction Rate Values, $-R_A \times 10^6$ (mol/g cat.s)					
T,K	2A	2A1	2A2	2A3	2A4
333	0.0000	0.0000	0.0000	0.0000	0.0000
343	0.0615	0.1329	0.0000	0.0000	0.0000
353	0.0919	0.1421	0.1054	0.1208	0.0826
363	0.3270	0.2992	0.4855	0.2557	0.5296
370	1.3220	0.8291	1.0729	0.4204	1.0844

Table C.1.4 Experimental Data for Heat Treated Catalysts for 2M2B+Ethanol Mixture (C_{A0}: 16.36 M, C_{B0}: 0.45 M)

Conversion Values For Different Catalysts, X_{Af}				
T,K	Amb-15	Amb-15-1	Amb-15-2	Amb-15-3
333	0.0009	0.0009	0.0009	0.0000
343	0.0023	0.0038	0.0013	0.0008
353	0.0094	0.0123	0.0050	0.0013
363	0.0302	0.0169	0.0152	0.0040
370.3	0.0435	0.0321	0.0162	0.0152
Reaction Rate Values, $-R_A \times 10^6$ (mol/g cat.s)				
T,K	Amb-15	Amb-15-1	Amb-15-2	Amb-15-3
333	0.0756	0.0685	0.0723	0.0000
343	0.1862	0.3061	0.1017	0.0625
353	0.7590	0.9886	0.4007	0.1009
363	2.4338	1.3638	1.2271	0.3222
370	3.5018	2.5859	1.3060	1.2241

C.2 Batch-Reflux-Recycle Reactor Data

For each experiment, samples were taken from the reboiler and reflux sections at the same time. In the following tables, data analyzed with GC for both reboiler and reflux samples are presented

EXPERIMENT: 1

Feed:4.6 mol % 2M2B, 95.4 mol % MeOH
Reboiler Temperature (°C): 94
Operating Gauge Pressure Range (bar): 3.2-2.5
Catalyst Amount (gr/plate): 7.5 gr/plate (Total Plate: 8)

Table C.2.1 Experimental data of reaction of 2M2B+Methanol, Experiment: 1

Time, min	Reboiler Data (Bottom Product)			Reflux Data (Top Product)		
	X_{2M2B}	X_{MeOH}	X_{TAME}	X_{2M2B}	X_{MeOH}	X_{TAME}
60	0.0421	0.9468	0.0111	0.5062	0.4243	0.0694
90	0.0304	0.9492	0.0204	0.2871	0.6516	0.0613
120	0.0270	0.9457	0.0272	0.2786	0.6614	0.0600
150	0.0224	0.9452	0.0324	0.2369	0.7022	0.0609
180	0.0202	0.9437	0.0361	0.2008	0.7352	0.0640
210	0.0185	0.9433	0.0382	0.1681	0.7684	0.0635
240	0.0151	0.9444	0.0405	0.1633	0.7700	0.0667
270	0.0144	0.9431	0.0424	0.1422	0.7911	0.0668
300	0.0121	0.9439	0.0440	0.1336	0.7995	0.0668
330	0.0123	0.9386	0.0491	0.1351	0.7959	0.0690
360	0.0120	0.9432	0.0448	0.1346	0.7943	0.0711
390	0.0107	0.9430	0.0463	0.1183	0.8116	0.0700
420	0.0088	0.9432	0.0481	0.1098	0.8296	0.0606
450	0.0084	0.9468	0.0448	0.1185	0.8177	0.0638
480	0.0085	0.9456	0.0459	0.1102	0.8233	0.0665
510	0.0083	0.9446	0.0470	0.1061	0.8264	0.0676
540	0.0079	0.9467	0.0454	0.0947	0.8386	0.0667
570	0.0079	0.9473	0.0449	0.0930	0.8396	0.0674
Reboiler	0.0068	0.9434	0.0499			

EXPERIMENT: 2

Feed: 6 mol % 2M2B, 94 mol % MeOH

Reboiler Temperature (°C): 94

Operating Gauge Pressure Range (bar): 3.5-2.5

Catalyst Amount (gr/plate): 7.5 gr/plate (Total Plate: 8)

Table C.2.2 Experimental data of reaction of 2M2B+Methanol, Experiment: 2

Time, min	Reboiler Data (Bottom Product)			Reflux Data (Top Product)		
	X_{2M2B}	X_{MeOH}	X_{TAME}	X_{2M2B}	X_{MeOH}	X_{TAME}
40	0.0341	0.9593	0.0067	0.4661	0.4345	0.0995
55	0.0359	0.9559	0.0082	0.3427	0.5894	0.0679
80	0.0294	0.9554	0.0152	0.2893	0.6511	0.0596
140	0.0252	0.9476	0.0272	0.2312	0.7095	0.0592
200	0.0178	0.9428	0.0394	0.1863	0.7471	0.0666
260	0.0122	0.9430	0.0449	0.1581	0.7734	0.0685
320	0.0108	0.9414	0.0478	0.1476	0.7827	0.0698
380	0.0099	0.9416	0.0485	0.1348	0.8007	0.0645
440	0.0088	0.9449	0.0463	0.1286	0.8056	0.0658
500	0.0071	0.9485	0.0444	0.1193	0.8176	0.0630
560	0.0074	0.9480	0.0446	0.1129	0.8253	0.0618
Reboiler	0.0072	0.9440	0.0489	-	-	-

EXPERIMENT: 3

Feed:10 mol % 2M2B, 90 mol % MeOH
Reboiler Temperature (°C): 94
Operating Gauge Pressure Range (bar): 4-3.5
Catalyst Amount (gr/plate): 7.5 gr/plate (Total Plate: 8)

Table C.2.3 Experimental data of reaction of 2M2B+Methanol, Experiment: 3

	Reboiler Data (Bottom Product)			Reflux Data (Top Product)		
Time, min	x_{2M2B}	x_{MeOH}	x_{TAME}	x_{2M2B}	x_{MeOH}	x_{TAME}
40	0.0528	0.9275	0.0198	0.9095	0.0087	0.0818
55	0.0480	0.9301	0.0219	0.3699	0.5603	0.0698
80	0.0495	0.9155	0.0350	0.2840	0.6474	0.0685
140	0.0336	0.9137	0.0527	0.2558	0.6640	0.0802
200	0.0280	0.9103	0.0617	0.2353	0.6872	0.0775
260	0.0232	0.9114	0.0654	0.2149	0.7021	0.0830
320	0.0161	0.9151	0.0689	0.2045	0.6951	0.1004
380	0.0165	0.9111	0.0724	0.1880	0.7270	0.0851
440	0.0175	0.9074	0.0751	0.1967	0.7204	0.0828
500	0.0186	0.9019	0.0795	0.2143	0.6919	0.0938
560	0.0173	0.9101	0.0725	0.2025	0.7116	0.0859
620	0.0185	0.9083	0.0732	0.2090	0.7033	0.0877
680	0.0177	0.9056	0.0768	0.2159	0.6974	0.0867
740	0.0174	0.9061	0.0765	0.2129	0.7010	0.0861
800	0.0184	0.9051	0.0765	0.2072	0.7096	0.0832
Reboiler	0.0184	0.9060	0.0759			

EXPERIMENT: 4

Feed: 25 mol % 2M2B, 75 mol % MeOH

Reboiler Temperature (°C): 94

Operating Gauge Pressure Range (bar): 4.6-4

Catalyst Amount (gr/plate): 7.5 gr/plate (Total Plate: 8)

Table 2.2.4 Experimental data of reaction of 2M2B+Methanol, Experiment: 4

Time, min	Reboiler Data (Bottom Product)			Reflux Data (Top Product)		
	x_{2M2B}	x_{MeOH}	x_{TAME}	x_{2M2B}	x_{MeOH}	x_{TAME}
40	0.2009	0.7831	0.0160	0.3165	0.6267	0.0568
55	0.1849	0.7985	0.0166	0.4575	0.4574	0.0851
80	0.1712	0.7993	0.0295	0.5021	0.4032	0.0947
140	0.1498	0.8066	0.0436	0.4960	0.4076	0.0964
200	0.1280	0.8063	0.0656	0.4431	0.4537	0.1032
260	0.1261	0.7817	0.0922	0.4416	0.4579	0.1004
320	0.1105	0.7678	0.1217	0.4180	0.4879	0.0942
380	0.0983	0.7651	0.1366	0.4373	0.4688	0.0939
440	0.1005	0.7481	0.1514	0.4337	0.4749	0.0914
500	0.0889	0.7485	0.1626	0.3475	0.5541	0.0984
560	0.0772	0.7325	0.1903	0.3400	0.5447	0.1153
620	0.0848	0.7111	0.2041	0.3391	0.5502	0.1107
680	0.0805	0.7153	0.2042	0.3528	0.5321	0.1151
740	0.0735	0.7373	0.1893	0.3534	0.5321	0.1145
800	0.0721	0.7262	0.2016	0.3462	0.5400	0.1138
Reboiler	0.0693	0.7307	0.1999			

EXPERIMENT: 5

Feed: 6 mol % 2M2B, 94 mol % MeOH

Reboiler Temperature (°C): 72

Operating Gauge Pressure Range (bar): 2.1

Catalyst Amount (gr/plate): 7.5 gr/plate (Total Plate: 8)

Table C.2.5 Experimental data of reaction of 2M2B+Methanol, Experiment: 5

	Reboiler Data (Bottom Product)			Reflux Data (Top Product)		
Time, min	X_{2M2B}	X_{MeOH}	X_{TAME}	X_{2M2B}	X_{MeOH}	X_{TAME}
40	0.0463	0.9529	0.0008	0.40085	0.53765	0.06150
55	0.0451	0.9537	0.0012	0.45749	0.45738	0.08513
80	0.0434	0.9525	0.0040	0.45208	0.45686	0.09106
140	0.0417	0.9510	0.0073	0.38923	0.52351	0.08725
200	0.0395	0.9496	0.0109	0.34031	0.58087	0.07882
260	0.0372	0.9486	0.0143	0.29616	0.62404	0.07980
320	0.0369	0.9419	0.0213	0.24464	0.67997	0.07539
380	0.0305	0.9441	0.0253	0.22244	0.69218	0.08538
440	0.0261	0.9431	0.0308	0.19720	0.71342	0.08938
500	0.0201	0.9466	0.0332	0.18629	0.72248	0.09123
560	0.0160	0.9490	0.0350	0.16449	0.74575	0.08976
620	0.0131	0.9489	0.0380	0.12911	0.78022	0.09067
680	0.0118	0.9493	0.0388	0.12270	0.79315	0.08416
740	0.0106	0.9484	0.0409	0.12253	0.78902	0.08845
800	0.0095	0.9496	0.0409	0.12046	0.79113	0.08842
860	0.0087	0.9506	0.0407	0.11435	0.79985	0.08580
920	0.0079	0.9492	0.0429	0.10917	0.80737	0.08346
980	0.0069	0.9495	0.0437	0.10684	0.81137	0.08179
1040	0.0069	0.9492	0.0440	0.10364	0.81507	0.08130
1100	0.0061	0.9454	0.0485	0.10264	0.81626	0.08109
1160	0.0056	0.9471	0.0472	0.09902	0.82212	0.07886
1220	0.0052	0.9476	0.0472	0.09660	0.82602	0.07739
1280	0.0052	0.9475	0.0473	0.09639	0.82656	0.07704
Reboiler	0.00522	0.94565	0.04915			

EXPERIMENT: 6

Feed: 6 mol % 2M2B, 94 mol % MeOH

Reboiler Temperature (°C): 82

Operating Gauge Pressure Range (bar): 2.3

Catalyst Amount (gr/plate): 7.5 gr/plate (Total Plate: 8)

Table C.2.6 Experimental data of reaction of 2M2B+Methanol, Experiment: 6

	Reboiler Data (Bottom Product)			Reflux Data (Top Product)		
Time, min	X_{2M2B}	X_{MeOH}	X_{TAME}	X_{2M2B}	X_{MeOH}	X_{TAME}
40	0.0455	0.9486	0.0059	0.35807	0.58699	0.05494
55	0.0475	0.9456	0.0069	0.41528	0.50745	0.07727
80	0.0378	0.9539	0.0083	0.41042	0.50692	0.08267
140	0.0318	0.9389	0.0293	0.34867	0.57317	0.07816
200	0.0246	0.9423	0.0331	0.30140	0.62879	0.06981
260	0.0195	0.9434	0.0371	0.26009	0.66982	0.07008
320	0.0159	0.9395	0.0446	0.21253	0.72198	0.06549
380	0.0134	0.9362	0.0504	0.19279	0.73321	0.07400
440	0.0117	0.9374	0.0509	0.17022	0.75264	0.07715
500	0.0097	0.9377	0.0527	0.16052	0.76087	0.07861
560	0.0091	0.9390	0.0520	0.14111	0.78189	0.07700
620	0.0070	0.9358	0.0572	0.10960	0.81523	0.07517
680	0.0057	0.9417	0.0526	0.10784	0.81432	0.07784
740	0.0051	0.9395	0.0554	0.11049	0.81348	0.07602
800	0.0046	0.9482	0.0472	0.10851	0.81604	0.07545
Reboiler	0.0065	0.9434	0.0502			

EXPERIMENT: 7

Feed: 6 mol % 2M2B, 94 mol % MeOH

Reboiler Temperature (°C): 104

Operating Gauge Pressure Range (bar): 4.7-3.8

Catalyst Amount (gr/plate): 7.5 gr/plate (Total Plate: 8)

Table C.2.7 Experimental data of reaction of 2M2B+Methanol, Experiment: 7

Time, min	Reboiler Data (Bottom Product)			Reflux Data (Top Product)		
	x_{2M2B}	x_{MeOH}	x_{TAME}	x_{2M2B}	x_{MeOH}	x_{TAME}
40	0.0275	0.9690	0.0035	0.3581	0.5870	0.0549
55	0.0395	0.9494	0.0111	0.4153	0.5074	0.0773
80	0.0339	0.9538	0.0123	0.4104	0.5069	0.0827
140	0.0334	0.9444	0.0222	0.3487	0.5732	0.0782
200	0.0280	0.9324	0.0396	0.3014	0.6288	0.0698
260	0.0190	0.9285	0.0525	0.2601	0.6698	0.0701
320	0.0177	0.9232	0.0591	0.2125	0.7220	0.0655
380	0.0144	0.9268	0.0588	0.1928	0.7332	0.0740
440	0.0120	0.9298	0.0582	0.1702	0.7526	0.0771
500	0.0102	0.9346	0.0552	0.1605	0.7609	0.0786
560	0.0097	0.9348	0.0555	0.1411	0.7819	0.0770
Reboiler	0.0091	0.9376	0.0534			

EXPERIMENT: 8

Feed: 4 mol % 2M2B, 96 mol % EtOH

Reboiler Temperature (°C): 94

Operating Gauge Pressure Range (bar): 2-1.9

Catalyst Amount (gr/plate): 7.5 gr/plate (Total Plate: 8)

Table C.2.8 Experimental data of reaction of 2M2B+Ethanol, Experiment: 8

Time, min	Reboiler Data (Bottom Product)			Reflux Data (Top Product)		
	x_{2M2B}	x_{EtOH}	x_{TAEE}	x_{2M2B}	x_{EtOH}	x_{TAEE}
30	0.0274	0.9708	0.0018	0.7424	0.2576	0.0000
60	0.0237	0.9742	0.0021	0.1065	0.8929	0.0006
120	0.0218	0.9719	0.0063	0.2667	0.7313	0.0020
180	0.0198	0.9708	0.0093	0.2521	0.7276	0.0203
240	0.0213	0.9680	0.0107	0.2506	0.7280	0.0214
300	0.0203	0.9673	0.0124	0.2358	0.7419	0.0222
360	0.0160	0.9690	0.0149	0.2443	0.7335	0.0222
420	0.0164	0.9684	0.0152	0.2291	0.7477	0.0233
480	0.0164	0.9687	0.0149	0.2142	0.7619	0.0239
540	0.0160	0.9686	0.0154	0.2163	0.7589	0.0248
Reboiler	0.0186	0.9652	0.0162			

EXPERIMENT: 9

Feed: 10 mol % 2M2B, 90 mol % EtOH

Reboiler Temperature (°C): 94

Operating Gauge Pressure Range (bar): 2.9-2.4

Catalyst Amount (gr/plate): 7.5 gr/plate (Total Plate: 8)

Table C.2.9 Experimental data of reaction of 2M2B+Ethanol, Experiment: 9

Time, min	Reboiler Data (Bottom Product)			Reflux Data (Top Product)		
	x_{2M2B}	x_{EtOH}	x_{TAEE}	x_{2M2B}	x_{EtOH}	x_{TAEE}
30	0.0677	0.9267	0.0057	0.7557	0.2370	0.0073
60	0.0666	0.9264	0.0070	0.4597	0.5095	0.0308
120	0.0615	0.9236	0.0149	0.4311	0.5303	0.0386
180	0.0555	0.9212	0.0233	0.4100	0.5527	0.0372
240	0.0492	0.9185	0.0323	0.3980	0.5620	0.0399
300	0.0499	0.9130	0.0371	0.3932	0.5652	0.0416
360	0.0475	0.9121	0.0404	0.3848	0.5718	0.0434
420	0.0468	0.9110	0.0421	0.3658	0.5876	0.0466
480	0.0437	0.9119	0.0444	0.3690	0.5879	0.0431
540	0.0457	0.9078	0.0466	0.3644	0.5918	0.0439
Reboiler	0.04484	0.91433	0.04083			

APPENDIX D

CALCULATIONS

D.1 Calculation of Reaction Rate in a Packed Continuous Differential Reactor
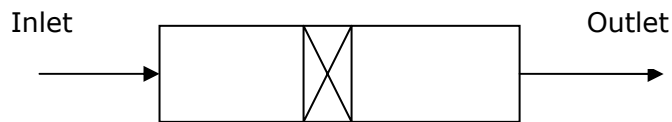
C_5 reactive olefins; F_{A0} $F_{Af} = F_{Ao} (1-X_{Af})$

Ethanol; F_{Bo} $F_{Bf} = F_{Bo} - F_{Ao} X_{Af}$

Ether, TAEE; $F_{Co} = 0$ $F_{Cf} = F_{Ao} X_{Af}$

For species A, the steady state material balance equation is given by;

$dF_{Ao} - dF_{Af} + (- R_A) dV = 0$

$dF_{Ao} - dF_{Ao} (1-X_{Af}) + (- R_A) dV = 0$

$$\int \frac{dV}{F_{Ao}} = \int \frac{dX_A}{(-R_A)}$$

-RA values can be taken as constant since the reaction rate does not change much throughout the reactor. Therefore, reaction rate expression given above can be simplified;

$$-R_A = \frac{F_{Ao}X_A}{V}$$

The reaction rate can be expressed in terms of catalyst amount:

$$-R_A' = \frac{-R_A}{(1-\epsilon_b)\rho_{cat}}$$

$$-R_A = (-R_A')(1-\epsilon_b)\rho_{cat} = \frac{X_{Af}F_{Ao}}{V}$$

$$-R_A' = \frac{X_{Af}F_{Ao}}{V(1-\epsilon_b)\rho_{cat}} = \frac{X_{Af}F_{Ao}}{m}$$

Therefore the reaction rate is obtained in terms of mol/g cat.s.

D.2 Calculate (-)ΔV/Δ(logD) vs. Pore Diameter by using Porosimetry Data

Sample calculation of (-)ΔV/Δ(logD) of heat treated Amberlyst-15 and Amb-1-1 catalysts are given in Table D.2.1, D.2.2.

Table D.2.1 Calculated (-)ΔV/Δ(logD) vs. Pore Diameter Data of Amberlyst-15

Amberlyst-15					
Pressure	Pore Diameter	Cum.Intr. Vol		log(D2-D1)	
Psia	D, µm	V, cc/g	ΔV	ΔlogD	(-)ΔV/Δ(logD)
2004.6	0.0902	0.0024			
3012.6	0.0600	0.0095	0.0071	-0.1771	0.0401
4988.5	0.0363	0.0261	0.0166	-0.2182	0.0761
7468.4	0.0242	0.1021	0.0760	-0.1761	0.4316
9956	0.0182	0.2563	0.1542	-0.1237	1.2461
10956	0.0165	0.2730	0.0167	-0.0426	0.3921
11956	0.0151	0.2850	0.0120	-0.0385	0.3116
12948	0.0140	0.2919	0.0069	-0.0328	0.2101
14931.9	0.0121	0.3014	0.0095	-0.0633	0.1500
17419.9	0.0104	0.3086	0.0072	-0.0658	0.1095
19915.9	0.0091	0.3133	0.0047	-0.0580	0.0810
20907.9	0.0087	0.3157	0.0024	-0.0195	0.1229
24883.9	0.0073	0.3181	0.0024	-0.0762	0.0315

Table D.2.2 Calculated (-)ΔV/Δ(logD) vs. Pore Diameter Data of Amb-15-1

Amb-15-1					
Pressure	Pore Diameter	Cum.Intr. Vol		log(D2-D1)	
Psia	D, µm	V, cc/g	ΔV	ΔlogD	(-)ΔV/Δ(logD)
1000.7	0.1807	0.0053			
2012.7	0.0899	0.0106	0.0053	-0.3032	0.0175
2996.7	0.0604	0.0160	0.0054	-0.1727	0.0313
4980.7	0.0363	0.0266	0.0106	-0.2211	0.0479
7476.5	0.0242	0.1915	0.1649	-0.1761	0.9364
10964.4	0.0165	0.2767	0.0852	-0.1663	0.5122
12948.4	0.0140	0.2926	0.0159	-0.0714	0.2228
17428.4	0.0104	0.3086	0.0160	-0.1291	0.1239
20908.4	0.0087	0.3192	0.0106	-0.0775	0.1367
22908.4	0.0079	0.3299	0.0107	-0.0419	0.2554

D.3 Calculation of Hydrogen Ion-Exchange Capacity

In the calculation of hydrogen ion-exchange capacity of Amb-15-1 catalyst, amount of consumed acid vs. measured pH values are shown in Figure D.3. Hydrogen ion-exchange capacity value is calculated by using Eqn.4.1.

Amount of Catalyst= 3.474 g

Amount of washed catalyst with 1 M HNO_3 solution in 0.1 N NaOH= 2.422 g

$$\% \text{ Solid} = \frac{0.9577g}{2.422g} \times 100 = 40$$

Consumed HCl from graph= 15.3 ml

$$\text{Hydrogen ion-exchange capacity} = \frac{(200 \times 0.1 N_{NaOH}) - 10 \times (15.8 \times 0.1)}{3.474 \times \dfrac{40}{100}} = 3.4$$
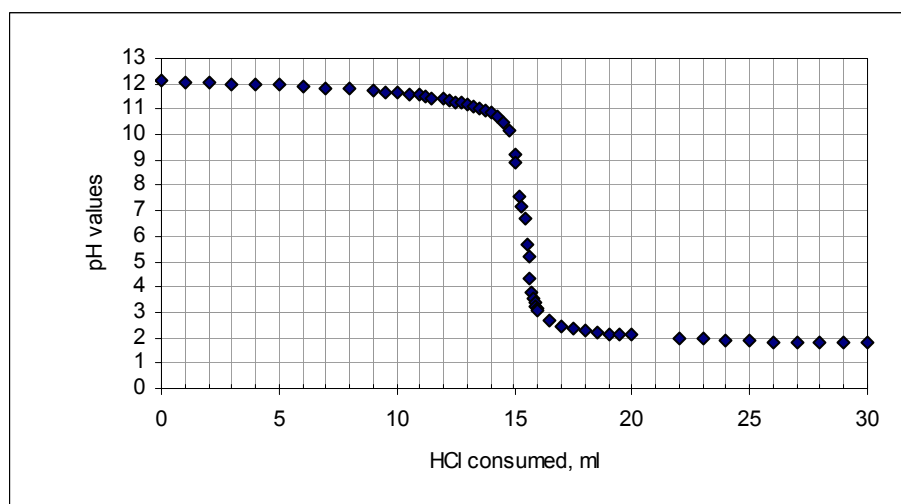
Figure D.3 Amount of consumed acid vs. measured pH values for Amb-15-1

D.4 Sample Calculation on the batch Reflux-Recycle-Reactor

Sample calculation of reaction rate constant k_1 (cm^3/ g.s) for Experiment: 2
(Feed: 6 mol % 2M2B, 94 mol % MeOH, T = 94°C)

Time= 40 min

Pg= 2.8 bar

Pabs=2.8+.8875=3.7 bar

Reboiler: XA = 0.03406 (liquid)   yAin = 0.2118 (vapor)

                  XB = 0.95928   from WSM MAIN: yBin = 0.7858

                  XC = 0.00667   yCin = 0.0024

Ctotal (reboiler, liquid)=ρ/MW=0.7914/32.04 = 0.0247 mol/cm^3 (for methanol)
(Assumptions: Total concentration of liquid is constant)

Ctotal (reboiler)= 24.7 mol/lt

Ctotal (vapor)= P/RT=0.126 mol/lt

CA=XA*Ctotal

CB=XB*Ctotal

CC=XC*Ctotal

yAin=KxyA*XA $\rightarrow$ find KxyA, KxyB, KxyC

yBin=KxyB*XB

yCin=KxyC*XC

$\rightarrow$ find   KA=(KxyA*Ctotal,vapor)/(Ctotal, reboiler)

$\rightarrow$ find   CAin=(Ctotal,vapor)*yAin

           CBin=(Ctotal,vapor)*yBin

CCin=(Ctotal,vapor)*yCin

Calculating volumetric flow rate, Q (cm^3/s):

qin(J/s)=Q1 (CAin,v λ_A + CBin,v λ_B +CCin,v λ_C) + Q2 (CA$_{top}$ C$_{PA}$ + CB$_{top}$ C$_{PB}$ + CC$_{top}$ C$_{PC}$) (Tboiler-Treflux)

In these calculations liquid phase CpA values are used.

λA, λB, λC are heat of vaporization.

It can be assumed Q1=Q2 since the calculated Q1 and Q2 are quite close to each other. But in our calculations we used corrected Q1 values.

Space time, s=Vreactor/Q1

Vreactor= 3.14*(2.5 cm)^2*39.3 cm = 771 cm^3

$$\frac{dC_{IA}^{L}}{dt} = -\frac{QK_{IA}}{V}\xi_{IA,e}^{V}\left[1-\exp\left(-\frac{(M+1)}{(M+\xi_{IA,e}^{V})}\frac{k_{1}W}{Q}\right)\right]C_{IA}^{L}$$

From above eqn. k$_1$ is calculated.

D.4.1 Calculation of Liquid Phase C_{pA} Calculation

liquid phase Cp calculation			$Cp= A+BT+CT^2+CT^3$				
	T°C	T(K)	A	B	C	D	J/mol.K Cp
2M2B	72	345	132.9	-1.48E-01	7.51E-04	-8.82E-08	168
	82	355	132.9	-1.48E-01	7.51E-04	-8.82E-08	171
	94	367	132.9	-1.48E-01	7.51E-04	-8.82E-08	176
	104	377	132.9	-1.48E-01	7.51E-04	-8.82E-08	179
meoh	72	345	74.86	-1.02E-01	4.07E-04	0.00E+00	88
	82	355	74.86	-1.02E-01	4.07E-04	0.00E+00	90
	94	367	74.86	-1.02E-01	4.07E-04	0.00E+00	92
	104	377	74.86	-1.02E-01	4.07E-04	0.00E+00	94
Tame	72	345	192.88	-2.50E-01	9.41E-04	2.02E-08	220
	82	355	192.88	-2.50E-01	9.41E-04	2.02E-08	224
	94	367	192.88	-2.50E-01	9.41E-04	2.02E-08	229
	104	377	192.88	-2.50E-01	9.41E-04	2.02E-08	234
etoh	72	345	100.92	-1.12E-01	4.99E-04	0.00E+00	122
	82	355	100.92	-1.12E-01	4.99E-04	0.00E+00	124
	94	367	100.92	-1.12E-01	4.99E-04	0.00E+00	127
	104	377	100.92	-1.12E-01	4.99E-04	0.00E+00	130
Taee	72	345	218.41	-2.09E-01	8.56E-04	0.00E+00	248
	82	355	218.41	-2.09E-01	8.56E-04	0.00E+00	252
	94	367	218.41	-2.09E-01	8.56E-04	0.00E+00	257
	104	377	218.41	-2.09E-01	8.56E-04	0.00E+00	261

APPENDIX E

DERIVATIONS

E.1 Derivations of A General Criterion to Test the Importance of Diffusion Limitations in Bidisperse Porous Catalysts (Doğu and Doğu, 1980)

In the analysis of solid catalyzed reactions, it is very important to know whether transport processes within the micro- and macropore regions have any effect on the observed reaction rate.

The effectiveness factor of a spherical bidisperse porous catalyst can be expressed as

$$\eta = \frac{9}{R_0^3 r_0^3 r_A(C_{A0})} \int_0^{R_0} \int_0^{r_0} \left[r_s(C_i) r^2 dr \right] R^2 dR \tag{E.1}$$

where C_i is the concentration of reactant in the micropores. The rate is expanded in a Taylor series about the surface concentration of particles, C_a, which is the concentration of reactant in the macropores, and second-order and higher order terms are neglected. For negligible diffusion effects ($\eta > 0.95$), a general criterion for bidisperse porous catalysts obtained.

$$\frac{R_A^{'}(C_{A0})}{R_A(C_{A0})}\left[(R_A\rho_p)S\frac{R_0^2}{D_a}\right](1+G) - \frac{1}{15}\frac{R_A^{''}(C_0)}{R_A(C_0)}\left[R_A\rho_pS\frac{R_0^2}{D_a}\right]G < \frac{3}{4} \qquad (E.2)$$

where

$$G = \left(\frac{r_o}{R_o}\right)^2\frac{D_a}{D_i(1-\varepsilon_a)}$$ and S is the surface area of per unit mass of

the catalyst.

Magnitude of G is determined by the ratio of diffusion times in the micro and macro-pores.

According to this criterion, the following relation should be satisfied for negligible diffusional effects.

$$\left(\frac{(R_A\rho_p)R_o^2}{C_{Ao}D_a}\right)(1+G) \ll \frac{3}{4} \qquad (E.3)$$

E.2 Derivation of Moment Equations for Batch Adsorber

When the dynamic mass balances of the adsorbate in the particle side and bulk liquid solution were solved together for the batch adsorber with the initial and boundary conditions, the dimensionless concentration profile of the tracer in the adsorber was found in Laplace Domain as follows:

$$\frac{D_a}{R^2} \frac{\partial}{\partial R} \left(R^2 \frac{\partial q}{\partial R} \right) = \frac{\partial q}{\partial t}$$

at R=R$_0$ q=KC

at R=0 $\dfrac{dq}{dR} = 0$

$$q = KC \left(\frac{R_0}{R} \right) \frac{\sinh\left(\left(\dfrac{s}{D_a} \right)^{1/2} R \right)}{\sinh\left(\left(\dfrac{s}{D_a} \right)^{1/2} R_0 \right)}$$

$$\frac{dC}{dt} = -D_a m_s \frac{3}{R_0} \frac{\partial q}{\partial R} \Big|_{R=R_o}$$

$$\frac{C - C_\infty}{C_0 - C_\infty} = \frac{1 + \delta_0}{\delta_0} \left(\frac{1}{s + \dfrac{3D_a}{R_0^3} \left[R_0 \left(\dfrac{s}{D_a} \right)^{1/2} \cosh\left(\left(\dfrac{s}{D_a} \right)^{1/2} R_0 \right) R_0 - \sinh\left(\left(\dfrac{s}{D_a} \right)^{1/2} R_0 \right) \right]} \right) - \frac{1}{s\delta_0}$$

where $\delta_0 = \dfrac{C_0}{C_\infty} - 1$

CIRRUCULUM VITAE

NEZAHAT BOZ

PERSONEL INFORMATION

Gender: Female
Marital Status: Married
Date of Birth: 01.01.0969
Date of Place: Cerkes/TURKEY

EDUCATION:

1998-2004 Ph.D. Degree: METU Chemical Engineering, June 2004.

Topic: Kinetic Studies For The Production of Tertiary Ethers Used As Gasoline Additives
Advisors: Prof. Dr. Timur Doğu and Prof.Dr. Gülşen Doğu

1993-1996 M. Sc. Degree: Stevens Institute of Technology Chemical Engineering, May 1996.

Topic: Rheological Behavior and Extrusion Flow of a Concentrated Suspension with an Elastomeric Binder
Advisor: Prof. Dr. Dilhan M. Kalyon

1985-1989 B.S. Degree: Gazi University Chemical Engineering, August 1989.

*Graduated in top 5% of the class.

Journal Papers produced basing on this work:

Dogu, T., Aydin, E., **Boz, N.**, Murtezaoglu, K., Dogu, G., 2003, "Diffusion Resistances and Contribution of Surface Diffusion in TAME and TAEE Production Using Amberlyst-15", Int. J. Chem. Reac. Eng. 1, Article A6.

Dogu, T., **Boz, N.**, Aydin, E., Oktar, N., Murtezaoglu, K., Dogu, G., 2001, "DRIFT Studies for the Reaction and Adsorption of Alcohols and Isobutylene on Acidic Resin Catalysts and the Mechanism of ETBE and MTBE Synthesis", Ind. Eng. Chem. Res., Vol. 40, pp. 5044-5051.

Boz, N., Dogu, T., Murtezaoglu, K., Dogu, G., 2004, "Effect of hydrogen ion-exchange capacity on activity of resin catalysts in tert-amyl ethyl ether (TAEE) synthesis", Applied Catalysis A: General, vol. 268, pp. 175-182.

Boz, N., and Dogu, T., 2004, "Reflux-Recycle-Reactor for High Yield and selectivity in TAME & TAEE Production", AICHE (in press).

Boz, N., Dogu, T., Murtezaoglu, K., Dogu, G., 2004, "Mechanism of TAME and TAEE Synthesis From Diffuse Reflectance FTIR Analysis", Cataly. Today. (in review).

Symposium Presentations related to this work:

Oktar, N., **Boz, N.,** Murtezaoglu, K., Dogu, G., Dogu, T., "Sulfonated Polymeric Catalysts for the Etherification of 2-Methyl 1-Butene with Ethanol", Clean Processes and Environment: The Catalytic Solution Conference, Lyon, France, 1999.

Oktar,N., **Boz, N.,** Murtezaoglu, K., Dogu, G., Dogu, T., "Preparation of Acidic Polymeric Membranes for Obtaining Environmentally Benign Gasoline", 5th National Symposium of Combustion and Air Pollution Control, Elazig, July 19-21, 2000.

Boz, N., Oktar, **N.,** Murtezaoglu, K., Dogu, G., Dogu, T., "Drift Studies for the production of MTBE over Amberlyst 15", 4th National Symposium of Chemical Engineering, Istanbul, September 4-7, 2000.

Boz, N., Dogu, T., Murtezaoglu, K., Dogu, G., "Synthesis and Activity of Acidic Mesoporous Polymeric Catalyst for the Etherification Reaction" 2nd Chemical Engineering Conference for Collaborative Research in Eastern Mediterranean (EMCC), May 20-24, 2001.

Dogu, T., **Boz, N.**, Aydin, E., Oktar, N., Murtezaoglu, K., Dogu, G., "Drift Studies for the Reaction and Adsorbtion of Alcohols and Isobutylene on Acidic Resin Catalysts and the Mechanism of ETBE and MTBE Synthesis", Chemical Reactor Engineering 2001: Novel Reactor Engineering for The New Millennium, Barga-Italy, June 24-29, 2001.

Dogu, T., Aydin, E., **Boz, N.**, Murtezaoglu, K., Dogu, G. "Diffusion Studies for Ethanol, Methanol and Isoamylene in a Macroreticular Resin Catalyst by Batch Adsorption Moment" 17th International Symposium on Chemical Engineering (ISCRE 17), Hong Kong, August 25-28, 2002.

Boz, N., Dogu, G , Murtezaoglu, K., Dogu, T., "Kinetic Studies on Etherification of Isoamylenes and DRIFTS Results for TAME and TAEE Production" 3rd Chemical Engineering Conference for Collaborative Research in Eastern Mediterranean (EMCC-3), Thessaloniki, Greece, May 13-15, 2003.

Dogu, T., **Boz, N**., Murtezaoglu, K., Dogu, G., "Effect of Hydrogen Ion-Exchange Capacity on Activity of Resin Catalysts and Mechanism of Tame and Taee Synthesis", Chemical Reaction Engineering IX: Chemical Reactor Engineering, Meeting the Challanges for New Technology (CRE-XI), Quebec City, Canada, June 29 –July, 2003.

Boz, N., Dogu, G., Dogu, T., Murtezaoglu, K., "TAME and TAEE Production in a Batch Reflux-Reactor", International Symposium on Multifunctional Reactors (ISMR-3) and Colloquium on Chemical Reaction Engineering (CCRE-18), University of Bath, UK, August 27-30, 2003.

Varışlı,D., **Boz, N.**, Doğu, T., Doğu, G., Mürtezaoğlu, K., "Performances of Batch Reactive Distillation and Batch Reflux Recycle Reactors in the Production of Tert-amyl-ethyl-ether", 4th Int. Conference on Unsteady–State Processes in Catalysis", USPC4, Montreal, Canada (October 2003).

Boz, N., Dogu, T., Murtezaoglu, K. and Dogu, G., "Mechanism of TAME and TAEE Synthesis from Diffuse-Reflectance FT-IR Analysis", 11th Nordic Symposium on Catalysis, 22- 25 May, 2004.